MODELLING HYDROLOGICAL RESPONSE TO DYNAMIC LAND USE LAND COVER CHANGES IN BIG AKAKI WATERSHED, ETHIOPIA

BAYISA TULU AREDA

A THESIS SUBMITTED TO

THE DEPARTMENT OF WATER RESOURCES ENGINEERING

SCHOOL OF CIVIL ENGINEERING AND ARCHITECTURE

PRESENTED IN PARTIAL FULFILLMENT OF THE REQUIREMENT FOR THE DEGREE OF MASTER'S IN WATER RESOURCES ENGINEERING

(SPECIALIZATION IN HYDROLOGY AND WATER RESOURCES MANAGEMENT)

OFFICE OF GRADUATE STUDIES
ADAMA SCIENCE AND TECHNOLOGY UNIVERSITY

JUNE 2022
ADAMA, ETHIOPIA

Modelling Hydrological Response to Dynamic Land Use Land Cover Changes in Big Akaki Watershed, Ethiopia

Bayisa Tulu Areda (ID: PGR/22408/13)

Advisor: Dereje Birhanu Mitiku (PhD)

A Thesis Submitted to

The Department of Water Resources Engineering

School of Civil Engineering and Architecture

Presented in Partial Fulfillment of the Requirement for the Degree of Master's in Water Resources Engineering

(Specialization in Hydrology and Water Resources Management)

Office of Graduate Studies
Adama Science and Technology University

June 2022

Adama, Ethiopia

APPROVAL PAGE

I, the advisor of the thesis entitled **"Modelling Hydrological Response to Dynamic Land Use Land Cover Changes in Big Akaki Watershed, Ethiopia"** and developed by Bayisa Tulu Areda, hereby certify that the recommendation and suggestions made by the board of examiners are appropriately incorporated into the final version of the thesis.

Dereje Birhanu Mitiku (PhD)	------------------------	----------------------
Major Advisor	Signature	Date

We, the undersigned, members of the Board of Examiners of the thesis by Bayisa Tulu Areda have read and evaluated the thesis entitled **"Modelling Hydrological Response to Dynamic Land Use Land Cover Changes in Big Akaki Watershed, Ethiopia"** and examined the candidate during the open defense. This is, therefore, to certify that the thesis is accepted for partial fulfillment of the requirement of the degree of Master of Science in Water Resources Engineering (Specialization in Hydrology and Water Resources Management).

________________________	________________	________________
Chairperson	Signature	Date
________________________	________________	________________
Internal Examiner	Signature	Date
________________________	________________	________________
External Examiner	Signature	Date

Final approval and acceptance of the thesis is contingent upon the submission of its final copy to the Office of Postgraduate Studies (OPGS) through the Department Graduate Council (DGC) and School Graduate Committee (SGC).

________________________	________________	________________
Department Head	Signature	Date
________________________	________________	________________
School Dean	Signature	Date
________________________	________________	________________
Office of Postgraduate Studies, Dean	Signature	Date

DECLARATION

I hereby declare that this Master Thesis entitled **"Modelling Hydrological Response to Dynamic Land Use Land Cover Changes in Big Akaki Watershed, Ethiopia"** is my original work. That is, it has not been submitted for the award of any academic degree, diploma, or certificate in any other university. All sources of materials that are used for this thesis have been duly acknowledged through citation

Bayisa Tulu Areda ______________________ _______________

Name of student Signature Date

RECOMMENDATION

I, the advisor of this thesis, hereby certify that I have read the revised version of the thesis entitled **“Modelling Hydrological Response to Dynamic Land Use Land Cover Changes in Big Akaki Watershed, Ethiopia”** prepared under my guidance by Bayisa Tulu Areda submitted in partial fulfillment of the requirements for the degree of masters of science in Water Resources Engineering (Specialization in Hydrology and Water Resources Management). Therefore, I recommend the submission of a revised version of the thesis to the department following the applicable procedures.

Dereje Birhanu Mitiku (PhD)	______________________	_______________
Major Advisor	Signature	Date

ACKNOWLEDGEMENT

First of all, I would like to thank the Almighty God for providing me the audacity, wisdom, sustainable strength, and hope to proceed successfully in my academic journey. Next, I wish to express my deepest appreciation for those who helped, assisted and guided me for the successful accomplishment of this research work.

I would like to express my deepest gratitude to my advisor Dereje Birhanu Mitiku (PhD) for giving me a constructive and valuable support, advice, and guidance throughout my research work. His wide and deep knowledge especially on hydrological modeling and software help me to do my research work effectively and efficiently on time. Really, I appreciate his limitless kindness, effort, commitment, support, and assistance for the accomplish of this research work successfully. I am very happy and feel honor to work under his guidance. I also express my heartfelt thanks to Kassa Tadele (Dr.Ing) and Mulugeta Musie (PhD) who thought me Programming and Computational Methods, Hydroinformatics, GIS and RS and Hydrological modelling, respectively. I would also like to extend my appreciation to Achenafi Teklay (PhD) and Mr. Alen Verser (member of SWAT-LUT model developers), who assisted me on how to incorporate dynamic LULC land use update in SWAT model.

I am thankful to Adama Science and Technology University (ASTU) for awarding me the scholarship opportunity to undertake my MSc study in Water Resources Engineering and financing to complete the research work on time. I appreciate the kind collaboration of the National Meteorological Agency of Ethiopia (NMA) and Ministry of Water and Energy (MoWE) Department of Hydrology and Water Quality Directorate during data collection. I have very big respect and thanks for all staff of ASTU Water Resources Engineering Department especially; Mekonnen Ayana (PhD), Mesfin Benti (PhD), Mr. Million Teshome, Mr. Taddesse Tufa, Mr. Mitiku Teshome and Mr. Bekele Kushu for their continuous support and encouragement starting from grass root from undergraduate to my MSc studies.

Last but not least, I would like to extend my deepest gratitude to my family especially Keneni Dumecha (mother), Alem Tulu, Deme Tulu, Taru Tulu, Habtamu Bekele, Yewbnesh Abebe, Bekele Balcha, Tirunesh Birusa and my best friend Abebe Gizaw.

TABLE OF CONTENTS

LIST OF TABLES

LIST OF FIGURES

LIST OF TABLES IN THE APPENDIX

LIST OF FIGURES IN THE APPENDIX

ACRONYMS

AAWSA	Addis Ababa Water and Sewerage Authority
ASTER	Advanced Space borne Thermal Emission and Reflection Radiometer
ARS	Agricultural Research Service
CFSR	Climate Forecast System Reanalysis
CN	Curve Number
DEM	Digital Elevation Model
DMC	Double Mass Curve
DN	Digital Number
ENVI	Environment for Visualizing Images
ERDAS	Earth Resources Data Analysis System
EROS	Earth Resources Observation and Science
ET	Evapotranspiration
ETM+	Enhanced Thematic Mapper Plus
FAHP	Fuzzy Analytical Hierarchy Process
FAO	Food and Agriculture Organization
GCPs	Ground Control Points
GDEM	Global Digital Elevation Model
GIS	Geographic Information System
GLUE	Generalize Likelihood Uncertainty Estimation
GPS	Geographic Positioning System
GWQ	Groundwater Flow
GWR	Groundwater Recharge
HEC-HMS	Hydrologic Engineering Center-Hydrologic Modeling System
HRU	Hydrologic Response Unit
HSG	Hydrologic Soil Group
HWSD	Harmonized World Soil Database
IFOV	Instantaneous-Field-of-View
IR	Infrared
ISO-DATA	Iterative Self-organizing Data Analysis Technique

LULC	Land Use Land Cover
LatQ	Lateral Flow
MCMC	Markov Chain Monte Carlo
MDG	Millennium Development Goal
MIKE SHE	MIKE System Hydrological European
MoWE	Ministry of Water and Energy of Ethiopia
MSS	Multispectral Scanner
MUSLE	Modified Universal Soil Loss Equation
NMA	National Meteorological Agency of Ethiopia
NASA	National Aeronautics and Space Administration
NDBI	Normalized Difference Built-up Index
NDVI	Normalized Difference Vegetation Index
NDWI	Normalized Difference Water Index
NSE	Nash-Sutcliff Efficiency
OLI	Operational Land Imager
ParaSol	Parameter Solution
PBIAS	Percent of Bias
PET	Potential Evapotranspiration
PSO	Particle Swarm Optimization
R^2	Coefficient of determination
RS	Remote Sensing
SCS	Soil Conservation Service
SDG	Sustainable Development Goal
SPOT	Satellite Pour I'Observation de la Terre
SUFI-2	Sequential Uncertainty Fitting version 2
SurfQ	Surface Runoff
SVM	Vector Support Algorithm
SWAT	Soil and Water Assessment Tool
SWAT-CUP	SWAT calibration and uncertainty program
SWAT-LUT	SWAT Land Update Tool
SWAT-LUU	SWAT Land Use Update

SWM	Stanford Watershed Model IV
SYLD	Sediment Yield
TIRS	Thermal Infrared Sensor
TM	Thematic Mapper
USACE	United States Army Corps of Engineers
USGS	United States Geological Survey
UTM	Universal Transverse Mercator
WYLD	Water Yield

ABSTRACT

This study investigates the hydrological responses to dynamic land use land cover (LULC) changes in the big Akaki watershed, upper Awash River basin, Ethiopia. The population growth and socio-economic flux have forced people to clear forests for agriculture and settlement which causes the LULC changes. Thus, these LULC changes have a negative impact on water balance components. Quantifying and assessing the state of hydrological responses to dynamic LULC changes is very important for sustainable water resources development and management. The main objective of this study was to model hydrological response to dynamic LULC changes at basin and sub-basin levels in the study area of the big Akaki watershed. The Soil and Water Assessment Tool (SWAT) model was used to quantify the effects of LULC changes on hydrological responses and sediment yield. The LULC trends and dynamics were assessed using Landsat imagery of 2000, 2010, and 2020 in ERDAS Imagine 2015 with a supervised classification technique of maximum likelihood algorithm. The overall accuracy and kappa coefficient values were 90.50%, 90.00%, and 89.10% and 0.83, 0.82, and 0.81, respectively for the periods of 2000, 2010, and 2020. The classified LULC of the three land-use periods showed that absolute change of built-up, forest land, shrub land, and bare land areas were increased by 3.47%, 0.28%, 0.47%, and 0.06% whereas the agricultural land, grass land, and water body were decreased by 2.65%, 1.43%, and 0.19%, respectively. The SWAT model runs were performed using static and dynamic LULC inputs to assess the impacts of LULC change on hydrological responses and sediment yield between 2000 and 2020. The static model setup used only the 2000 land use map, whereas the dynamic model setup used 2000, 2010, and 2020 land use data. Sensitivities of input parameters including auto-calibration and validation have been performed using the SUFI-2 algorithm in SWAT Calibration Uncertainties Program (SWAT-CUP). The two model performance was found to be satisfactory to predict the spatio-temporal water balance components with R^2 of 0.8 (0.82), NSE of 0.73 (0.61), and P_{Bias} of 21.4 (37.7), respectively for streamflow and R^2 of 0.84 (0.68), NSE of 0.81 (0.54) and P_{Bias} of 17.1 (39.1), respectively for sediment yield. Due to the expansion of built-up and reduction of agricultural land and grassland, the basin level average annual surface runoff (SurfQ), water Yield (WYLD), and sediment yield (SYLD) were increased by 2.51mm, 0.67mm, and 10.83t/ha, respectively whereas lateral flow (LatQ), groundwater flow (GWQ), groundwater recharge (GWR) and evapotranspiration (ET) were decreased by 1.18mm, 0.63mm, 0.56mm and 2.9mm, respectively. However, at the sub-basin level, the rapid expansion of built-up resulted in an increase of SurfQ and WYLD by 10.15mm and 8.78mm in sub-basin 13, respectively. Whereas the GWQ, ET, and SYLD were decreased by 2.58mm, 32.34mm, and 4.74t/ha in sub-basins 5, 9 and 6, respectively. The outcome of this study work revealed that incorporating the dynamic LULC approach into the SWAT model simulation gives a better representation of spatio-temporal variability of LULC changes. Thereby improving the accuracy of spatio-temporal estimation of water balance components by integrating better LULC evolution than the static LULC model approach.

Key Words: Dynamic LULC, Static LULC, SWAT Model, Hydrological Responses, Big Akaki Watershed

1. INTRODUCTION

1.1. Background

Land use refers to how humans and their habitats utilized the land where as land cover refers to the physical condition of the earth's surface, captured in the distribution of vegetation, water, soil, and other physical features of the land which includes man-made activities (Rawat & Kumar, 2015).

Land use land cover (LULC) change is a crucial issue that incorporates global dynamics and their response to hydrologic characteristics of soil and water management in a catchment (Welde & Gebremariam, 2017). The LULC's impact on hydrological processes such as runoff, evapotranspiration, infiltration, etc. are the integrated indicators of the water conditions (Shawul et al., 2019). LULC changes from natural vegetation to other LULC can result in a shortage of water, degraded watersheds tend to accelerate the overland flow which reduces the soil moisture and groundwater recharge and soil erosion, flood risk and thus contributes to the deterioration of living conditions (Munoth & Goyal, 2020; Shawul et al., 2019). This is due to natural and man-induced factors on global land cover change, especially in terms of change from forest cover to other land covers, has been one of the important issues in global change research (Assfaw, 2020). So understanding the impacts of LULC changes on water resources is an important research issue for watershed management (Munoth & Goyal, 2020).

Like many other developing countries across the globe, significant land-cover changes have been observed in Ethiopia due to anthropogenic activities, because rapid population growth and socio-economic flux has forced people to clear forest for cultivation and forest products and settlements (Gebresamuel et al., 2010; Shawul & Chakma, 2019). The Ethiopian highlands have experienced intense levels of land use dynamics and forest cover transformations over the past few decades. Multiple socio-economic, demographic, bio-physical, and policy and institutional factors have driven such transformations (Deribew & Dalacho, 2019). The research done on the upper Awash River basin depicted that a continuous increment in the spatial extent of cropland and urban areas were observed between the periods 1974 to 2014. The urban area was found to increase by 606.20% from the year 1972 to 2014 and cropland has also increased by 47.30% and it is expected to increase due to the higher population growth rate and socio-economic development in the region (Shawul & Chakma, 2019). Due to these changes, a 9.06% increase in depth of surface runoff, a 16.30% decrease in lateral flow, 0.98% reduction in Evapotranspiration, and a 0.10% decrease in Groundwater recharge (Shawul et al., 2019)

The upper Awash River basin is one of the most highly populated, irrigated, and urbanized parts of Ethiopia where densely populated cities such as Addis Ababa and Adama exist. In recent years, sizeable rural-urban migration and rapid growth in population for the search of a job due to much concentration of economic development in this area is observed (Shawul & Chakma, 2019). Uncontrolled urban growth and haphazard land developments are one of the crucial problems in Addis Ababa and the surrounding Oromia special zone causing environmental degradation and rural-urban land base conflicts. This is mostly because of the rapidly increasing built-up area that conquered large tracts of natural green spaces and prime agricultural lands (Mohamed & Worku, 2019). To improve this problem, reliable information on the water balance components currently and their future changes is a prerequisite for sustainable water management. Mainly, these components are under the strong influence of land-use dynamics (Kumar et al., 2017).

Comprehensive and improved procedures that integrate different techniques such as hydrologic modeling, remote sensing, and statistical approaches are required to identify the influence of LULC change on the hydrologic variability of a river basin (Shawul et al., 2019). Many hydrologic models have been developed over time to allow for a better understanding of the hydrologic and erosion processes which occur in agricultural watersheds (Biru & Kumar, 2018). These models are often categorized into three types namely empirical, conceptual, and physically-based (Merritt et al., 2003). The hydrological responses to LULC change can be assessed by using various hydrologic models, such as SWAT(Abraham & Nadew, 2018; Shawul et al., 2019; Welde & Gebremariam, 2017), HEC-HMS (Aliye et al., 2020; Ben Khélifa & Mosbahi, 2021), and MIKE SHE (Aredo et al., 2021).

Through comparison of hydrological models for assessing the effect of different land management practices, distributed hydrological models are efficient tools as they could account for spatial heterogeneity and consequently, they have higher accuracy for predicting the effect of LULC on hydrological processes (Aghsaei et al., 2020). Soil and Water Assessment Tool (SWAT) is by far the most widely used physical hydrological model all over the world to evaluate the effect of LULC on watershed hydrological processes. For example, SWAT was used in the Tennesse River watershed to assess the long-term hydrological impact of land use/ land cover change (Zhu and Li, 2014). Yan et al. (2013) also evaluate the impact of land-use changes on stream flow and sediment yield at a basin-scale using the SWAT model. A research done by Biru and Kumar (2017) on Modjo watershed in Ethiopia indicated that SWAT performed well with $R^2 = 0.75$, NSE = 0.76 and PBIAS = 10.90 during calibration and for validation $R^2 = 0.71$, NSE = 0.70 and PBIAS = 9.50 for stream flow. Similarly, Shawul et al. (2019) showed that SWAT hydrological model performed well in the upper Awash River basin at Hombole, Melka Kuntre, Modjo, Akaki and Teji sub-basins.

However, most of the hydrological model applications used the static LULC data to assess the effects of LULC change on hydrological processes (Aghsaei et al., 2020; Teklay et al., 2019). Correct parameterization is an important process in model calibration and must be based on the knowledge of the hydrologic processes and variability in soil, land use, slope, and location. The LULC affects many hydrological processes such as evapotranspiration, surface runoff, infiltration, and soil erosion. Hence, it is advisable to use dynamic LULC to minimize the problem of over parameterization during model calibration due to utilizing a static land use over the simulation period to fit the predicted data to measured data that naturally includes the changes in land use over time. The static land use approach in SWAT modeling applications does not adequately estimate the spatio-temporal hydrological variations (Wagner et al., 2016). The use of dynamic LULC data may improve the accuracy of spatio-temporal model simulation by integrating better LULC evolution.

The big-Akaki watershed is one of the major tributaries of the upper Awash basin, which includes most of the city of Addis Ababa which is the capital city of Ethiopia. The city has grown very rapidly since its founding and the rapid transformation of land from rural to the urban area has occurred more than anywhere else in Ethiopia. There was a serious transformation of rural land to urban development such as buildings, transport networks, shopping centers, and various types of industries, parks, and recreational areas during the last ten decades. Thus the objective of this study is to assess the hydrological response to dynamic LULC change using SWAT hydrological model in the big Akaki watershed

1.2. Statement of the Problem

The LULC change is one of the main global environmental problems for humanity (Teklay et al., 2019). The rapid LULC change and climate variability potentially lead to an increase in hydrologic impact (Shawul et al., 2019). The LULC change has a significant impact on the surface runoff, groundwater recharge, base flow, sedimentation, and extreme events (Teklay et al., 2019, Aghsaei et al., 2020)

Land and water resource degradation are the major problems in the Ethiopian highlands. Poor land-use practices and improper management systems have played a significant role in causing a flood, high soil erosion rates, sediment transport, and loss of agricultural nutrients (Andualem & Gebremariam, 2015). More than 90% of the Ethiopian uplands were formerly forested. Today, the percentage of forest cover decreases considerably because of the invasion of humans. This is due to large-scale deforestation that has led to severe soil erosion and increased soil degradation throughout the country in general and in the uplands in particular. Soil erosion and sediment production include the processes of detachment, transport, and deposition of sediments by the impact of rain and running water (Zeberie, 2020).

Akaki watershed is a place where densely populated, a large number of industries and irrigation practices are active (Tolera and Chung, 2021). Addis Ababa consists of about 23% of the total urban population in Ethiopia. The city’s population had approached approximately 3,774,000 (CSA, 2021). To accommodate the increasing population, industrial concentration, and commercial expansion, Addis Ababa city has been expanding horizontally towards its peri-urban areas. The rapid growth of Addis Ababa city in the Akaki watershed causes unexpected flooding and sedimentation problems on reservoirs during the wet season and water scarcity during the dry season. This is due to the watershed has been experienced huge LULC changes such as the construction of industrial parks, real estate, condominiums, and infrastructures at the expense of cropland and other natural vegetation. This LULC conversion from other land cover types to urban land causes an increment of surface runoff that lead to extreme flood in the watershed that damage human life and properties and affects the groundwater recharge as well. Therefore properly assessing the impact of LULC change on hydrological responses of the catchment using a physical hydrological model is curial in order to quantify and suggest appropriate mitigation measures for watershed conservation and management. Hence accurate assessment of the impact of dynamic land use approach is particularly very important to represent the change in a more realistic manner using land use update module and hydrological model.

1.3. Objective of the Study

1.3.1. General objective

The overall objective of this study was to assess the impact of dynamic LULC change on hydrological responses of the big Akaki watershed using SWAT hydrological model.

1.3.2. Specific objectives

The following three specific objectives were formulated to achieve the general objective of the study.

- To assess the spatio-temporal LULC change of the big Akaki watershed for a period of two decades (2000 - 2020).
- To evaluate the SWAT hydrological model performance in simulating the long-term water balance components in the big Akaki watershed.
- To quantify the hydrological and sediment yield responses of the big Akaki watershed to dynamic LULC change using SWAT hydrological model.

1.4. Research Questions

The three research questions were formulated as follows to achieve the specific objectives of this study.

- How the spatio-temporal variations of LULC change in the big Akaki watershed look like?
- How well does the SWAT hydrological model simulate the hydrological processes in the big Akaki watershed?
- How does the hydrology of the big Akaki watershed respond under dynamic LULC change during the study period?

1.5. Significance of the Study

It is essential to have an understanding of the impact of historic LULC changes on the watershed hydrological system, to predict the potential future impact of LULC change on water balance components on river flow. Moreover, detecting and simulating the effects of LULC change and management on hydrological processes requires a new and improved procedure to instrument watersheds based on the hydrological sensitivity due to LULC changes at sub-watershed levels (Tadele and Förch, 2007). LULC change can also have a significant impact on catchment hydrology, and these impacts can be strongly interrelated (Kibria et al., 2016).

Big Akaki watershed is exposed to extreme LULC dynamics due to rapid population growth, socio-economic development, expansion of urbanization, and infrastructures. The LULC changes in the study area have caused extreme flooding during the rainy season and water scarcity during the dry season. These treat the agricultural productivity, water pollution, and water allocation problems in the area. Thus, this study will play a big role in supporting the local governments and policy makers by providing crucial information about the influence of the LULC change on the hydrological process of the watershed which assists to take appropriate measures and implement an effective strategy to mitigate the undesirable impact of LULC changes.

1.6. Scope and Limitation of the Study

In this study, it is planned to evaluate the impact of dynamic LULC change on the hydrological responses using the hydrological model in the big Akaki watershed which has a drainage area of 833.2 Km^2. The study used a hydrological model by evaluating the performance of SWAT hydrological model. This study was achieved through the combined use of GIS and RS techniques to investigate and analyze LULC and hydrological model (SWAT) to predict the hydrological processes**.** It includes the Landsat image processing in ERDAS imagine 2015 for LULC classification through supervised classification technique of maximum likelihood algorithm for a period of 2000, 2010, and 2020. The accuracy assessment was conducted for the classified LULC map using an error matrix. The R-program (Climatol package), double mass curve, and rainbow software were used to fill the missed climate data, to check the consistency and homogeneity of climate data, respectively. The LULC, soil, and slope were used in this study by dividing the watershed into sub-watersheds and further divided into the HRUs to identify the critical sub-watersheds in terms of hydrological processes and sediment yield. This was achieved through SWAT hydrological model. The dynamic land use update for the dynamic SWAT model setup is integrated using the SWAT-LUT tool. However, the study doesn't include the best management practice to minimize the negative impact of dynamic LULC change on hydrological processes. Furthermore, the study doesn't investigate the future LULC change impacts on hydrological responses.

1.7. Thesis Organization

This thesis study is organized into five chapters. The first chapter is the introduction which consists of the background, statement of the problem, objective of the study, research questions, significance of the study, scope, and limitation of the study. The second chapter is the literature review which describes the concept of LULC and its changes. It also discussed the driving factor that causes LULC changes, the application of RS and GIS in LULC data acquisition, and change detection. The status of LULC change on a global and Ethiopia scale were assessed in this chapter. The impact of LULC changes on hydrological responses and sediment yields, the description of different hydrological models, and its classification and selection criteria are also discussed well in chapter two. The SWAT hydrological model concept and its application in the different watersheds were reviewed in detail. The materials and methods are incorporated in chapter three. The description of the study area, its climate characteristics, topography, soil, and LULC condition were highlighted. Materials and software tools, input data sources and data analysis, and the step-by-step methodologies applied to address the objective of the study. Chapter four describes the result and discussion of the study that addresses the objective of the research described in chapter one. Finally, chapter five provides conclusions and recommendations.

2. LITERATURE REVIEW

2.1. Land Use Land Cover Change

According to FAO definition, Land is a delineable area of earth's terrestrial surface, encompassing all attributes of the biosphere immediately above or below this surface, including near-surface climate, the soil and terrain forms, the surface hydrology (Lakes, Rivers, Marshes, and Swamps), the near-surface sedimentary layers and associated groundwater reserve, the plant and animal populations, the human settlement patterns and physical results of past and present human activities (terracing, water storage or drainage structure, roads, buildings, etc.) (FAO, 2002).

Land use and Land Cover are two different terminologies (Rawat and Kumar, 2015). Land cover can be defined as the biophysical state of the earth's surface and immediate subsurface that includes the type of vegetation that covers the land surface, soils, biodiversity, surfaces, groundwater, and human structures such as buildings and pavements, whereas Land Use refers to the manner in which the biophysical attributes of the land are utilized and the intent underlying that utilization and the purpose for which land is used. (Kassa, 2009; Rawat and Kumar, 2015; Turner et al., 1995). Meyer and Turner, (1994) also explain the difference between Land Use and Land Cover. They indicated that Land Cover represents the physical, chemical or biological categorization of the terrestrial surface. For example grassland, forest, building or pavement; whereas Land Use denotes the functions or purposes associated with the land cover. For example: living in a building, raising cattle on grassland, and recreational activities in a forest area.

LULC change is a change in the aerial extent of land use or land cover type. It is a shift in an extent and management constitutes land use and land cover. LULC change can be categorized into LULC conversion and LULC modification. LULC conversion is the change of one land cover or land use type to another. For instance: the expansion of urban and cultivated land at the expense of forests due to deforestation. On the other hand, LULC modification indicates the maintenance of land cover or land use type in the face of change in its attributes. Modification involves the alterations of structure, function without a whole change from one land use or land cover type to another (Kassa, 2009; Lambin et al., 2003).

The study of LULC change requires a comprehensive understanding and monitoring of all the factors which cause it (Rahman et al., 2012). LULC change is occurred due to natural and socio-economic factors and their utilization by the human in time and space (Rawat and Kumar, 2015; Tewabe and Fentahun, 2020). Human activities such as agricultural expansion, burning activities or fuel wood consumption, deforestation, urbanization and construction works are responsible for LULC change (Munoth & Goyal, 2020; Welde and Gebremariam, 2017). This is due to population growth, economic growth and physical factors such as topography, slope, soil type, and climate variability (Lambin et al., 2003).

The changes in LULC have been reported since 1700 as a human being induced changes. Agricultural land and settlement has expanded at the expense of forest land, grassland, and stepper in all parts of the world due to population growth to meet the demand for food and shelter (Lambin et al., 2003). They revealed that these changes reduced the global forest land coverage by 16.10 million ha/yr during the 1990s, which is around 4.20% of forest loss yearly. According to Richard (1990), the agricultural land is estimated to have increased by 466.00% from 1700 to 1980 across the world. Some parts of the world such as Russia, South Asia, Latin America and North America experienced a faster expansion of agricultural land than other parts of the world.

Worldwide research has been conducted by many researchers to assess the LULC change evolution (Abdulkareem et al., 2018; Barakat et al., 2019). In many regions of the world, still continue to have experienced huge LULC change (Zhang et al., 2020). Urban population growth and urban sprawl accelerated LULC changes and land transformation. Land transformation process cannot be stopped but it can be regulated. Rahman et al. (2012) revealed that the agricultural land decreased by 27.35% from 92.06% in 1972 to 64.71% in 2003. Whereas the built-up area was 3.00% in 1972 which expanded to 28.00% in 2003 due to natural increase of the population and the migration of rural population in seeking for better living in the north-west district of Delhi, India. The forest land coverage declined to 119.09ha in 2003 from 173.45ha of total area in 1972. The major LULC change was recorded from agricultural land to urban in the south district of the study area (Rahman et al., 2012).

Barakat et al. (2019) assessed the LULC change and its environmental impact in Ben-Mellal district, Morocco using remote sensing, geographical information system, and fuzzy analytical hierarchy process (FAHP) from 2002 to 2016. The supervised classification method by the vector support algorithm (SVM) was applied to each image using the ENVI 5.3 software and the image of 2002 and 2016 have been classified into five classes namely: arboriculture, arable fields, forest, bare soil and built up. The analysis of the changes in the study area showed that the arboriculture has been decreased from 32.73 Km^2 to 19.43 Km^2, which was a 13.30% decrement. The arable land, built ups and barren land showed that an increment, whereas the forest has been decreased during the period between 2002 and 2016 due to human activities such as overgrazing and overexploitation of wood resources (Barakat et al., 2019).

Research conducted to examine the impact of LULC in the Midwestern United States using the HEC-HMS model resulted that the dominant LULC was agriculture (60.06% in 2001 and 57.95% in 2011 which was 3.51% decrement). The developed land was the second dominant LULC category with 25.80% in 2001 and 28.66% in 2011 with 11.21% increment. The forest and water bodies also the other categories of LULC in the watershed with no change shown between the period 2001 and 2011 (Hu and Shrestha, 2020). Rawat and Kumar (2015) have used the Landsat thematic mapper (TM) of 1990 and 2010 and processed the images in ERDAS Imagine and used indices such as normalized difference vegetation index (NDVI), normalized difference water index (NDWI) and normalized difference built-up index (NDBI). Using the maximum likelihood algorithm of supervised classification methods the LULC of the study area classified as vegetation, agriculture, barren land, built up and water bodies. They revealed that in 1990, the land cover were 54.75% of vegetation, 31.69% of agriculture, 11.65% of barren land, 1.01% of built up and 0.90% of water bodies. Whereas in 2010, 58.26% of vegetation, 30.17% of agriculture, 6.19% of barren land, 4.56% of built up and 0.82% of water bodies. From 1990 to 2010, the vegetation and built up has increased by 3.51% and 3.55%, respectively, whereas agriculture, barren land and water body has decreased by 1.52%, 5.46% and 0.08%, respectively.

The LULC dynamics in the Anzali wetland catchment in the Gilan region of Iran showed that six LULC classes were extracted using ERDAS Imagine and Arc GIS software and classified as forest, agriculture, grassland, wetland, water body and urban areas (Aghsaei et al., 2020) and compared the LULC of 1990, 2000 and 2013. They proved that the most LULC changes occurred in the agriculture and forest LULC classes. From 1990 to 2013, agricultural land increased by 7.00% at the expense of forest coverage, whereas forest, grassland and wetland showed a decline by 6.80%, 1.00% and 0.70%, respectively. Urban area was increased by 100.00% in 2013 compared to the year of 1990.

The LULC changes are at an alarming rate in East Africa due to the region is highly dependent on rain-fed agriculture. The land resource holding in the region has been decline in the size per household, so to meet the demand for the land resources holding, the forest has been cleared to human settlement, urban centers, agriculture, and grazing land (Guzha et al., 2018). The forest has decreased at a rate of 1.00% annually as the population increased at a rate of 2.00% in the region from 1990 to 2015.

2.2. Land Use and Land Cover Change in Ethiopia

Conversion of natural vegetation to agricultural land and settlement land due to population growth and socio-economic development has been one of the major issues today. Expansion and intensification of agricultural land, built-up area and deforestation accelerate to satisfy the (Andualem and Gebremariam, 2015) needs of ever growing population (DeFries and Eshleman, 2004). LULC change highly pronounced in developing countries like Ethiopia, that their economies are dominantly based on agriculture and an emerging and unstoppable horizontal urban expansion and rapidly increasing population.

Land and water resources degradation are one of the important issues in Ethiopian highlands (Andualem and Gebremariam, 2015) due to population growth, socio-economic development and land tenure insecurity due to institutional and policy reforms that lead to poor land use practices and improper management system. The continuous change in LULC has influenced the hydrology and water resources of a given watershed by altering the quantity and pattern of hydrological components such as surface runoff, groundwater flow, evapotranspiration, total sediment yield and nutrient concentration (Aghsaei et al., 2020; Andualem and Gebremariam, 2015).

Several previous studies have quantified the LULC change through the remote sensing and GIS techniques in different parts of Ethiopian River catchments. According to FAO, the forest land in Ethiopia has decreased from 13.30% (14.69 million ha) in 1993 to 11.40% (12.54 million ha) in

2016 with an estimated annual rate of change 0.80% (104,600 ha·year-1), whereas the agricultural
land has increased from 27.66% (30.54 million ha) in 1993 to 32.83% of (36.26 million ha) in 2016. Andualem and Gebremariam (2015) has classified the LULC of Gilgel Abay watershed in the Lake Tana sub-basin as agricultural land, water, grassland, shrub land and forest land classes for the 1986, 2000 and 2011. They showed that the agricultural land dominated at the middle portion of the watershed, grassland at north and northwestern, shrub land at northeastern and southeastern portions of the watershed. The agricultural land increased by 24.12% from 1986 to 2000, whereas forest land, grassland and shrub land showed a significant decrease. Generally the agricultural land increased at the rate of 33.79% from 1986 to 2011, whereas forest land, shrub land, grassland and water body were decreased at 1.40%, 7.41%, 24.45% and 0.55%, respectively. The change in LULC observed in the study area was due to rapid population growth by 2.30% and socio-economic, political, ecological and cultural significance (Andualem and Gebremariam, 2015).

Similarly, the study conducted in northwest Ethiopia in Lake Tana Basin showed that the LULC change has been assessed using remote sensing and come up with the study area categorized into six LULC classes namely: water body, bush land, grassland, forest land, agricultural land and residential land classes. The result indicated that the agricultural land constituted the largest proportion while bush land was the second dominant LULC. The forest land, bush land and grassland had decreased while agricultural land and settlement areas had increased due to the population growth and high demand for agricultural activities. Agricultural land and settlement areas were increased by 13.00% and 9.10%, respectively while forest land, bush land and grassland were decreased by 2.30%, 9.80% and 10.00%, respectively (Tewabe and Fentahun, 2020). Birhanu et al. (2019) suggested that the LULC class of Gumara catchment were dominated by agricultural land, grassland and forest land. Agricultural land increased from 70.00% to 82.00% between 1986 and 2015 while forest land, grassland were decreased from 11.00% to 5.00% and 18.00% to 10.00%, respectively. They conclude that the largest conversion was recorded from grassland to agriculture and from forest to agriculture. Another research done at the Megech dam watershed in northwest Ethiopia depicted that bare land, agricultural land, grassland, shrubland, urban and forest land were the dominant LULC classes in the area. The agricultural land increased by 6.48%, while forest land reduced by 0.94% from 1998 to 2016 due to the expansion of agricultural land which was caused by human population growth. The grassland and bare land were also reduced due to the urban and agricultural land expansion (Assfaw, 2020).

On the other hand, Gebresemuel et al. (2010) analyzed the LULC change in the period from 1964 to 2006 in the highland of Tigray in two catchments using remote sensing and GIS techniques and come up with a conclusion that there were agricultural land, grassland, and plantation and area ex-closure. They concluded that agricultural land accounted for the largest land use and accounted for 77.00%, 70.00% and 80.00% of total land use in 1964, 1994 and 2006, respectively at Gum Selassa catchment, whereas at Maileba catchment, the agricultural land accounted for 76.00, 72.00 and 62.00%, respectively. The agricultural land slightly increased at Gum Selassa, whereas decreased at Maileba catchment due to the plantation areas and area ex-closures were under the protection of the Government. The forest land and woodland suffered more changes and losing their entire cover due to the deforestation for the purpose of fuel, construction and as a source of income. The significant changes were observed on shrubland, open grassland and agricultural land at Gum Selassa than at Maileba. Shrubland declined from 9.30% in 1964 to 1.50% in 2006 in Gum Selassa, whereas in Maileba the shrubland increased from 33.20ha to 49.20ha from 1964 to 2006. Similarly, Welde and Gebremariam (2017) conducted an assessment of the effects of LULC dynamics at Tekeze dam watershed in Tigray and come up with a result of dominant LULC were agricultural land, bare land, and shrub land in both 1986 and 2008 land use references which accounts for 91.00% of total area.

Shawul and Chakma (2019) carried out LULC change detection analysis and came up with a conclusion that there were a significant expansion of cropland and urban area while decreasing trends in forest land, shrubland and pasture land coverage in upper Awash basin. From 1972 to 2014, urban area was increased by 606.20% and the cropland also increased by 47.30% whereas, the forest land, pasture, shrubland and water body were decreased by 25.10%, 87.40%, 28.80% and 21%, respectively. From the four sub basins in upper Awash basin, Akaki sub basin which is the more urbanized area showed a linearly increasing urbanization trend during the study period with more than 8.07 times the area of 1972 in 2014. Another study in Awash River basin over 30 years study period (1988 to 2018) revealed that six land use classes were identified as cropland, shrubland, built-up, forest land, wetland and water body. According to the researchers, Awash River basin is dominated by shrubland and followed by cropland over the study period. At sub basin level, upper Awash basin is dominated by cropland whereas, in the middle and lower Awash basin, the dominant land classification was shrubland followed by cropland (Tadese et al., 2020). Keleta watershed in the Awash River basin exhibited that farmland and Settlement areas were the dominant land use. The farmland and settlement area expanded from 49.70% in 1985 to 67.50% in 2011, whereas grassland cover was significantly declined from 29.60% to 19.00% from the period 1985 to 2011 (Bekele et al., 2019). They concluded that the major land use transitions were from grassland to farmland and settlement.

Recently, Aragaw et al. (2021) showed that agroforestry, cultivated area, evergreen-forest and grassland cover a significant portion of the watershed during the study period from 1988 to 2018 on Gidabo River basin. In contrast to other similar studies, they depicted that from the year of 2000, the areal extent of agroforestry and shrubland started to increase from 42.86% and 1.11% to 46.86% and 1.90%, respectively, while the evergreen-forest and grassland cover decreased significantly from 2000 to 2018.

The LULC changes and socio-economic dynamics have a strong relationship because as the population increases, the demand for agricultural land, grassland, fuel wood, and settlement areas also increases to meet the growing demand for food and energy, and livestock population. Population pressure, lack of awareness and improper management are the major causes for the deforestation and degradation of natural resources in Ethiopia (Bekele et al., 2019; Gashaw et al., 2018; Kassa, 2009).

2.3. Application of RS and GIS for Land Use Land Cover Analysis

Change detection analysis is a key for development planning and management activities and considered as an essential aspect for modeling the earth system. It is important for monitoring change in LULC on multi-temporal satellite images by mapping LULC. Remote Sensing (RS) and Geographic Information System (GIS) are the technologies widely used for detecting and analyzing spatio-temporal changes of LULC (Tadele and Förch, 2007). The advances in GIS and RS instruments and techniques enable the researchers, policy makers and managers to effectively model the change observed in LULC dynamics (Halefom et al., 2018). Mapping of land use changes using RS techniques provides a quantitative description of land transformation that can help to identify the rates, extents, and patterns of land-use dynamics (Tadese et al., 2020).

Remote sensing (RS) is the science, technology and art of obtaining information about an earth's surface, atmosphere, object, area or phenomenon through the analysis of data acquired by a device that is not in contact with the earth surface, object or area under investigation using sensors onboard air-borne such as aircraft and balloons or space-borne sensors such as satellites and space shuttle platforms (Chipman et al., 2015; Weng, 2010). RS and GIS are valuable data source from which LULC change information can be extracted efficiently and used to generate, map and manage LULC change. They are widely used in the detection of LULC dynamics (Abdulkareem et al., 2018; Barakat et al., 2019; Rahman et al., 2012). GIS is the most commonly used tool to explore and derive information derived from the remote sensing images and used to detect the LULC change. GIS provides a platform for collecting, storing, analyzing and displaying digital data necessary for LULC change detection. GIS links spatial data with geographical information about a particular feature on a map. This information is stored as attributes of a graphically represented feature. GIS uses these attributes to compute new information about map features (Khan, 1998).

Digital RS images can be input into a GIS for use; analog data also can be used in GIS through analog-to-digital conversion. RS data are interpreted and analyzed through various methods of information extraction to provide data layers for the GIS (Jensen, 2015). Jensen (2015) categorized four basic resolution characteristics to understand RS images. Namely:

Spatial resolution**:** is a measure of the smallest angular or linear separation between two objects that can be resolved by the RS system. It is the minimum distance between two objects. Many satellite RS systems use optics that has constant instantaneous-field-of-view (IFOV) which the spatial resolution is defined as the ground-projected IFOV in meters or feet. Pixels are normally represented on computer or hardcopy images as rectangles with length and width (e.g. 10X10m or 30X30m resolution) (Jensen, 2015). The relationship between the geographic scale of the study area and the spatial resolution of RS image has been explored (Weng, 2010).

Temporal resolution**:** is refers to how often and when the sensor records imagery of a particular area of the earth's surface. It is the amount of time it takes for the sensor to return to a previously imaged location. The temporal resolution also has an important role in LULC change detection. The changes over time such as vegetation, and forest deforestation (Weng, 2010).

Radiometric resolution**:** is the sensitivity of a RS to detect or to a difference in signal strength as it records the radiant flux reflected, emitted or back-scattered from the terrain. It measures how much change in radiance there must be on the sensor before a change in recorded brightness value takes place (Jensen, 2015; Weng, 2010). Jensen (2015) showed that radiometric resolution can have a significant impact on the ability to measure the properties of scene objects. The Landsat 1 multispectral Scanner (MSS) recorded reflected energy with a precision of 6 bits (values ranges from 0 to 63) whereas Landsat 4 and 5 Thematic Mapper Sensor (TM) recorded data with a precision of 8 bits (values ranges from 0 to 255). The Landsat TM sensors had improved radiometric resolution compared to the Landsat MSS. High radiometric resolution increases the probability that phenomena will be more accurately the RS image.

Spectral resolution**:** is refers to the number and dimension (size) of wavelength intervals (bands or channels) in the electromagnetic spectrum to which a remote sensing instrument is sensitive. The Landsat TM sensor collects seven spectral bands including; Blue (0.45-0.52µm), Green (0.52-0.60 µm), Red (0.63-0.69 µm), Near-IR (0.76-0.90 µm), Short IR (1.55-1.75 µm), Thermal IR (10.4-12.5 µm) and Short IR (2.08-2.35 µm).

Images with various levels of detail have been available since the 1960s with low resolution and oblique angles. But since the advent of the Landsat satellite program in the 1970s and the SPOT satellite program in the 1980s near-vertical multispectral and panchromatic images with higher resolutions useful for earth resources mapping have been available. Satellite images with 1 m or below 1m resolutions have become available after the launch IKONOS satellite in 1999 which was the first commercially developed satellite (Chipman et al., 2015).

The Landsat program is the United States' oldest land-surface observation satellite system, having obtained data since 1972. The ERTS-1 satellite, launched on July 23, 1972, was the first experimental system designed to test the feasibility of collecting Earth resource data by unmanned satellites. Prior to the launch of ERTS-B on January 22, 1975, NASA renamed the

ERTS program Landsat, distinguishing it from the Seasat oceanographic RADAR satellite launched on June 26, 1978 (Jensen, 2015). The Landsat satellites have provided space-based images of the earth's land surface, which serve as valuable resources for LULC change research. The primary sensor onboard Landsat 1, 2, and 3 was the Multispectral Scanner (MSS), with a resolution of 79 meters in four spectral bands ranging from the visible green to the near-infrared (IR) wavelengths. Landsat 4 and Landsat 5 also carried the MSS, along with the Thematic Mapper (TM) sensor. The TM sensor included an improved spatial resolution of 30 meters for the visible, near-IR, and SWIR bands; and the addition of a 120-meter thermal IR band. Landsat 7 carries the Enhanced Thematic Mapper Plus (ETM+), with 30-meter visible, near-IR, and SWIR bands; a 60-meter thermal band; and a 15-meter panchromatic band. Landsat 8, launched as the Landsat data continuity mission on February 11, 2013, contains the push-broom Operational Land Imager (OLI) and the Thermal Infrared Sensor (TIRS). OLI collects data with a spatial resolution of 30 meters in the visible, near-IR, and SWIR wavelength regions, and a 15-meter panchromatic band. OLI also contains a deep blue band for coastal-aerosol studies and a band for cirrus cloud detection (USGS, 2016).

Table 2.1 Landsat mission dates (USGS, 2016)

Satellite	**Launch**	**Decommissioned**	**Sensors**
Landsat 1	July 23, 1972	January 6, 1978	MSS/RBV
Landsat 2	January 22, 1975	July 27, 1983	MSS/RBV
Landsat 3	March 5, 1978	September 7, 1983	MSS/RBV
Landsat 4	July 16, 1982	June 15, 2001	MSS/TM
Landsat 5	March 1, 1984	2013	MSS/TM
Landsat 6	October 5, 1993	Did not achieve orbit	ETM
Landsat 7	April 15, 1999	Operational	ETM+
Landsat 8	February 11, 2013	Operational	OLI/TIRS

To extract LULC information from digital remote sensor data, it is important to classify the RS images using several digital image processing software such as ERDAS Imagine, ENVI, and PCI Geomatica. Image classification uses spectral information represented by digital numbers in one or more spectral bands and attempts to classify each pixel based on the spectral information. The objective is to assign all pixels in the image to particular classes or themes (e.g., water, forest, residential, commercial, etc.) and to generate a thematic "map." There are various approaches for image classification. Pal and Pal (1993) categorized the image classification techniques into three general groups as shown in figure 2.1 below.

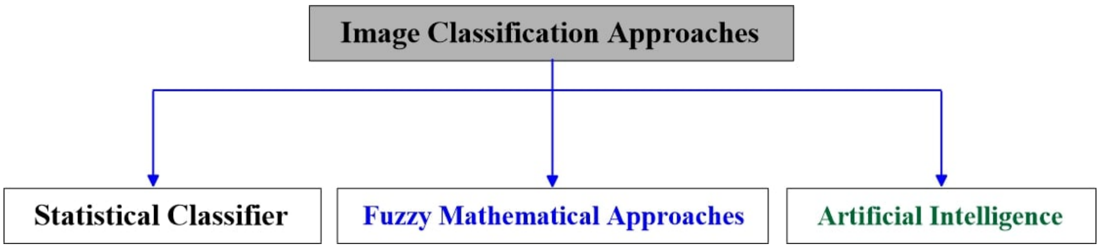

Figure 2. 1 Major approaches to image classification

Generally, there are two statistical approaches to image classification: supervised and unsupervised classification approaches (Al-Fares, 2013; Liu and Mason, 2009).

Supervised classification**:** is one type of classification approach in which the image analyst "supervises" the pixel categorization process by specifying to the computer algorithm, numerical descriptors of the various land cover types present in a scene. Representative sample sites of known cover types, called training areas are used to compile a numerical "interpretation key" that describes the spectral attributes for each feature type of interest. Each pixel in the data set is then compared numerically to each category in the interpretation key and labeled with the name of the category it "looks most like."(Chipman et al., 2015). The three basic stages of the supervised classification procedure are the training stage, classification stage, and Output stage. The types of algorithms applied in supervised classification are minimum-distance-to-means, parallelepiped, and maximum likelihood classifiers (Jensen, 2015; Tso and Mather, 2009; Weng, 2010).

Unsupervised classification**:** is also referred to as clustering which is an effective method of RS image data processing in multispectral feature space and extracting land-cover information (Exelis ENVI, 2013). It is the process whereby numerical operations are performed that search for natural groupings of the spectral properties of pixels, as examined in multispectral feature space. Unsupervised classification requires only a minimal amount of initial input from the analyst. The clustering does not require training data (Jensen, 2015). Spectral classes are first grouped based solely on digital numbers in the imagery, which then are matched by the analyst to information classes. The user specifies sonly the number of clusters to be generated, and the classifier automatically constructs the clusters by minimizing some predefined error function. The classes that result from unsupervised classification are spectral classes. Because of they are based solely on the natural groupings in the image values, the identity of the spectral classes will not be initially known. The analyst must compare the classified data with some form of reference data (such as larger-scale imagery or maps) to determine the identity and informational value of the spectral classes (Chipman et al., 2015). The algorithms employed in unsupervised classification are K-means clustering and Iterative Self-organizing Data Analysis Technique (ISO-DATA).

At the end of the process of producing LULC classification from RS image, errors in area estimates may occur in the distribution of pixels of the various remotely acquired on the ground features due to the spatial resolution of the satellite image used. The error may occur due to observation and recoding errors, miss-location of test data sites, differences caused by changes in land cover between the time of observation and the date of imaging (Tso and Mather, 2009). Therefore assessment of LULC classification accuracy is essential to measure classification performance. Accuracy assessment means the level of agreement between labels assigned by the classifier and class allocations based on ground data collected by the user, known as test data. The widely used LULC classification accuracy assessment method is the Error matrix method. Error matrix is also called confusion matrix or a contingency table which is a square array of dimension n X n (where n is the number of classes) that shows the relationship between pixels or polygons in the RS derived classification map and ground reference test data obtained at the location. The columns in an error matrix represent the ground reference or test data whereas the rows represent the labels assigned by the classifier from remotely sensed data (Chipman et al., 2015; Jensen, 2015; Tso and Mather, 2009). According to Congalton and Green (2009), there are two major statistical analysis of classification accuracy that can be obtained from the error matrix. They are univariate statistical analysis (such as Producer's accuracy, User's accuracy and Overall accuracy) and multivariate statistical analysis (such as Kappa coefficient)

The overall accuracy of the classification map is determined by dividing the total number of correctly classified pixels (i.e. the sum of the diagonal in the error matrix) by the total number of pixels in the error matrix (N).

$$\text{Overall accuracy} = \frac{\text{Total number of correctly classified pixles (Diagonal)}}{\text{Total number of reference pixles}} * 100 \quad (2.1)$$

The producer's accuracy is determined by the total number of correct pixels in a class divided by the total number of pixels of that class as determined from the ground reference data (i.e., the column total).

$$\text{Produce accuracy} = \frac{\text{Number of correctly classified pixles in each category}}{\text{Total number of reference pixles in that catecory (the column total)}} * 100 \quad (2.2)$$

The User's accuracy is determined by dividing the total number of correct pixels in a class by the total number of pixels that were actually classified in that category. It is a measure of commission error.

$$\text{Useraccuracy} = \frac{\text{Number of correctly classified pixles in each category}}{\text{Total number of classified pixles in that catecory (the row total)}} * 100 \quad (2.3)$$

Kappa analysis is a discrete multivariate technique of use in accuracy assessment. The method was introduced to the remote sensing community in 1981 and then published in a remote sensing journal in 1983 (Congalton, 1981; Congalton et al., 1983). It is a measure of the difference between the actual agreement between reference data and an automated classifier and the chance agreement between the reference data and a random classifier.

$$\textit{Kappa coefficient (K)} = \frac{(Total\ Sample * Total\ Corrected\ Sample) - \sum(Column\ Total * Row\ Total)}{Total\ Sample^2 - \sum(Column\ Total - Row\ Total) Total\ number\ of\ classified\ pixles\ in\ that\ catecory\ (the\ row\ total)} * 100 \quad (2.4)$$

The kappa coefficient values > 0.8 are very good, values between 0.6 and 0.79 are good, and values <= 0.59 are poor.

2.3.1. ERDAS imagine software

The ERDAS IMAGINE was among the first commercial software applications to provide a raster graphics editor and remote sensing application since 1992. Model maker was introduced as a graphic flowchart model building editor in 1993 (Beaty, 2021). It is designed for geospatial raster data processing and allows the user to prepare, display and enhance digital images for use in GIS or other similar application software. It is a toolbox allowing the users to perform various operations on an image and generate a solution to specific geographical questions by providing a graphical user interface to assist in visualizing imagery used in mapping, vector GIS data, and creating maps.

By manipulating data placement in the imagery it is possible to see features that would not normally be visible. The level of brightness or reflectance of light from the surfaces in the image can be helpful with vegetation analysis, prospecting for minerals, etc. Other usage examples include linear feature extraction, generation of processing chains ("spatial models" in ERDAS IMAGINE), import/export of data for a wide variety of formats, ortho-rectification, mosaicing of imagery, stereo and automatic feature extraction of map data from imagery (Nelson and Khorram, 2019).

2.4. Impact of Land Use Land Cover Changes on Hydrological Response

LULC change is one of the dominant driving forces of watershed hydrological change (Zhang et al., 2020). Expansion of agricultural land, urban areas, deforestation, and the day-to-day activities of human beings caused to spatio-temporal change in LULC that have affected watershed hydrology and water balance (Rawat and Manish, 2015). Increase in impervious surfaces often increases streamflow, runoff volume and increases peak discharge, all of which lead to degrade the hydrology of a watershed (Hu and Shrestha, 2020). Hence hydrological responses to the LULC changes require a detailed assessment to ensure sustainable management of water resources. Understanding of hydrological process is important for investigating the impact of LULC on water resources (Zhang et al., 2020). The spatial and temporal analysis of LULC trends and relationships between the factors driving the variations would allow for better management LULC (Barakat et al., 2019).

The impact of LULC on hydrology and water resources can be quantified by three major methods: The **"**Paired catchment" experimental method**:** which consider two catchments with similar areas, shapes, climate, vegetation and soil. The first 3 to 5 years including wet, normal and dry year are considered as a control period with no experimental measures. The LULC of one of the catchment will be artificially changed whereas the other catchment remain the same and serve as a reference catchment. The runoff in the two experimental catchments is compared and analyzed and the impact of LULC changes on water resources is investigated. These method are suitable only for small catchments (Bosch and Hewlett, 1982). The Time series analysis method: can be used to analyze the change trend of hydrologic and climate data, however, the spatial heterogeneity of the catchment and the mechanisms of LULC and climate change in hydrology and water resources cannot be determined (Li and Fox, 2012). The Hydrological model method: are widely used to determine the LULC change impacts on the hydrology of watersheds. Hydrological models provide a framework for conceptualizing and studying the relationships between climate change, land use change and the water cycle (Zhang et al., 2020).

Various studies were conducted in a different parts of the world on the impact of LULC change on hydrological components such as surface runoff, evapotranspiration, infiltration, lateral flow and groundwater recharge rate and water balance of watershed. Zhang et al. (2020) revealed that monthly surface runoff increased under deforestation and urbanization while decreased under afforestation in the north John-stone River catchment, Australia. Surface runoff increased by 25.00mm due to the reduction of forest by 11.50% and also surface runoff increased by 16mm under the scenario of the expansion of urban area by 2.30% and the decrement of surface runoff by 26.00mm due to the increment scenario of forest by 14.10%. However, the annual changes in lateral flow and groundwater recharge were decreased under urbanization scenarios. The impact of LULC change on peak discharge in the Richard Creek watershed was assessed using HEC-HMS and concluded that the peak discharges have been increasing from 2001 to 2011 due to an increase of impervious surface derived by sub-urban sprawl. The expansion of impervious surfaces by 11.21% increased the peak discharge from 125.00% to 175.00% (Hu and Shrestha, 2020).

On the other hand Aghsaei et al. (2020) applied the SWAT model to assess the impact of both static and dynamic land use to analyze its spatio-temporal impacts on hydrological components and sediment yields of the Anzali watershed and come up with the result of 0.90%, 1.00% and 2.30% increment of evapotranspiration, water yield and surface runoff, respectively. Groundwater flow and lateral flow were decreased due to the conversion of forest to irrigated paddy fields. At the sub-basin scale, the effect of LULC change on the hydrological response was more discernible than at the basin level.

Koneti et al. (2018) showed that cropland expansion and urbanization at expense of forest land leads to a decrease in the evapotranspiration and infiltration with an increase in runoff. Similarly, Zhu and Li (2014) revealed that the overall streamflow of the whole watershed of Little River Tennessee is increased by 3.00% for the study period of 1984 to 2010. The streamflow increment differs from sub-watershed to sub-watershed due to the spatial variation of land cover. The higher streamflow increment occurred at lower sub-watershed due to the land cover dominated by urban expansion. Munoth and Goyal (2019) also used SWAT hydrological model to investigate the impact of LULC change on runoff and sediment yield of the upper Tapi River watershed and come up with the conclusion that the surface runoff and water yield has increased by 36.13% and 21.78%, respectively due to the expansion of agricultural land and reduction of forest and rangeland.

Welde and Gebremariam (2017) revealed that due to the expansion of intensive agricultural land and expansion of bare land, the mean annual streamflow of Tekeze dam watershed was increased by 6.20% during the study period of over 22 years (1986 -2008). The hydrological impacts of human activities on Katar and Meki watersheds of Lake Ziway basin showed that due to the change in land use, annual surface runoff and water yield were increased in the Katar watershed, whereas for Meki watershed the evapotranspiration was increased (Musie et al., 2020). The annual surface runoff and water yields of Katar watershed increased by 11.00mm and 9.80mm from the year of 1984 to 2000 and 3.30mm and 2.10mm from the year of 2000 to 2017, respectively, whereas the percolation decreased by 12.90mm and 1.40mm from 1984 to 2000 and from 2000 to 2017, respectively. In contrast to the Katar watershed, in the Meki watershed, the annual surface runoff and water yield decreased by 1.40 and 0.90, respectively, while the annual percolation and evapotranspiration increased by 5.40mm and 3.30mm, respectively. They concluded that when compared to climate variability, the land use change has smaller impacts on the monthly streamflow.

Another research on Gilgel Abay watershed in Lake Tana sub-basin revealed that the amount of streamflow were increased by 17.54m^3/s during the wet season due to an expansion of agricultural land by 33.79% whereas streamflow were decreased by 0.65m^3/s during dry season which indicated that the base flow has decreased. The surface runoff showed an increment by 37.62mm and 51.60mm for the study period of 1986 to 2000 and 2000 to 2011, respectively, whereas groundwater flow decreased by $34.60 m^3/s$ for the study period of 1986 to 2000 due to the increase of agricultural land which leads to a reduction of infiltration (Andualem & Gebremariam, 2015).

Similarly, Shawul et al. (2019) showed the response of water balance components to LULC change in the upper Awash River basin and come up with the result that the higher fluctuation of surface runoff and lateral flow compared to the change in groundwater flow and evapotranspiration. During 40 years of the study period (1974 -2014), the surface runoff increased by 18.40%, while the lateral flow, groundwater flow and evapotranspiration decreased by 24.00%, 2.10% and 0.10% , respectively due to the rapid expansion of urban and cropland areas as the socio-economic development and population growth. The impact of LULC changes were more pronounced at the sub-basin level because of the contrasting effects are not averaged by LULC variation contained in the whole basin. For instance: the Akaki sub-basin which is experienced higher urban expansion due to the growth of Addis Ababa city and larger decreases in grassland and shrubland caused to increase in the surface runoff by more than 75.00% (83mm) and decrement of groundwater by 9.60% compared to the whole basin (upper Awash basin) (Shawul et al., 2019).

Most of the hydrological model applications used static LULC data to assess the effects of LULC change on hydrological processes. The static land use approach used in watershed processes does not estimate accurately the spatio-temporal hydrological processes (Wagner et al., 2016; Teklay et al., 2019). Hence, the Dynamic LULC approach helps to analyze the impact of LULC change, climate change, and land management practices on watershed hydrological responses (Pai and Saraswat, 2011; Teklay et al., 2019), whereas the static LULC approach uses a single LULC data which results in stationarity in hydrological responses. The stationarity of watershed hydrological response can be resolved by applying LULC change module to hydrological modeling approaches (Saraswat et al.,2010; wagner et al., 2016). Land use update modules through linear interpolation among time stamps have been developed in SWAT. The land use update module developed recently includes SWAT2009_LUC (Pai and Saraswat, 2011), LUC-R script (Tam, 2020), and SWAT-LUT (Moriasi et al., 2019). The modules are used to provide realistic parameterization by reducing over parameterization and stationarity problems by incorporating multiple LULC categories in watersheds at once rather than using a single static

LULC. The dynamic integration of LULC change in hydrological modeling is not found adequately in the literature due to the limitation of the hydrological model to incorporate the dynamic LULC data in the model run simulation. A few examples are, Pai and Saraswat (2011) used the LULC module with the SWAT model and improved the spatio-temporal hydrological responses. Wagner et al. (2016) also conducted a study on the effects of dynamic versus static representations of LULC change in hydrologic impact assessment. Teklay et al. (2019) evaluated the effects of static and dynamic LULC data using the same meteorological, soil and DEM data and different LULC data. They were used the land use update (SWAT-LUU) tool to setup dynamic land use model in the SWAT. The result showed that dynamic LULC data setup simulated the detailed biophysical processes better than static model setup during calibration and validation because of the improved representation of the dynamic watershed characteristics. Similarly, Tram et al. (2021) conducted a study on the impacts of land use on a flow and sediment discharge in the Dakbla watershed, Vietnam. They were incorporate dynamic land use in SWAT by SWAT-LUT tool. The result depicted that the dynamic LULC change could improve flow and sediment simulation performance better than performance found with static land use approaches.

2.5. Impact of Land Use Land Cover Changes on Sediment Yield

Sediment yield is the total result of soil erosion and sediment deposition processes, so it depends on variables that control water and sediment discharge to reservoirs. Sediment yield reflects the impacts of climate, soil type, topography, LULC and drainage properties (stream network form and density) (Munoth and Goyal, 2019; Williams, 1975). Approximately 40.00% of the world's fertile lands are excessively degraded as a result of erosion (The Guardian, 2007).

Sedimentation is the outcome of the land erosion in its catchment area. Land erosion has an impact on the physical and chemical characteristics of soils and causes on-site nutrient loss and off-site sedimentation and nutrient enrichment of water resources (Welde and Gebremariam, 2017). The study conducted in China by Yan et al. (2013) depicted that the upper Du watershed has experienced a sediment yield of 630.30, 697.10, 510.90, and 543.80t/km^2 during the year of 1978, 1987, 1999 and 2007, respectively. The fluctuation in sediment yield was due to LULC dynamics in forest and farmland. Another finding in Be river catchment, Vietnam, showed that the sediment yield increased by 12.80% due to agricultural land expansion and deforestation during the study period of 1990 to 2001 (Khoi and Suetsugi, 2014).

Soil erosion in Ethiopia has reached the highest level and increasing under the combined pressure of increasing population and deforestation. Soil erosion is one of the serious problems in Ethiopia's highland area that increased the sedimentation of reservoirs and lakes. The amount of soil erosion generated from the Ethiopian highland was estimated at 130.00 t/ha/yr for agricultural land (Molla et al., 2020). The sediment yield increased from 91.20 to 175.42% due to the expansion of farmland at the expense of forest and grazing land between 1984 and 1999 land use period, whereas a decrease from 119.88 to 45.62% due to the expansion of forested area and soil and water conservation practice between 2000 and 2009, however between 2010 and 2014, the sediment yield increased from 75.00% to 137.50% in the Baressa watershed in upper Blue Nile basin (Worku et al., 2017). Generally, Worku et al. (2017) concluded that the agricultural land and settlement area expansion by 18.20% and 59.70% at the expense of other natural vegetation resulted in the increment of sediment yield by 4332 t/yr in the Beressa watershed.

Similarly, Andualem and Gebremariam (2015) conducted a research and come up with a result that the amount of sediment yield from the Gilgel Abay watershed was increased by 40.01 t/km^2 and 22.77t/km^2 due to an expansion of agricultural land by 24.12% and 9.67% between 1986 and 2000, and 1986 and 2011, respectively. They conclude that the change in agricultural land has shown a direct relationship with sediment yield, while grassland and shrubland showed indirect relation in the Gilgel Abay watershed of Ethiopia. Welde and Gebremariam (2017) also articulated that the Tekeze dam watershed located in northern Ethiopia, which is vulnerable to intensive agricultural land and bare land experienced that 17.39% increment of sediment yield for the study period of 1986 to 2008.

2.6. Hydrological Models

2.6.1. Hydrological model concepts

Hydrology can be an important subject for the people and their surrounding environment that assess water of the earth, their occurrence, formulation, circulation and distribution, their physical and chemical properties, and their reaction with the environment including living things.

It studies the phase of the hydrologic cycle and the relationship of water with the environment (Devia et al., 2015). Dramatic changes have been observed in hydrologic systems due to population growth, socio-economic development, agricultural land expansion, forest clearing, rapid urban and industrial expansion, LULC, and climate change. These changes have an impact on the hydrology of watershed. To find out the effects of human activities and natural phenomena on the hydrological process of watersheds, hydrological models have been developed.

A model is a simplified representation of real-world system. It is used for understanding hydrological processes and predicting the behavior of a hydrologic system. The best model is one that gives results close to the observed one with the use least parameters and model complexity. Hydrological models are the abstraction of reality that is used to simulate natural systems. These models are power-full techniques that integrate hydrological systems and comprise a set of mathematical expressions of the hydrologic cycle to simulate real-world hydrologic processes. They are based on a set of mathematical equations to transform physical laws, which govern complex natural phenomena (Kassa, 2009). A watershed hydrological model is an assemblage of mathematical expressions of components of the hydrologic cycle (Singh and Woolhiser, 2002). Watershed hydrologic models have been developed for many different reasons and therefore have many different forms. However, they are in general designed to meet one of the two primary objectives. One objective of watershed modeling is to gain a better understanding of the hydrologic processes in a watershed and of how changes in the watershed may affect these phenomena. Another objective of watershed modeling is the generation of synthetic sequences of hydrologic data for facility design or for use in forecasting. They are also providing valuable information for studying the potential impacts of changes in land use or climate. The variety of uses and the rapid increase both in scientific understanding and in technical support, from data collection systems and computer technology, have produced an enormous range in levels of sophistication (Kassa, 2009).

2.6.2. Classification of hydrological models

Many hydrological models have been developed and refined during the past four decades and it is required to fully understand their characteristics to easily apply them. Classification of hydrological models is not exact and different hydrologists may give different definitions due to the nature of models is often the same but many models have overlapping characteristics. Unique and common characteristics of many models make classifications of hydrological models an important issue, which would be vital for accurate identification of the capabilities and limitations of each model (Paul et al., 2021). There are different characteristics of a catchment in models, resulting in a plentiful of mathematical models for the watershed simulation used in the evaluation of surface and groundwater flow modeling (Alam et al., 2011). The classification of hydrological models may vary depending on justification (Gosain et al., 2009; Singh and Frevert, 2006).

Hydrological models vary in many ways: time step, spatial scale, whether the model simulates single events or on a continuous basis, and how different hydrological components are computed. Depending upon the way the hydrological processes are described, the models can be also classified as deterministic, stochastic, or mixed. In a deterministic model, outcomes are precisely determined through known relationships among states and events, without any room for random variation. In such models, two equal sets of input always yield the same output if run through the model under identical conditions. On the other hand, if a model has at least one component of random character which is not explicit in the model input, but only implicit or hidden ‘it is called a stochastic model. If the model components are described by a mix of deterministic and stochastic components, the model is called a stochastic-deterministic or hybrid model. A vast majority of the models are deterministic, and virtually no model is fully stochastic. Based on the process description, the hydrological models can be classified into three main categories: lumped models, semi-distributed models, and distributed models (Kassa, 2009). The lumped modeling approach considers a watershed as a single unit for computations where the watershed parameters and variables are averaged over this unit (Cheng, 2011; Magar & Jothiprakash, 2011). A distributed model can make predictions that are distributed in space by dividing the entire catchment into small units, usually square cells or triangulated irregular networks so that the parameters, inputs, and outputs can vary spatially (Daofeng et al., 2004; Moradkhani and Sorooshian, 2008). The semi-distributed models partition the whole catchment into sub-basins or HRUs that partially allow parameters to vary in space by dividing the basin into a number of smaller sub-basins (Daofeng et al., 2004).

According to Devia et al., 2015, rainfall-runoff models are classified based on model input and parameters and the extent of physical principles applied in the model. One of the most important classifications is empirical model, conceptual models, and physically-based models.

Empirical models (Metric models) are observation-oriented models which take only the information from the existing data without considering the features and processes of the hydrological system hence these models are also called data-driven models. It involves mathematical equations derived from concurrent input and output time series and not from the physical processes of the catchment. These models are valid only within the boundaries. Statistically based methods use regression and correlation models and are used to find the functional relationship between inputs and outputs. Unit hydrograph, artificial neural network and fuzzy regression are some examples of this method.

Conceptual methods (Parametric models) describe all of the component hydrological processes. It consists of a number of interconnected reservoirs which represents the physical elements in a catchment in which they are recharged by rainfall, infiltration and percolation and are emptied by evaporation, runoff, drainage etc. Semi-empirical equations are used in this method and the model parameters are assessed not only from field data but also through calibration. A large number of meteorological and hydrological records is required for calibration. The calibration involves curve fitting which makes the interpretation difficult and hence the effect of land use change cannot be predicted with much confidence. Many conceptual models have been developed with varying degrees of complexity. Stanford Watershed Model IV (SWM) is the first major conceptual model developed by Crawford and Linsley in 1966 with 16 to 20 parameters.

Physically-based models are mathematically idealized representations of a real phenomenon. These are also called mechanistic models that include the principles of physical processes. It uses state variables that are measurable and are functions of both time and space. The hydrological processes of water movement are represented by finite difference equations. It does not require extensive hydrological and meteorological data for their calibration but the evaluation of a large number of parameters describing the physical characteristics of the catchment are required. In this method, a huge amount of data such as soil moisture content, initial water depth, topography, topology, dimensions of the river network, etc. are required. The physical model can overcome many defects of the other two models because of the use of parameters having physical interpretation. It can provide a large amount of information even outside the boundary and can be applied to a wide range of situations. SHE/ MIKE SHE model is an example (Abbott et al., 1986).

2.6.3. Guidelines for model selection

Most developed countries usually have their own hydrologic models, whereas the majority of developing countries have limited hydrologic capabilities due to the relatively poor ability in the model maintenance, computational costs and technical capacity for model simulation (Paul et al., 2021). An issue in many hydrological studies is determining which model is best applied to a catchment in any modeling exercise. No model can be identified as ideal for the range of hydrological conditions and catchments that exist. When selecting a model, we are not solely reliant on its predictive performance but will also take into account the modeler's preference and familiarity in using particular models, the aim of the modeling task, the time available to develop and apply a model and the level of accuracy required. In addition to these issues, significant attention is also paid to the performance of the model when applied to a specific catchment (Marshall et al., 2005).

Therefore an appropriate selection of hydrological model, at first the purpose of the study should be clear and then identifying the problem, requirement of input data spatio-temporal resolution of the model, model credibility and the hydrologic processes that need to be modeled, its applicability to simulate the impact of land use and climate change and also prediction performance. Model functionality and complexity can become major criteria in model selection. The model functionality differs in terms of hydrologic process representation, the equations adopted to simulate these processes and model discretization. In addition, model complexity can be defined by the estimated data, resources, time, and cost that are required to parameterize and calibrate a model, as well as the professional judgment and experience required to operate these models (Dwarakish & Ganasri, 2015; Paul et al., 2021)

There are numerous criteria that can be used for choosing the right hydrologic model. These criteria are always project-dependent, since every project has its own specific requirements and needs. Some models are data-intensive that often does not exist or are not available in full (Kassa, 2009). Among the various project-depended selection criteria, there are four common, fundamental ones that must be always answered:

i) Output needed from the model that is important to the project and therefore to be estimated by the model (Does the model predict the variables required by the project such as peak flow, event volume and hydrograph, long term sequence of flows?)

ii) Hydrologic processes that are required to be modeled to estimate the desired outputs adequately (Is the model capable of simulating required reservoir operation and single event or continuous processes?)

iii) Availability of input data (Can all the inputs required by the model be provided within the time and cost constraint of the project?)

iv) Price (Does the investment appear to be worthwhile for the objective of the project?)

Based on the criteria listed above, SWAT hydrological model is selected for this study.

2.7. Soil and Water Assessment Tool (SWAT) Model

The Soil and Water Assessment Tool (SWAT) model was developed by the United States Department of Agriculture, Agricultural Research Service (ARS). SWAT operates on a daily time step and is designed to predict the impact of land use and management on water, sediment, and agricultural chemical yields in ungagged watersheds (Arnold et al., 1998, 2012). The model is process-based, computationally efficient, and capable of continuous simulation over periods long time (Neitsch et al., 2012). Major model components include weather, hydrology, soil temperature and properties, plant growth, nutrients, pesticides, bacteria and pathogens, and land management. In SWAT, a watershed is divided into multiple sub-watersheds, which are then further subdivided into hydrologic response units (HRUs) that consist of homogeneous land use, management, topography, and soil characteristics. The HRUs are represented as a percentage of the sub-watershed area and may not be contiguous or spatially identified within a SWAT simulation. Alternatively, a watershed can be subdivided into only sub-watersheds that are characterized by dominant land use, soil type, and management. Climatic inputs used in SWAT include daily precipitation, maximum and minimum temperature, solar radiation, relative humidity, and wind speed data, which can be input from measured records and/or generated. Relative humidity is required if the Penman-Monteith (Monteith, 1965) or Priestly-Taylor (Priestly and Taylor, 1972) evapotranspiration routines are used; wind speed is only necessary if the Penman-Monteith method is used. Measured or generated sub-daily precipitation inputs are required if the Green-Ampt infiltration method (Green and Ampt, 1911) is selected. The average air temperature is used to determine if precipitation should be simulated as snowfall. The maximum and minimum temperature inputs are used in the calculation of daily soil and water temperatures (Arnold et al., 2012; Gassman et al., 2007).

In the SWAT, water, sediment and nutrient transformations and losses determined in each HRU are aggregated at the sub-basin level and routed to the catchment outlet through the channel network. The hydrologic sub-model is based on the water balance equation in the soil profile, where the simulated processes include precipitation, infiltration, surface runoff, evaporation, lateral flow and percolation (Fan and Shibata, 2015).

SWAT is used in many countries all over the world for the analysis, evaluation, assessment and estimation of streamflow, sediment yield, agricultural chemicals and management measures in the river watersheds. Several research studies are conducted using the SWAT model to predict streamflow, sediment yield and best management practices for a variety of watershed. The SWAT model was applied in the upper kharun catchment, India to investigate the impact of land use change on water resources (Kumar et al., 2017); SWAT also used in the Tennesse River watershed to assess long term hydrological impact of land use/ land cover change (Zhu and Li, 2014), Yan et al. (2013), evaluate the impact of land use changes on streamflow and sediment yield at a basin-scale using SWAT model.

SWAT also has been successfully applied in many parts of Ethiopian watersheds. It was used in the upper Awash River basin (Amin & Nuru, 2020; Daba, 2018; Shawul et al., 2019; Tolera et al., 2018), Blue Nile Basin (Andualem & Gebremariam, 2015; Birhanu et al., 2019; Getachew et al., 2021); SWAT also applied in Lake Ziway watershed to assess the impact of LULC dynamics, climate variability and human activity on water balance (Abraham and Nadew, 2018; Desta and Lemma, 2017; Musie et al., 2020); SWAT model also evaluated at Weyib River Basin in simulating catchment hydrology and the performance of the model appears to be reasonable (Serur and Sarma, 2016; Shawul et al., 2016).

3. MATERIALS AND METHODS

3.1. Description of the Study Area

3.1.1. Location

The study area, the big Akaki watershed (Figure 3.1) is located in central Ethiopia in Oromia regional state and parts of Addis Ababa administrative zones along the western margin of a rift valley. The watershed is one of the tributaries of Akaki River that is suited at the northwestern of Awash River with $8^{\circ}\ 52'00''$ N to $9^{\circ}\ 14'\ 00''$ N latitude and $38^{\circ}\ 45'00''$E to $39^{\circ}14'56''$ E longitude and has a land area of 833.20 Km^2. The watershed is bounded by Intoto Mountain in the north, Bilbilo and Guji Mountains in the south, Gara Bushu Mountain hills in the southeast, Yerer Mountain in the east, Andode and Salo Gora Mountains in the west. Addis Ababa and other cities are found in this watershed. Big Akaki watershed consists of Kebena, Ginfle, Bentyketu, and Abo Rivers as tributaries and flows southwards across the Addis Ababa city towards Lake Aba Samuel which is an artificial Lake constructed for hydropower generation. Surface water reservoirs exist in the watershed are Legedadi reservoir and Dire dam.

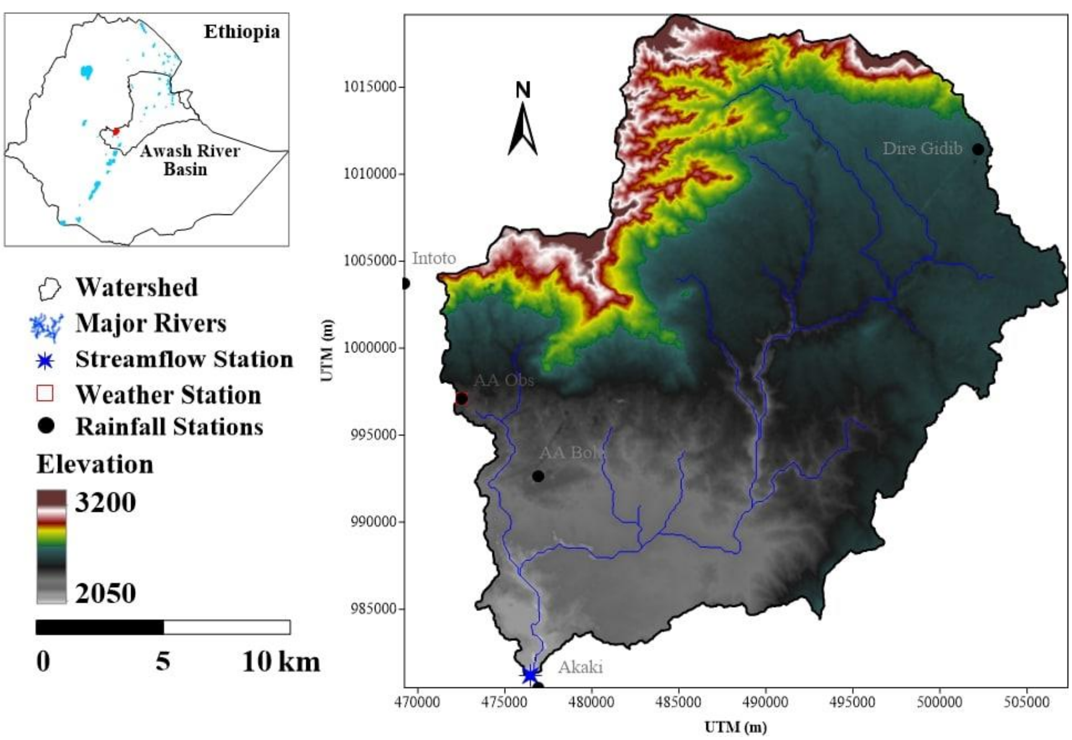

Figure 3. 1 Location map of the Study Area

3.1.2. Climate

Ethiopian climate pattern is governed by the Inter-Tropical Convergence Zone (ITCZ) and influenced by the Indian Monsoon. The ITCZ creates dry and rainy seasons when the ITCZ is northernmost; the equator air stream direction is southeast in southern Ethiopia and southwest in central to northern Ethiopia. Ethiopia's climate is categorized into five main climatic zones based on elevation as Wurch, Dega, Woyna Dega, Kolla, and Bereha (Kassa, 2009).

Table 3.1 Ethiopia's agro-climatic zone (Kassa, 2009)

Agro-climatic zone	Characteristics		
	Altitude (m)	Precipitation (mm)	Temperature (^{o} C)
Wurch (Alpine)	>3000	>2200	<13
Dega (Humid)	2300-3000	1200-2200	13-16
Woyna Dega (Sub-humid	1500-2300	800-1200	16-18
Kolla (Semi-arid)	800-1500	200-800	18-20
Bereha (Hyper-arid)	<800	<200	>20

The climate of the big Akaki watershed is characterized by two main season climate patterns. The main rainy season is from mid-June to mid-September which contributes more than 76.00% of the total annual rainfall. The second moderate rainy season is from mid-February to mid-April which consists of the remaining rainfall. The dry season is from October to February. The mean annual and mean monthly rainfall for five weather stations located in the period of 2000 to 2018 of the big Akaki watershed is 1048.34 mm and 87.36mm, respectively. The maximum monthly rainfall of 273.60mm was recorded in August; whereas the minimum monthly rainfall of 6.30mm was recorded in December. The mean monthly maximum temperature ranges from 18.16^{0}C to 26.48^{0}C, while the mean monthly minimum temperature ranges from 8.50^{0}C to 11.11^{0}C, respectively as shown in figure 3.2 and 3.3.

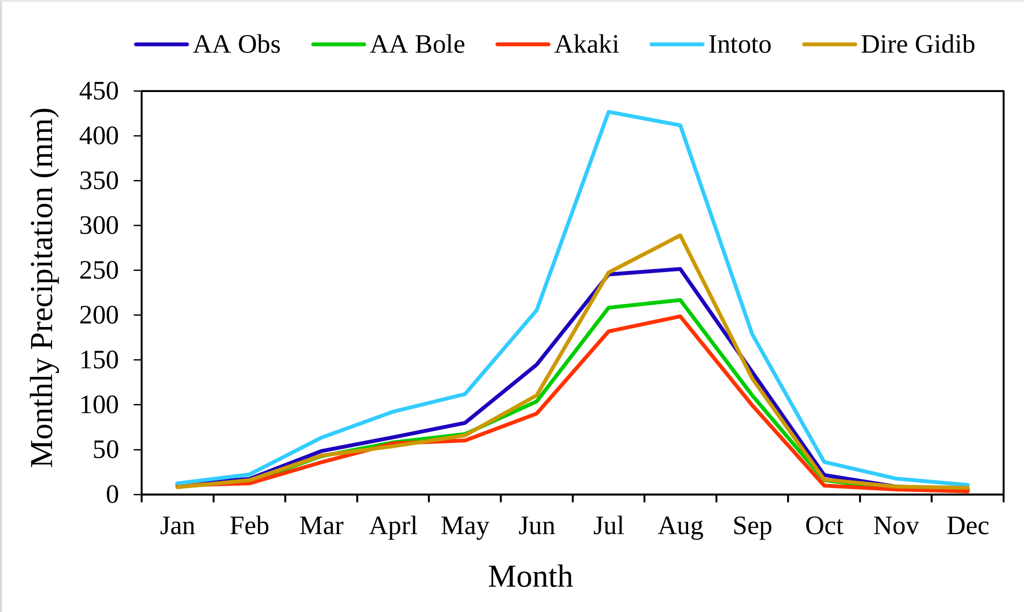

Figure 3. 2 Mean monthly precipitation distribution of the Study Area

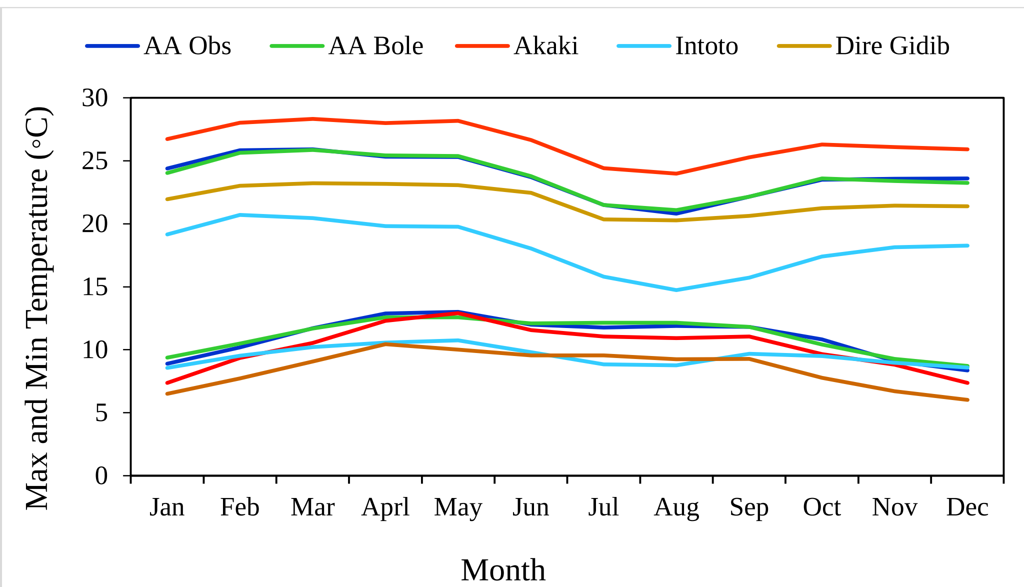

Figure 3. 3 Mean monthly maximum and minimum temperature distribution of the Study Area

3.1.3. Topography, geology, and soils

The big Akaki watershed has an elevation ranges from 2022 to 3210m above mean sea level. The topography of the study area is increasing from the downstream (around big Akaki gauge station) in south to the upstream (around Intoto Mountain) in north direction. The physiographic component of the area are steep slope in north and form plateau in central and gentle to flat in the southern part. The geology of big Akaki watershed is an integral part of the evolution and development of the Ethiopian rift system. The geological unit in big Akaki watershed is categorized into Alaji Formation, Addis Ababa Basalts, Younger Volcanic and Recent Deposits. The Alaji Formation such as rhyolites, trachyte, tuff, agglomerate and alphianitic basalt. It is mainly dominated in the northern and central zone of the watershed (Grimay and Assefa, 1979). The Addis Ababa basalts overlay with the Intoto silicics and cover the central and southern parts of the big Akaki watershed (Tsehayu and Hailemariam, 1990). The Younger Volcanic unit is another geological unit that incorporates the Nazareth group and Bishoftu formation. It includes the aphianitic basalts, welded tuffs, ignimbrites trachyte and rhyolites. The Recent Deposits include alluvial, residual and lacustrine deposits (AAWSA et al., 2000). The watershed is covered by volcanic rocks, fluvial and residual soils in which the black cotton soils are the predominant varying in thickness. The basalt, rhyolites, trachyte, scoria, trachy-basalts, ignimbrites and tuff. Since the watershed is located at the edge of the Ethiopian rift, there are a number of fault systems having a general trend of the rift system (AAWSA et al., 2000). The major soil types in the big Akaki watershed are ET1266 (69.40%), ET1137 (17.10%), ET1189 (8.40%), ET1154 (3.90%) and ET957 (1.20%).

3.2. Materials and Software Tools

The following materials and software were used to achieve the objective of the study to assess the impact of dynamic LULC change on hydrological responses of the big Akaki watershed. The R-studio (Climatol package) and Rainbow software packages were used for filling the missing climate data and homogeneity test of climate data, respectively. The Geographic Information System (GIS) 10.4 was used for processing the spatial data such as land use data, soil data and used as an interface for the SWAT hydrological model. The Earth Resources Data Analysis System (ERDAS) Imagine 2015 was used for the processing and analysis of the satellite Landsat image, LULC image classification, and generation and its accuracy assessment. Soil and Water Assessment Tool (SWAT) 2012 was used to simulate, assess and analyze the hydrological components and sediment yield of the watershed. The SWAT-LUT software was used to process multi-year land use data and develop land use update files for SWAT simulation scenarios. The sequential Uncertainty Fitting-2 (SUFI-2) algorithm which is one of the five uncertainty analysis techniques incorporated in SWAT Calibration and Uncertainty Program (SWAT-CUP) software was used for model sensitivity analysis, calibration, validation, and uncertainty analysis of SWAT model simulation.

3.3. Hydrological Model Data Input and Sources

The hydrological models require input data that describe the watershed. Some of the most important input data are weather data, hydrological data, topography (DEM), soil map, and property and LULC map. These data were collected from different sources.

3.3.1. Weather data

Weather data are the essential input data for SWAT hydrological model which is used for simulation of the hydrology of watershed. The daily precipitation, maximum and minimum temperature, relative humidity, wind speed and solar radiation at 5 meteorological stations within and around the study watershed namely Addis Ababa Bole (AA Bole), Addis Ababa Observatory (AA Obs), Akaki, Intoto, and Dire Gidib meteorological stations were obtained from the National Meteorological Agency of Ethiopia (NMA) for a period of 2000 to 2018. The additional weather data was generated from the National Aeronautics and Space Administration (NASA) Power Data Access Viewer and from Climate Forecast System Reanalysis (CFSR) database.

Table 3.2 Weather Stations in and around the study area

No	Station Name	Lat	Long	Elev (m)	Parameters*					
					PCP	Tmax	Tmin	RHD	SLR	WS
1	AA Obs	9.02	38.75	2386	Yes	Yes	Yes	Yes	Yes	Yes
2	AA Bole	8.98	38.79	2354	Yes	Yes	Yes	Yes	Yes	Yes
3	Akaki	8.87	38.79	2057	Yes	Yes	Yes	No	No	No
4	Intoto	9.08	38.72	2903	Yes	Yes	Yes	No	No	No
5	Dire Gidib	9.15	39.02	2569	Yes	Yes	Yes	No	No	No

* PCP is Precipitation, Tmax and Tmin is Maximum and Minimum Temperature, RHD is Relative Humidity, SLR is Solar Radiation and WS is Wind Speed.

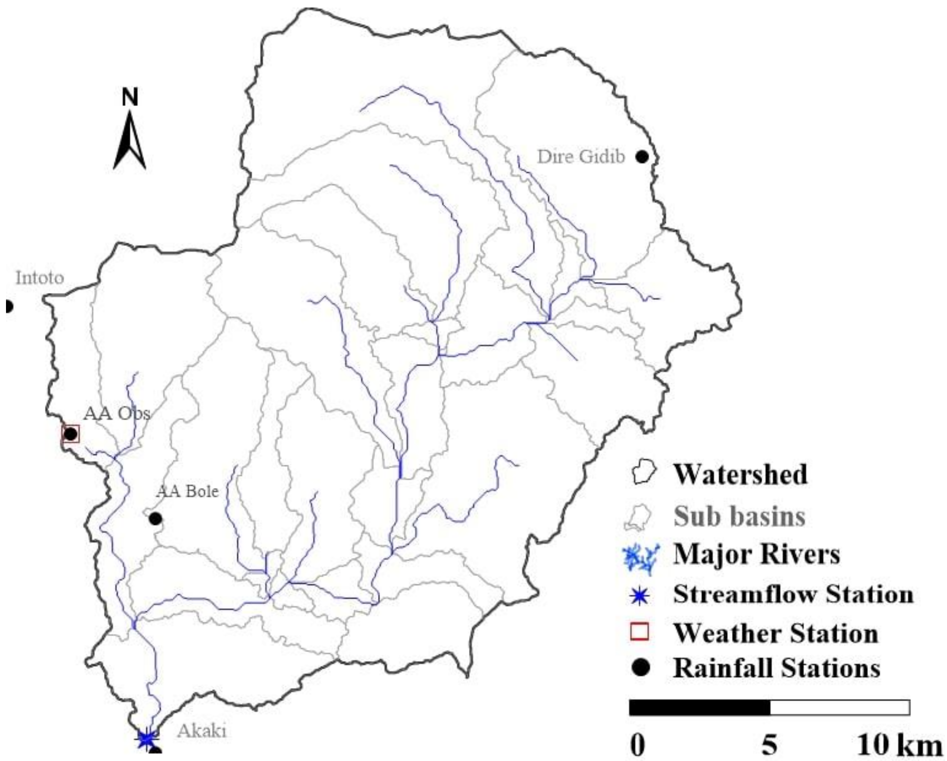

Figure 3. 4 Location of selected meteorological stations for big Akaki watershed

3.3.2. Hydrological data

3.3.2.1. Streamflow data

The streamflow data is required for performing sensitivity analysis, calibration, and validation of the SWAT hydrological model. The daily streamflow data of the big Akaki watershed at big Akaki gauge station for the period of 2000-2016 was collected from the hydrology department of the Ministry of Water and Energy of Ethiopia (MoWE). The peak discharge occurs from July to September (figure 3.5)

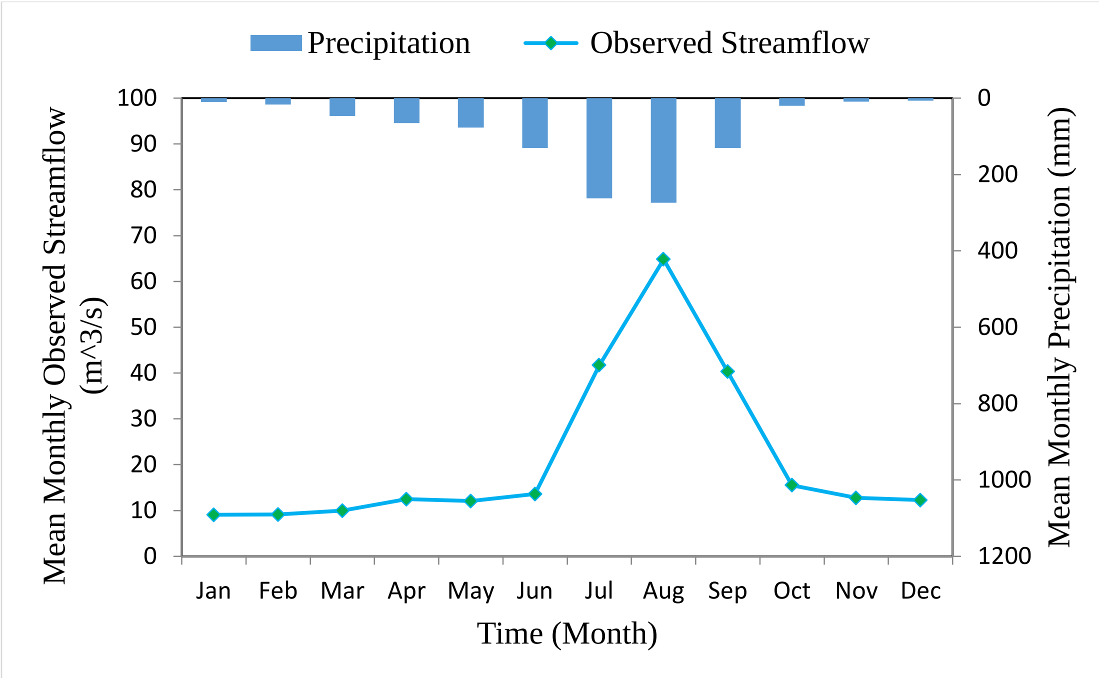

Figure 3. 5 Mean monthly streamflow of big Akaki gauge station (2000-2016)

3.3.2.2. Sediment yield data

The sediment yield data availability is a challenging task in most of Ethiopian River catchments since the measured sediment data taken from the Ministry of Water and Energy of Ethiopia (MoWE) was for only a short period and not in a continuous-time step. To solve the discontinuity problem, the empirical relationship between the streamflow and sediment load which is called a rating curve equation is established to allow the calculation of the suspended sediment (Jansson, 1996). The sediment data at the big Akaki gauge station was collected from the department of water quality directorate of the Ministry of Water and Energy of Ethiopia (MoWE). The sediment data obtained was on a concentration basis; hence it was converted to the suspended sediment yield using equation 3.1 as shown below (Andualem and Gebremariam, 2015).

$$Sy = 0.0864 * C * Q \quad (3.1)$$

Where Sy suspended sediment yield (t/day) is, C is sediment concentration (mg/l), Q is streamflow (m^3/s) and 0.0864 is a conversion factor.

The sediment data was prepared using the sediment rating curve by considering the streamflow and sediment yield relationships at the big Akaki gauge station using equation 3.2. The correlation coefficient of the streamflow and sediment data series was R^2 value of 0.90 as shown in figure 3.6 below. Different scholars such as Jansson (1996), Guzman et al. (2013), Andualem and Gebremariam (2015), Higgins et al. (2016), Razad et al. (2019) and Lemma et al. (2020) applied the sediment rating curve to estimate long-term sediment yield for sediment data-scarce catchments.

$$Sy = 26.23Q^{1.47} \tag{3.2}$$

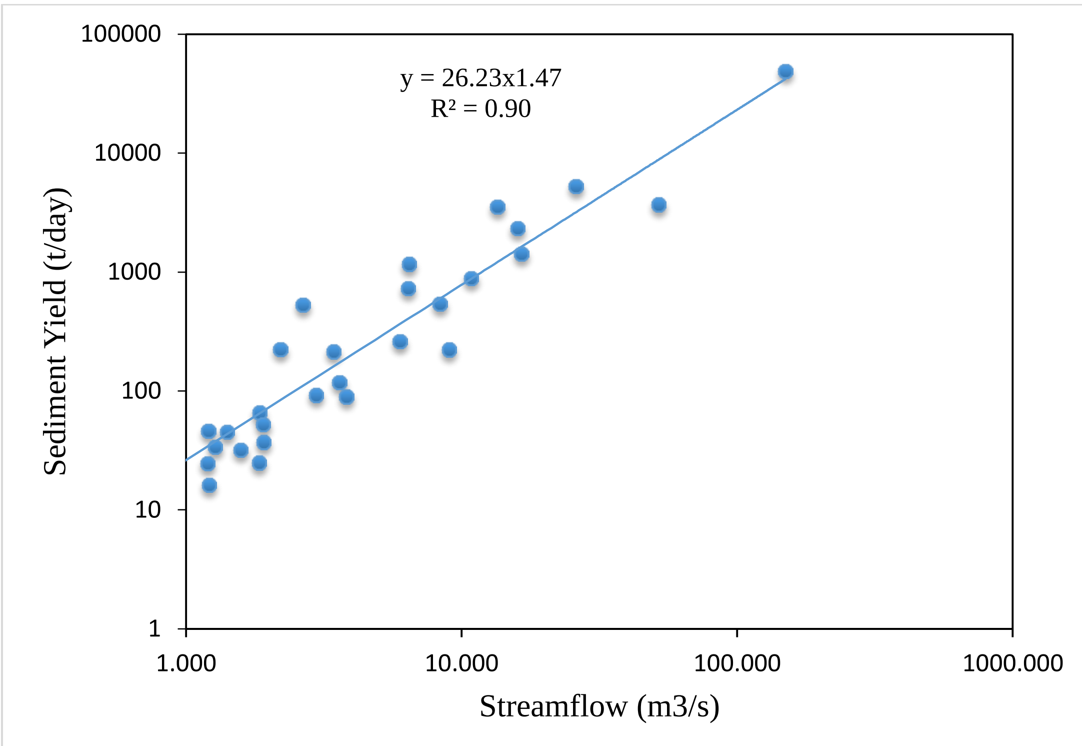

Figure 3. 6 Sediment rating curve for big Akaki gauge station

3.3.3. Digital elevation model data

The digital elevation model (DEM) is a digital topographic surface used to analyze watersheds into a number of sub-basins and to analyze the drainage pattern of the surface. The basin parameters such as slope length of the train, slope gradient and stream network characteristics such as channel length, slope and width and the hydrological parameters were generated from the DEM. The DEM with a spatial resolution of 30m obtained from the Advanced Spaceborne Thermal Emission and Reflection Radiometer (ASTER) Global Digital Elevation Model

(GDEM) website was extracted and processed using GIS (Arc map) by masking the big Akaki watershed shapefile and clipping the study area watershed for the sake of delineating the watershed. The extracted DEM of the study area was used as an input in SWAT hydrological model to delineate the watershed into a number of sub-watersheds and further into hydrologic response units (HRUs). The big Akaki watershed was classified into three land slope classes as 0-10%, 10-20% and >20% as indicated in figure 3.7 below. The slope class indicates that 60.89% of the watershed area is between the slope class of 0-10%, 24.68% between 10-20% and the remaining 14.42% is in the slope class of >20%. The land slope classes of the study area watershed indicate the existence of higher variation in topography of the big Akaki watershed.

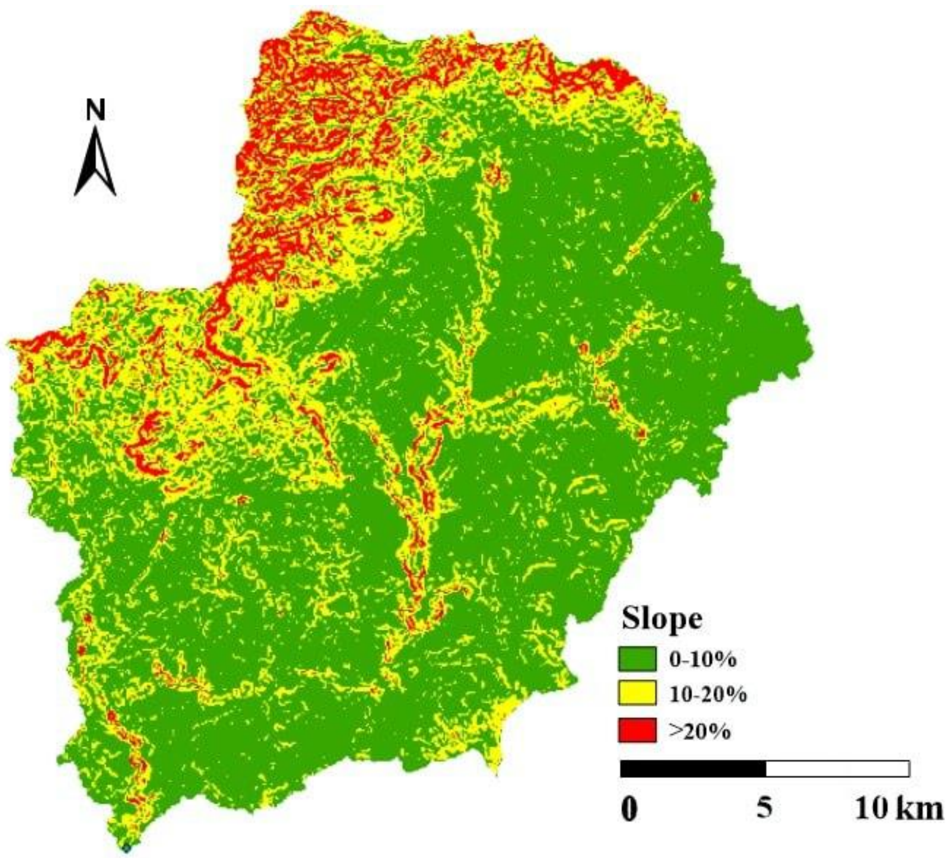

Figure 3. 7 Slope class of the study area

3.3.4. Soil data

Soil data is one of the spatial input data required for the modeling of streamflow and sedimentation in the physical-based hydrological models. A soil map and a database table of soil characteristics such as soil hydrologic group, maximum rooting depth of the soil profile, moist bulk density, soil texture, soil saturated hydraulic conductivity, grain size percentage, texture class, and soil available water for different soil layers are required by the hydrological models (Zhang et al., 2020).

Soil map and properties play an important role in hydrological modeling. The prediction of runoff, sediment yield and impacts of LULC depends on soil physical properties and the understanding of these data (Kassa, 2009). The SWAT hydrological model requires the detailed physical and chemical properties of the soils. Hence, the soil map and soil data of the study area were obtained from the Ministry of Water and Energy (MoWE) and Food and Agriculture Organization (FAO) Harmonized World Soil Database (HWSD) of soil classification to determine the soil type of the study area (FAO, 2002).

Since the soil data of the Ethiopian catchment is not available in SWAT user soil database, to integrate the soil map with SWAT model, a user soil table database that contains the physical and chemical properties of soil was prepared using the SWAT user soil template (Excel extension) and imported to SWAT user soil database.

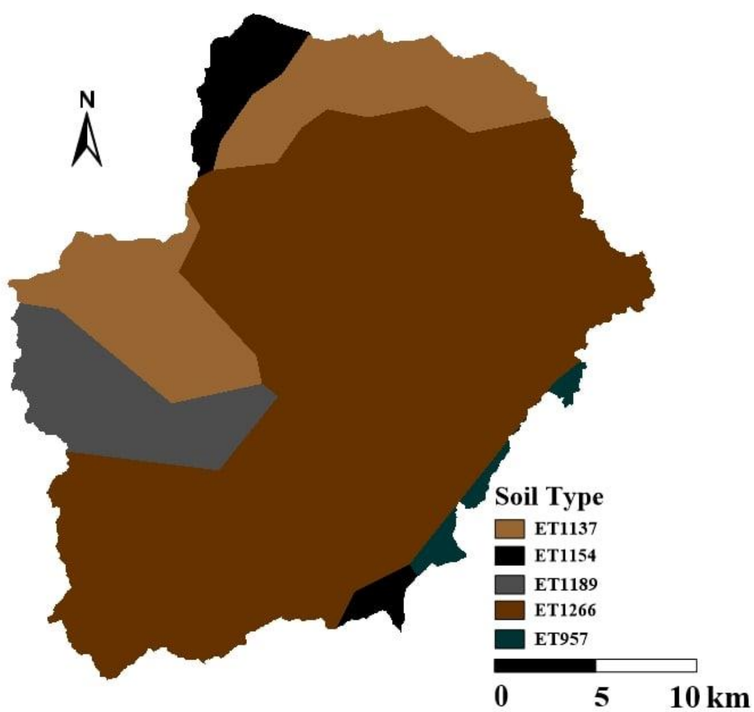

Figure 3. 8 Soil map of the study area

The FAO soil classification method was used and five different soil types were classified in the big Akaki watershed. The main soil types are 69.35% ET1266 (soil dominated by clay), 17.08% ET1137 (soil dominated by sandy clay loam), 8.37% ET1189 (soil dominated by clay), 3.95% ET1154 (soil mainly dominated by sandy clay loam) and 1.25% ET957 (soil mainly dominated by clay). The soil map of the study area is presented in figure 3.8. A detailed soil data description of the study area is presented in Appendix A.1.

3.3.5. Land use and land cover

Information derived from land use and land cover data is important to land conservation, sustainable development and management of water resources. LULC change affects the amount of evapotranspiration, groundwater infiltration and overland runoff (Tewabe and Fentahun, 2020). The LULC data is important for assessing the response of watershed characteristics for land use change for different periods. It is one of the important inputs for SWAT model to set the Hydrological Response Units (HRUs) of watersheds in addition to the Soil and slope map.

3.3.5.1. Land use land cover image pre-processing

The LULC data set for the three historical periods with 30m spatial resolution was obtained from multi-temporal series of Landsat images. The Landsat images were downloaded from the United States Geological Survey (USGS) earth explorer website (http://earthexplorer.usgs.gov) for the years 2000 and 2010 of Landsat 7 Enhanced Thematic Mapper Plus (ETM+), and year 2020 of Landsat 8 the Operational Land Imager (OLI) in path 168 and Row 54 as shown in Table3.3. The Landsat images for three historical periods were selected for the period of dry months of the same season as they are cloud-free and fewer vegetation variations in pattern and distribution.

ERDAS Imagine 2015 was chosen for processing land analysis of the satellite Landsat image before image classification and change detection. The Landsat ETM+ image for land use period of 2000 and 2010 and the Landsat OLI image for land use period of 2020 were captured a series of Geo-tiff files with separate TIFF files for each bands. Then the Landsat bands were unpacked for each image and these TIFF layer bands of Landsat were imported to ERDAS Imagine format (.img) from the initial format (.tif).

The Landsat bands were imported into ERDAS Imagine file (.img) for each image year of 2000, 2010 and 2020, respectively. The color composite is created from images obtained. There were different combinations of color composite to achieve an optimal one. The true color composite of the image data represented by the corresponding colors (red, green and blue) spectral areas were assigned red, green and blue image bands, respectively. The band combination in Landsat 7 ETM+ represented by band 3, 2 and1 whereas for Landsat 8 OLI/TRIF represented by band 4, 3 and 2. This allows us to easily differentiate different land use classes from each other. The color composition has been done using the ERDAS Imagine toolbar, raster/spectral/layer stack module. The individual layers of each land use period (2000, 2010 and 2020) were merged into single multi-layer file (.img). The separate bands were combined into single and multi-layer image format for land use period of 2000, 2010 and 2020 in (.img) format. To select the target study area, the image has been clipped using create subset image tool from the menu subset and chip. The clipped area was applied to all images (2000, 2010 and 2020) to accomplish an identical area of interest. The area of interest (AOI) layer file was created to identify the area of interest in the ERDAS Imagine viewer.

Table 3.3 Landsat satellite image used for LULC classification

Year	Satellite Name/Sensor	Acquisition data	Path	Row	Spatial resolution (m)	Projection
2000	Landsat 7 ETM+	2000/02/05	168	54	30	WGS84/ UTM, Zone 37
2010	Landsat 7 ETM+	2010/01/31	168	54	30	
2020	Landsat 8 OLI/TIRS	2020/04/08	168	54	30	

3.3.5.2. LULC classification

Image classification uses spectral information represented by digital numbers in one or more spectral bands and attempts to classify each individual pixel based on the spectral information. The Landsat images were assigned per-pixel signatures and differentiating the watershed on the basis of the digital number (DN) value of different land classes into seven land use classes. The delineated classes for big Akaki watershed as shown in Table 3.4 were agricultural land, forest land, grassland, shrubland, water body, built-up and bare land.

The supervised image classification of statistical approach of maximum likelihood algorithm was applied for all Landsat images of 2000, 2010 and 2020, respectively using ERDAS Image 2015 software (Rawat & Kumar, 2015; Shawul & Chakma, 2019; Tadese et al., 2020; Tso and Mather, 2009). For each the LULC periods, the training samples of 500 were selected by delimiting a polygon around the representative sites. The spectral signatures for each LULC types extracted from the Landsat image were recorded. The training sample for major LULC classes such as agricultural land, built-up and forest land were over 100. The predefined LULC classes were developed with the help of Google Earth Pro 7.3.3 software which is integrated with ERDAS Imagine 2015. Google Earth provides powerful information that can be used for LULC-related studies with higher resolution, suitable accuracy, and less cost.

Table 3.4 Land use and land cover categories of big Akaki watershed

LULC Class	SWAT Code	Description
Agricultural Land	AGRR	Land areas used for the purpose of crop cultivation and rural scattered settlement are associated with cultivated fields.
Built-Up	URBN	Areas used for permanent building and other man built artificial structures such as transportation facilities, industrial and commercial area
Forest Land	FRST	Land areas covered with high density of trees which include deciduous broadleaf forest, evergreen forest, mixed forest and plantation.
Grass Land	RNGE	Land areas covered predominantly by grassland with cover density over 10%.
Shrub Land	RNGB	Land areas covered with shrubs and cover density over 30%.
Water Body	WATR	Areas covered with liquid water bodies such as River, Lake, reservoir etc.
Bare Land	BARR	Land areas covered with little or no vegetation. It includes rocky area, desert, gravel ground etc.

3.3.5.3. Accuracy assessment

At the end of the process of producing LULC classification from RS image, errors in area estimates may occur in the distribution of pixels of the various remotely acquired on the ground features due to the spatial resolution of the satellite image used. Therefore, assessment of LULC classification accuracy is essential to measure classification performance. Accuracy assessment means the level of agreement between labels assigned by the classifier and class allocations based on ground data collected by the user, known as test data. The LULC classification accuracy assessment was done for three LULC supervised classifications by comparing the classified image using ERDAS Imagine 2015 with the reference ground truth data for the LULC classification of 2000, 2010 and 2020 period. The ground control points (GCPs) of 2000, 2010 and 2020 was generated from historical high resolution Google Earth imageries captured on February 05, 2000, January 31, 2010 and April 08, 2020, respectively.

Error matrix accuracy assessment method which is a square array of dimension nXn (n is number of classes) that shows the relationship between pixels or polygon in the RS derived classification map and ground reference test data was used to assess the accuracy of LULC classification of big Akaki watershed. Generally, a total number of 201 ground truth points were taken randomly for each LULC period. The statistical analysis of classification accuracies (Gongalton and Green, 2009) such as producer's accuracy, user's accuracy, overall accuracy, and Kappa coefficient statistical analysis were used.

3.3.5.4. LULC change detection analysis

LULC change detection is a process to determine which LULC class is changing to the other. It is the determination of the change in land use classes from one to another using the spatio-temporal multi-temporal datasets. There are different LULC change detection methods. The most commonly used methods are image overlay, classification comparisons of land cover Statistics, change vector analysis, principal component analysis, image rationing and differencing of normalized difference vegetation index (NDVI). In this study, a classification comparison of land cover statistics had used. The areal coverage of classified LULC maps for the stated periods was calculated and the areal change was quantified between 2000-2010, 2010-2020 and 2000-2020 years of period. The absolute change in LULC classes was computed by considering the difference between two consecutive LULC maps for instance area of LULC 2010 minus the area of LULC 2000. A LULC change between each period was also developed to understand the spatio-temporal variations in the LULC classes, whereas the rate of LULC change over the study period was obtained by dividing the LULC area difference between two periods. Moreover, the relative change in LULC categories between each consecutive time horizon was estimated using the following

$$A = Af - Ai \tag{3.3}$$

Where A is absolute areal change in LULC classes, Af is area of the LULC class at final later period, Ai is area of the LULC at initial period.

$$A(\%) = \frac{Af - Ai}{Ai} \tag{3.4}$$

Where $A(\%)$ is a relative area change of LULC class between later periodAf, and initial period Ai.

3.4. Data Analysis

The hydro-meteorological data for water resources management studies should be stationary, consistent and homogeneous when used for hydrologic system simulation. The time-series data may be subject to jumps, inconsistency and non-homogeneity due to various driving factors. The hydro-meteorological data need an extensive analysis and investigation to represent the real process taking place in the environment and for a good estimation of the hydrologic process quantities (Dahmen and Hall, 1990).

3.4.1. Filling missing data

The meteorological data collected from the five stations (AA Bole, AA Obs, Akaki, Intoto and Dire Gidib) for this study have missing data for some time. There are different methods to fill the missed data such as Arithmetic Mean method, Normal Ratio method, Inverse Distance Weighting method etc. However, for this study, the R-program (Climatol package) in R studio software was employed to estimate the missing values of daily rainfall data series.

The R package Climatol (https://CRAN.R-project.org/package=climatol) contains functions for quality control, homogenization, and filling of the missing data in a set of data series of the climatic variable. Filling the missing data by estimates calculated from the closest series. This was done by adapting by averaging neighboring values and normalized by dividing them by their respective average rainfall. Climatol also offers the possibility of subtracting the means or applying a full standardization (Guijarro, 2018).

Guijarro (2018) considers letting mX and sX be the average and standard deviation of an X series, and introduces these options for their normalization:

i. Remove the mean: $x = X - mX$ (3.5)

ii. Divide by the mean: : $x = X/mX$ (3.6)

iii. Standardize: $x = (X - mX)/sX$ (3.7)

The Climatol first calculates these parameters with the available data in each series, fill in the missing data using these provisional averages and standard deviations, and recalculates them with the in-filled series. Then the data originally missing data are recalculated using the new parameters, which will lead to new means and standard deviations, hence repeating the process until no average changes when rounded up to the initial precision of the data. Once the means become stable, all data are normalized and estimated by means of the simple expression:

$$\widehat{Y} = \frac{\sum_{j=1}^{j=n} Wj * Xj}{\sum_{j=1}^{j=n} Wj} \tag{3.8}$$

Where $\widehat{Y}$ is a data item estimated from their corresponding nearest "n" data available at each time step, and Wj is the weight assigned to them.

The major advantages of R package climatol homogenization strategy are its ability to:

i. Automatically homogenize a large number of climate data series, including short term ones and without needing site metadata,
ii. Use the closest reference series even not sharing a common period with candidate series or presenting missing data; and
iii. Supply homogenized series, correcting anomalous data (quality control by spatial coherence), and filling in all the missing data (Azorin-Molina et al., 2019).

In the last few years Climatol has been widely applied to homogenize a variety of climate databases. For instance, Czerenecki et al. (2019) were applying R package for meteorological and hydrological data sets for environmental assessment. The daily peak wind also homogenized by R package climatol version 3.1 in Australia (Azorin-Molina et al., 2019). The research conducted by Nimac and Tadic (2017) in Croatia for interpolation of missing data and homogenization of climatological series for construction of 1981 to 2010 climatological normal applied the R package climatol. The climatol package and its programming code (algorithms) used in the big Akaki watershed for filling the missing data are illustrated in Appendix A.2.

3.4.2. Consistency test

The time series of hydro-meteorological data shows inconsistency due to outliers that arise from different errors. Inconsistency is a change in the amount of systematic error in recording data due to the use of different instruments and observation methods (Dahmen and Hall, 1990). The precipitation time series data of the study area stations may be subjected to outliers due to the replacement of a rain gauge, shifting of the instrument to a new location, precipitation observation errors, etc. The outlier that exists in the precipitation time series makes the data inconsistent.

A Double Mass Curve (DMC) was used to check the consistency of rainfall time series data for this study. A Double mass curve (DMC) is a graph of the cumulative of one quantity against the cumulative of another quantity during the same period plot as a straight line as long as the data are proportional, the slope of the line represents the constant of proportionality between the quantities. The DMC is plotted by taking the summation of a rainfall series for the rain gauge station whose consistency is to be checked against the summation of the average rainfall of the remaining rainfall gauge stations in the area under consideration (Khalil, 2021; Searcy and Hardison, 1960).

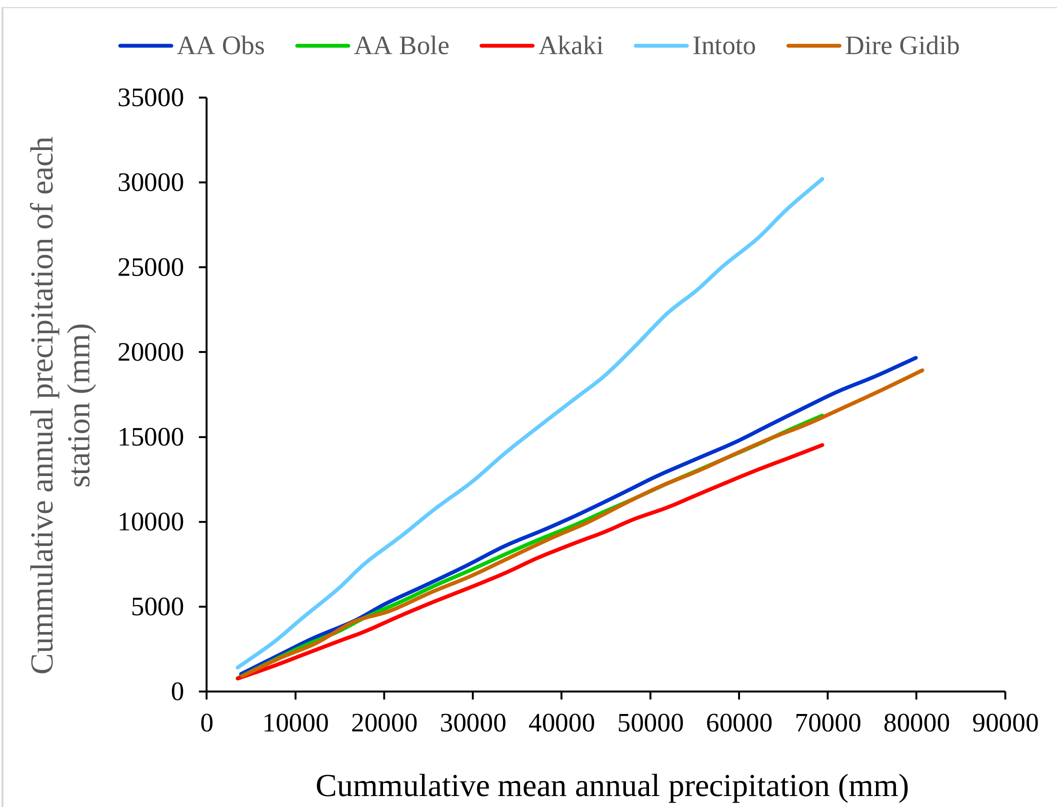

Figure 3. 9 Double Mass Curve for five representative stations of big Akaki Watershed

DMC analysis assumes a linear relationship between time series of precipitation data and is used for checking the consistency of precipitation data. The rainfall data are consistent when the DMC follows a straight line. A beak in the slope of DMC indicates the change in the constant of proportionality between two variables has occurred. All stations used in the study area should be tested for consistency by plotting it against the pattern and those records that are inconsistent should be eliminated from the pattern. The DMC is applicable in many studies all over the world to check the consistency of climate data for assessing hydrological process simulation. The cumulative rainfall for each station in the study area was plotted against the cumulative rainfall of other stations in the study area for this research. In this study as indicated in figure 3.9, the graphical inspection of DMC showed that no significant inconsistency in all stations used in the big Akaki watershed.

3.4.3. Homogeneity test

Non-homogeneity is a change in the statistical properties of the time-series data (Dahmen and Hall, 1990). Homogeneity tests are used to assess the impact of non-climatic factors such as instrument changes, observation practices, rain gauge station relocations, and station environments on climate time series data (Khalil, 2021). The common method to assess the impact are the Pettitt test, Standard normal homogeneity test (SNHT), Buishand test and Von Neumann test. The homogeneity test was conducted using RAINBOW software (Raes et al., 2006) for this study. RAINBOW is a software package developed by the Institute for Land and Water Management of the K.U. Leuven. The program is designed to test the homogeneity of hydrologic records and to execute a frequency analysis of rainfall and evaporation data. In RAINBOW software, the homogeneity test is based on the adjusted partial sums or cumulative deviations from the mean (Raes et al., 2006). One of the tests of homogeneity (Buishand, 1982) is based on the cumulative deviations from the mean:

$$S_k = \sum_{i=1}^{k}(X_i - \overline{X}) \qquad (3.9)$$

K= 1, 2,…,n :

Where X_i are the records from the series X1, X2…Xn and $\overline{X}$ the mean. The initial value of Sk=0 and last value Sk=n are equal to zero. When plotting the Sk's (also called a residual mass curve) changes in the mean are easily detected. For a record Xi above normal the Sk=i increases, while for a record below normal Sk=i decreases. For a homogenous record, one may expect that the Sk's fluctuate around zero since there is no systematic pattern in the deviations of the Xi's from their average value X.

When the cumulative deviation crosses one of the horizontal lines, the homogeneity of the dataset is rejected with 90%, 95% and 99% probability, respectively (Raes et al., 2006). For this study, the homogeneity of the datasets were evaluated and the cumulative deviation of the representative stations were not crossed the horizontal line at 90%, 95% and 99% probability, respectively as shown in figure 3.10 for AA Obs meteorological station and in Appendix B.1 for remaining stations.

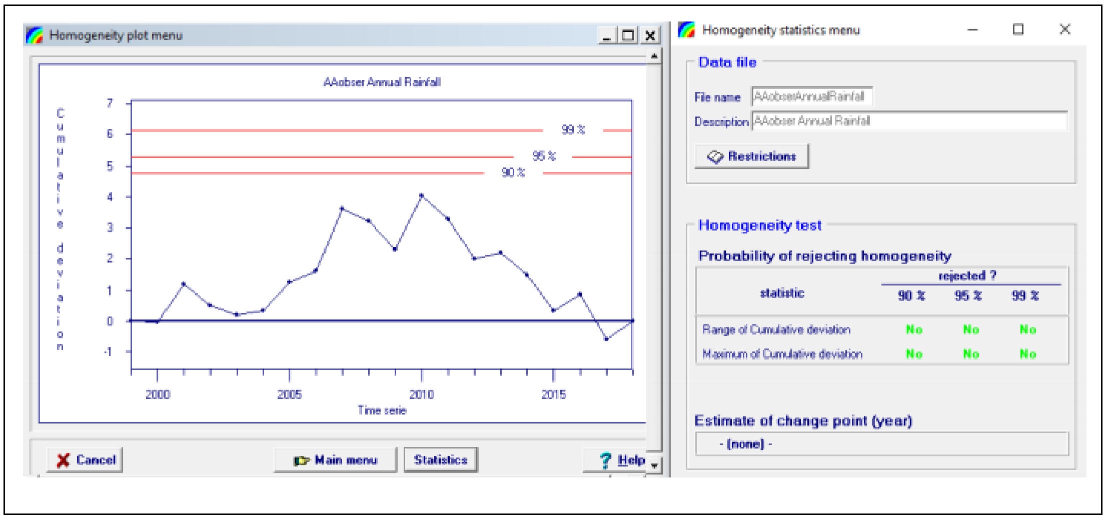

Figure 3. 10 Homogeneity test for AA Obs rainfall station

3.5. Hydrological Model Setup and Simulation

3.5.1. Hydrological components of SWAT

The Soil and Water Assessment Tool (SWAT) model is a semi-distributed physically-based model that operates on a daily time step and is designed to predict the impact of land use and management on water, sediment, and agricultural chemical yields and is computationally efficient and capable of continuous simulation over long periods (Arnold et al., 2012). The watershed hydrological simulation can be categorized into two major components. They are the land phase and the routing phase of hydrological cycle. The land phase of hydrological cycle regulates the amount of water, sediment, nutrient and pesticide loading to the main channel on each sub-basin. Hydrological components simulated inland phase of the hydrological cycle are surface runoff, evapotranspiration, infiltration, lateral subsurface flow, redistribution, canopy storage, ponds, tributary channels, and return flow. The routing phase of hydrological cycle can be defined as the movement or transport of water, sediment, nutrients, and pesticide loading through the channel network of the watershed to the outlet (Neitsch et al., 2011).

SWAT simulates the land phase of the hydrological cycle based on the water balance equation as follows:

$$SW_t = SW_0 + \sum_{i=0}^{t}\left(R_{day} - Q_{surf} - E_a - W_{sweep} - Q_{gw}\right) \qquad (3.10)$$

Where SW_t is the final soil water content (mm), SWo is the initial soil water content on day i (mm), t is the time (days), R_{day} is the amount of precipitation on day i (mm), Q_{surf} is the amount of surface runoff on day i (mm), E_a is the amount of evapotranspiration on day i (mm), W_{sweep} is the amount of water entering the vadose zone from the soil profile on day i (mm), and Q_{gw} is the amount of return flow on day i (mm).

3.5.1.1. Surface runoff

Surface runoff flow is a flow that occurs along a sloping surface and it occurs whenever the rate of water application to the ground surface exceeds the rate of infiltration (Neitsch et al., 2011). There are two method for estimating surface runoff in SWAT: the SCS curve number procedure (USDA SCS, 1972) and the Green and Ampt infiltration method (Green and Ampt, 1911). The SCS CN method was adopted in this study since the sub-daily rainfall data was not available to apply the Green and Ampt infiltration method. In SCS CN method, the ratio of actual retention to maximum retention is assumed to be equal to the ratio of direct runoff to rainfall minus initial abstraction (Kassa, 2009). The curve number equation (SCS, 1972) is:

$$Q_{surf} = \frac{\left[\left(R_{day} - Ia\right)\right]^2}{\left(R_{day} - Ia + S\right)} \qquad (3.11)$$

Where Q_{surf} is the accumulated runoff (mm), R_{day} the rainfall depth for the day (mm), Ia is the initial abstraction (mm, surface storage, canopy interception, infiltration prior to runoff) and S is the potential maximum moisture retention after runoff begins (mm).

The retention parameter varies spatially due to changes in soils, land use, management and slope and also temporally varies due to changes in soil water content. The retention parameter is computed as:

$$S = 25.4 * (\frac{1000}{CN} - 10) \tag{3.12}$$

Where CN is the curve number for the day. The initial abstractions, Ia is commonly approximated as 0.2 S.

$$Q_{surf} = \frac{[(R_{day} - 0.2S)]^2}{(R_{day} + 0.8S)} \tag{3.13}$$

SCS defines three antecedent moisture conditions: I-dry (wilting point), II-average moisture and III-wet (field capacity). The moisture condition I curve number is the lowest value the daily curve number can assume in dry conditions. The curve numbers for moisture conditions I and III are calculated as follows:

$$CN_1 = CN_2 - \frac{CN_2 - 20(100 - CN_2)CN_1}{[100 - CN_2 + \exp(2.533 - 0.0636(100 - CN_1))]} \tag{3.14}$$

$$CN_3 = CN_2[\exp(0.00673(100 - CN_2))] \tag{3.15}$$

Where CN1 is curve number for moisture condition I, CN2 is curve number for moisture condition II and CN3 is curve number for moisture condition III.

3.5.1.2. Evapotranspiration

Evapotranspiration (ET) is a combined process of evaporation and transpiration by which the water is converted to water vapor (Kassa, 2009). It is a term used to refer the sum of evaporation and transpiration from the Earth's land surface to the atmosphere. Evaporation is a process in which the water from rivers, lakes, reservoirs, seas and oceans, water tables at or close to the land surface changed to atmospheric water vapor, whereas transpiration is a process by which the water evaporated from vegetated surfaces, forests and woodland and other plants through leaf stomata (Yadeta et al., 2020). The current available evaporable water, and plant cover and soil characteristics are considered as a factor to categorize the ET as potential ET (PET) and reference ET (ETo). Consequently, PET is the evaporation from an extended surface of a short green crop that fully shades the ground, exerts little or negligible resistance to the flow of water, and is always well supplied with water (Kassa, 2009; Penman, 1956).

SWAT incorporated three methods to estimate PET: the Penman-Manteith method (Monteith, 1965), Priestley-Taylor method (Priestley and Taylor, 1972), and Hargreaves method (Hargreaves et al., 1985). Penman-Manteith method requires solar radiation, air temperature, relative humidity and wind speed. Priestley-Taylor method requires solar radiation, air temperature, and relative humidity. Hargreaves method requires only air temperature. Based on the availability of input data, the Penman-Monteith method was applied to estimate the PET of the study area.

3.5.1.3. Baseflow estimation

Baseflow is the volume of streamflow emerging from the groundwater (Kassa, 2009). SWAT classifies the aquifers into two in each sub-basin to simulate the system. The shallow (unconfined) aquifer is an aquifer that contributes to flow in the main channel or reach of the sub-basin. Deep (confined) aquifer is a type of aquifer that is assumed to contribute to streamflow outside of the watershed (Arnold et al., 1993; Neitsch et al., 2011). The contribution of groundwater to streamflow is simulated by creating shallow aquifer storage (which is recharged by percolation process). The water balance for the shallow aquifer in SWAT is calculated as:

$$Aqsh,i = Aqsh,i - 1 + Wrchrg,sh - Qgw - Wrevap - Wpump,sh \tag{3.16}$$

Where $Aqsh,i$ and $Aqsh,i-i$ is the shallow aquifer storage (mm) on day i and $i-i$ respectively, $Wrchrg,sh$ is the recharge entering the aquifer on day i (mm), Qgw is the groundwater flow or baseflow into the main channel on day i (mm), $Wrevap$ is the amount of water moving into the soil zone in response to water deficiencies on day i (mm), $Wpump,sh$ is the amount of water removed from the shallow aquifer by pumping on day i (mm).

The shallow aquifer contributes baseflow to the main channel or reaches within the sub-basin. The steady state response of groundwater flow to recharge is estimated as (Hooghoudt, 1940):

$$Qgw = \frac{8000 * Ksat}{Lgw} * hwtbl \tag{3.17}$$

Where Qgw is the groundwater or base flow into the main channel on day i (mm), $Ksat$ is the hydraulic conductivity of the aquifer (mm), Lgw is the distance from the ridge or sub-basin divide for the groundwater system to the main channel (m) and $hwtbl$ is the water table height (m)

Water table fluctuations due to non-steady state response of groundwater flow to periodic recharge are calculated (Smedema and Rycroft, 1983):

$$\frac{dhwtbl}{dt} = \frac{Wrchrg,sh - Qgw}{800 * \mu} \tag{3.18}$$

Where $\frac{dhwtbl}{dt}$ is the change in water table height with time (mm/day), $Wrchrg, sh$ is the amount of recharge entering the shallow aquifer on day i (mm), Qgw is the groundwater flow into the main channel on day i (mm), and μ is the specific of the shallow aquifer (m/m).

The water balance for the deep aquifer is calculated as:

$$Aqdp, i = Aqdp, i - 1 + Wdeep - Wpump, dp \tag{3.19}$$

Where $Aqdp, i$ is the amount of water stored in the deep aquifer on day i (mm), $Aqdp, i - 1$ is the amount of water stored in the deep aquifer on day $i - 1$ (mm), $Wdeep$ is the amount of water percolating from the shallow aquifer into the deep aquifer on day i (mm), and $Wpump, dp$ is the amount of water removed from the deep aquifer by pumping on day i (mm).

3.5.1.4. Flow routing

Manning's equation is used to define the rate and velocity of water flow (Neitsch et al., 2011). After the model determines flow to the main channel, SWAT incorporates two methods to route water through the channel network: Variable storage and Muskingum routing methods. The Muskingum routing method is one of the channel routing methods incorporated in the SWAT model that models the storage volume in a channel length as a combination of wedge storage and prism storage. The variable storage routing method was developed by Williams (1969) that used in the HYMO (Williams and Hann, 1973) and ROTO (Arnold et al., 1995) models have been used in this study. The variable storage method is based on the concept of the continuity equation.

$$Vi - Vout = \Delta Vstored \tag{3.20}$$

Where Vi is the volume of inflow during the time step (m^3), $Vout$ is the volume of outflow during the time step (m^3), and $\Delta Vstored$ is the change in volume of storage during the time step (m^3). The detail of this method is explained in the SWAT theoretical documentation version 2009.

3.5.1.5.Sediment component of SWAT

Sediment yield is the sum of the sediments produced by overland flow, gully, and stream channel erosion in a catchment. Sediment transport in the channel network is a function of degradation and aggradation (Neitsch et al., 2005). The SWAT model can be used for sediment yield predictions for planning and management of water resources and reservoir sediment controls at the catchment scale. The soil erosion caused by rainfall and runoff is computed using the Modified Universal Soil Loss Equation (MUSLE) (Williams, 1975) is used in SWAT model. In MUSLE, the rainfall energy factor is replaced by the runoff factor to improve the sediment yield prediction, eliminates the need for delivery ratios, and allows the equation to be applied to each storm events (Neitsch et al., 2011).

The MUSLE (Williams, 1975) is computed as follow in equation 3.21 for this study:

$$Sed = 11.8 * (Qsurf * qpeak * area_{hru})^{0.56} * K_{USLE} * C_{USLE} * P_{USLE} * LS_{USLE} * CFRG \quad (3.21)$$

where Sed is the sediment yield on a given day (metric tons), $Qsurf$ is the surface runoff volume (mm), $qpeak$ is the peak runoff rate (m^3/s), $area_{hru}$ is the area of the HRU (ha), K_{USLE} is the USLE soil erodibility factor (0.013 metric ton m^2 hr/ (m^3-metric ton cm)), C_{USLE} is the USLE cover and management factor, P_{USLE} is the USLE support practice factor, LS_{USLE} is the USLE topographic factor and $CFRG$ is the coarse fragment factor. The detail of this method is explained in the SWAT theoretical documentation version 2009.

3.5.2. SWAT model setup

SWAT model is a semi-distributed model that could best predict hydrology and sediment yield under land use dynamics. The SWAT model is a physically-based model designed to predict the impact of land management practices on water, sediment, and agricultural chemical yields in large complex watersheds with varying soil, land-use, and management conditions over long periods of time (Arnold et al., 2012). A basin is divided into a number of sub-basins. Sub-basins are also further divided into hydrological response units (HRUs) based on the homogeneity of soil types, land-use types, and slope classes. The SWAT model (Arnold et al., 2012) requires input data such as topography, soil, and land use along with hydro-meteorological data to simulate hydrological processes. The SWAT model setup incorporates the components such as Watershed delineation, Hydrologic Response Unit (HRU), Sensitivity analysis and calibration and Validation of the model. In this study, SWAT-2012 interface compatible with Arc GIS 10.4 (Arc SWAT 2012) was used to set up a SWAT model for the big Akaki watershed to assess the impact of dynamic LULC on hydrological responses by comparing the static and dynamic land use. Both model setups (static and dynamic) used the same input data, but different land use data. The static land use setup used only the 2000 land use data for the entire simulation period (2000-2018), whereas the dynamic land use setup used 2000, 2010 and 2020 land use data to simulate the hydrologic process. These land use data were applied using the SWAT Land Use Update Tool (SWAT-LUT) of the SWAT for dynamic model setup.

3.5.2.1. Watershed delineation

Watershed delineation is the first step in generating the SWAT model. After the preparation of spatial input data such as DEM, soil and land use data and project into the UTM zone 37 projection to assure map overlapping in Arc GIS 10.4 software, then the watershed was delineated in Arc SWAT in which the Arc GIS is an interface. The DEM of 30 m resolution was used for delineating the watershed and sub-watershed. The delineation process involves five major steps: DEM setup, stream definition, inlet-outlet definition, watershed outlet selection, and definition and calculation of sub-basin parameters. Once the DEM setup is completed and the DEM projection setup was selected, then the model automatically computes the flow direction and accumulation. The threshold area was required to determine the minimum drainage area for stream network definition. The smaller threshold area gives more detail of the drainage network, large number of sub-basins and HRUs and vice versa. For this study, the minimum threshold area of 2000ha proposed by the model was used to define the stream. The stream network, sub-basins, and sub-basin parameters were subsequently calculated using the respective tool. As the result, the big Akaki watershed was divided into 27 sub-basins as shown in Figure 3.11.

3.5.2.2. Hydrologic response unit's definition

Hydrologic Response Units (HRUs) are referred to as the smallest lumped land use area of the sub-basin that comprised of unique land cover, soil, slope, and management combinations and enable the model to reflect differences in precipitation, evaporation, infiltration, runoff and other processes for different land cover, soil and slope (Arnold et al., 2012). The HRU analysis in SWAT includes the delineation of HRUs by overlaying the spatial map of slope classes, land use, and soil data. Hydrologic simulations on the HRU level help to visualize the spatial variation of water balance components of the basin in a relatively smaller area which is vital for planning watershed interventions (Shawul et al., 2019).

The delineated watershed, land use, and soil map were overlapped 100%. The multiple slope option which is considering different slope classes for HRU definition was selected. The three slope classes (0-10%, 10-20% and >20%) were applied. The LULC, soil and slope map were reclassified to correspond with the parameters in the SWAT database. Then the classified LULC, soil and slope were overlaid for HRU definition. The other step in the HRU analysis was the HRU definition. The HRU distribution was determined by applying multiple HRU definition option. For this particular study a 5 % threshold value for land use, 10 % for soil and 20 % for slope were used to define the HRU. The minor LULC, soil and slope less than the threshold value was removed. The 2000 land use data was used to define the HRUs in both static and dynamic model setup since it represents the beginning phase of the model simulation period. For the dynamic model setup, the SWAT-LUT was selected in annual time step to reclassify the map for the period of 2000-2018 to test the linear land use update function. As a result, the watershed of big Akaki was divided into 141 HRUs for static LULC (2000 land use map) and 629 HRUs for dynamic LULC (2000, 2010 and 2020 land use map.

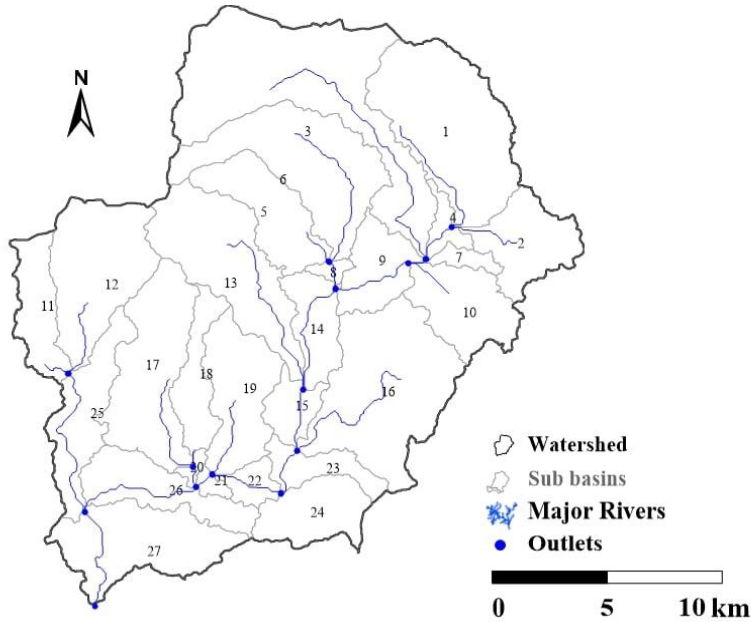

Figure 3. 11 Sub-basins of the study area

3.5.2.3. Weather data

The SWAT model simulation requires the daily precipitation, maximum and minimum temperature, relative humidity, solar radiation, and wind speed to carry out the watershed assessment. However, the meteorological stations in the study area except for AA Obs station has a limitation in relative humidity, solar radiation, and wind speed. To fill such data scarcity in the remaining meteorological stations, the SWAT model incorporates the weather generator (WGN) model to generate in measured records. AA Obs meteorological station was used to generate the missed weather parameter (relative humidity, solar radiation and wind speed) for the rest of the meteorological stations using the weather generator capabilities of SWAT models. The missed data were filled by assigning missed data by -99 identifier to allow the SWAT model to produce weather data from the average monthly value. Once the weather parameters were generated from WGN, it was imported into the SWAT database to generate the weather parameters for the rest of the meteorological stations.

3.6. Sensitivity Analysis, Calibration, and Validation

Physical-based hydrological models can simulate a continuous hydrological process on water resources development and management. The output from such models should be scientifically acceptable to use for decision-making activities on watershed management (Moriasi et al, 2007). The hydrological model simulation output is important in water resource development and decision-making for watershed management making performing sensitivity analysis, calibration, validation, and uncertainty analysis very vital when using the model (Kassa, 2009). The parameters of SWAT input should be within an acceptable uncertainty range. The SWAT Calibration and Uncertainty Program (SWAT-CUP) software package of Sequential Uncertainty Fitting 2 (SUFI-2) algorithm (Abbaspour et al., 2007) was employed for sensitivity analysis, calibration, and validation and uncertainty analysis of the SWAT model.

3.6.1. Sensitivity analysis

Sensitivity analysis is the process of that the rate of change in model output determined with respect to changes in model inputs (parameters). Parameter identification is a necessary process required for model calibration (Moriasi et al, 2007). A complex hydrologic model is generally characterized by a multiple of parameters. Due to spatial variability, measurement error, and incompleteness in the description of both the elements and processes present in the system, the values of many of these parameters are not exactly known. So to achieve a good fit between the observed and simulated data, models need to be conditioned to match reality by optimizing their internal parameters. A parameter sensitivity analysis provides insights on which parameters contribute most to the output variance due to input variability (Holvelt et al., 2005). Sensitivity analysis is conducted to determine the influence of a set of parameters on predicting total flow (Shawul et al., 2019). In SWAT model, parameter sensitivity analysis is carried out in two ways: One-Factor-At-a-Time sensitivity and Global sensitivity analysis.

One-factor-at-a-time sensitivity indicates the variable sensitivity to changes in a parameter if all other parameters are kept constant at some fixed value (Abbaspour, 2015). Latin Hypercube (LH) sampling and one-factor-at-a-time (OAT) are combined in SWAT to analyze the sensitive parameter. LH sampling is based on the Monte Carlo simulation but uses a stratified sampling approach that allows efficient estimation of the output statistics, whereas OAT is a technique that falls under the category of screening methods. Each model run involves perturbation of only one parameter in turn (Kassa, 2009; Saltelli et al., 2000). The disadvantage of one-at-a-time analysis is that the correct values of other parameters that are fixed are never known (Arnold et al., 2012).

In Global sensitivity analysis, the parameter sensitivities are determined by calculating the multiple regression system, which regresses the Latin hypercube generated parameters against the objective function values (Abbaspour, 2015). Global sensitivity analysis can be performed after iteration. Parameter sensitivities are determined by calculating the following multiple regression system, which regresses the Latin hypercube generated parameters against the objective function values.

$$g = \alpha + \sum_{i=1}^{m} \beta i b i \qquad (3.22)$$

Where g is the objective function value, α is the regression constant, and β is the parameter coefficient, b is the model parameter.

A t-test is then used to identify the relative significance of each parameter bi. The sensitivities given above are estimates of the average changes in the objective function resulting from changes in each parameter, while all other parameters are changing. This gives relative sensitivities based on linear approximations and, hence, only provides partial information about the sensitivity of the objective function to model parameters.

The global sensitivity analysis method in SWAT-CUP software package was used for sensitivity analysis for this study. In this analysis, the larger in absolute value, the value of t-stat and the smaller the p-value was accepted as the more sensitive the parameter (Abbaspour et al., 2007). The simulated and observed data and sensitive parameters are considered as input for sensitivity analysis. Once the stream flow sensitivity analysis was performed then sediment yield sensitivity analysis was followed. The parameters identified as more sensitive in influencing the simulated output was used to calibrate a model for this study.

3.6.2. Calibration and validation

Model calibration is the process of estimating model parameters by comparing model prediction (output) for a given set of assumed conditions with observed data for the same conditions. The calibration of the model has been done based on the assumption of there is a linear relation between the observed and the simulated one. That means all of the error variances is contained in the simulated values and the measured data are free of error. But in reality the measured data are not free of error (Moriasi et al, 2007). There are manual Calibration and automatic calibration tools method that incorporated in SWAT or SWAT-CUP (Abbaspour et al., 2007).

Manual calibration is performed manually and consists of changing model input parameter values to produce simulated values that are within a certain range of the measured data. Automatic calibration is a common calibration approach that incorporates the numerical algorithm in the optimization of the objective function intensively (Balascio et al., 1988).

SWAT calibration and uncertainty program (SWAT-CUP) software package (Abbaspour, 2013) is one of the most widely applied programs in SWAT model calibration and sensitivity analysis in many literatures such as Abbaspour et al. (2015); Zhang et al. (2020); Shawul et al. (2019) and Setegn et al. (2010). SWAT-CUP incorporates a semi-automated approach of sensitivity, calibration and uncertainty analysis to provide a decision-making framework (Shawul et al., 2019). Currently, there are five uncertainty techniques available in SWAT-CUP program: Generalized Likelihood Uncertainty Estimation (GLUE) (Beven and Binley, 1992), Particle Swarm Optimization (PSO) (Eberhart and Kennedy, 1995), Parameter Solution (ParaSol) (Griensven and Meixner, 2006), Sequential Uncertainty Fitting-2 (SUFI-2) (Abbaspour et al., 2004) and Markov Chain Monte Carlo (MCMC) (Kuczera and Parent, 1998B) algorithms.

In this study, a semi-automated SUFI-2 algorithm which is one of the uncertainty analysis techniques incorporated in SWAT-CUP was used for streamflow and sediment yield calibration and validation at the big Akaki gauge station.

Once the model was calibrated successfully, model validation was applied. Model validation is the process of demonstrating that a given site-specific model is capable of making sufficiently accurate simulations. Validation involves running a model using parameters that were determined during the calibration process and comparing the predictions to observed data not used in the calibration. Calibration and validation was conducted by splitting the observed hydrological data (streamflow and sediment yield) into a range of two datasets for the big Akaki gauging station. The entire model simulation was set to run for 2000-2018 period by taking the 2 years (2000-2001) as a warm-up period for model initialization. The dataset from 2002-2008 periods and 2009-2012 periods were used for the calibration and validation process, respectively.

3.6.3. Uncertainty analysis

Due to uncertainties such as model input uncertainty, model parameter uncertainty, model structural uncertainty and model response (output) uncertainty, watershed modeling, analysis and assessment become a challenging task. To overcome the uncertainty problem in watershed calibration and analysis, many uncertainty analysis techniques have been developed. Generalized Likelihood Uncertainty Estimation (GLUE) (Beven and Binley, 1992), Particle Swarm Optimization (PSO) (Eberhart and Kennedy, 1995), Parameter Solution (ParaSol) (Griensven and Meixner, 2006), Sequential Uncertainty Fitting-2 (SUFI-2) (Abbaspour et al., 2004) and Markov Chain Monte Carlo (MCMC) (Kuczera and Parent, 1998B) are among the most applicable uncertainty analysis techniques in different watershed across the world.

The goodness of fit and the degree to which the calibrated model accounts for the uncertainties can be assessed by two measures (P-factor and R-factor) in the Sequential Uncertainty Fitting, version 2 (SUFI-2) programs (SWAT CUP). P-factor refers to the degree to which all uncertainties are accounted and which is the percentage of measured data bracketed by the 95% prediction uncertainty (95PPU) whereas the R-factor is a measure of the quality of the calibration and indicates the thickness of the 95PPU and the average thickness of the 95PPU band divided by the standard deviation of the measured data (Abbaspour et al., 2007). In SUFI-2, parameter uncertainty accounts for all sources of uncertainties such as uncertainty in driving variables (e.g., precipitation), conceptual model, parameters, and measured data. The percentage of data captured by the prediction uncertainty is a good measure to assess the strength of our uncertainty analysis. The 95PPU is calculated at the 2.5% (L95PPU) and 97.5% (U95PPU) levels of the cumulative distribution of an output variable obtained through Latin hypercube sampling, disallowing 5% of very bad simulations. Theoretically, the value for P-factor ranges between 0 and 1, while that of R-factor ranges between 0 and infinity. A P-factor of 1 and R-factor of zero is a simulation that exactly corresponds to measured data. The degree to which we are away from these numbers can be used to judge the strength of our calibration. Generally, a P-factor values greater than 0.70 and R-factor less than 1.50 is recommended for the discharge data (Abbaspour et al., 2015).

3.7. Model Performance Evaluation

There are two methods to compare observed data with model predictions during the calibration and validation periods: graphical and statistical methods. Graphical techniques provide a visual comparison of simulated and measured constituent data and the first overview of model performance. According to Moriasi et al. (2007) recommendation the statistical methods namely Coefficient of determination (R^2), Nash-Sutcliffe efficiency (NSE) and Percent bias (PBIAS) were used for evaluating the performance of SWAT model statistically.

Coefficient of determination (R^2) refers to the squared ratio between the covariance and the multiplied standard deviations of the observed and predicted values. It estimates the combined dispersion against the single dispersion of the observed and predicted series (Krause et al., 2005). The value of R^2 ranges between 0 and 1 where, the R^2 value closer to 1 indicates the higher agreement between the simulated and the observed flow data, while the R^2 value close to 0 indicates the poor agreement. It can be calculated as:

$$R^2 = \frac{\left(\sum_{i=1}^{n}[Qo_i - \bar{Q}o][Qs_i - \bar{Q}s]\right)^2}{\sum_{i=1}^{n}[Qo_i - \bar{Q}o]^2[Qs_i - \bar{Q}s]^2} \tag{3.23}$$

Where, Qo_i is observed value, $\bar{Q}o$ is average observed value, Qs_i is simulated value and $\bar{Q}s$ is average simulated value.

Nash-Sutcliffe efficiency (NSE) is a normalized statistic that determines the relative magnitude of the residual variance (“noise”) compared to the measured data variance (“information”) (Nash and Sutcliffe, 1970). NSE indicates how well the plot of observed versus simulated data fits the 1:1 line. NSE values can range between -∞ to 1 and provide a measure how well the simulated output matches the observed data along a 1:1 line (regression line with slope equal to 1) (Arnold et al., 2012). An efficiency of lower than zero indicates that the mean value of the observed time series would have been a better predictor than the model. NSE can be calculated (Nash and Sutcliffe, 1970) as :

$$NS = 1 - \frac{\sum_{i=1}^{n}(Qo_i - Qs_i)^2}{\sum_{i=1}^{n}(Qo_i - \bar{Q}o)^2} \tag{3.24}$$

Where, Qo_i is observed value, $\bar{Q}o$ is average observed value, Qs_i is simulated value and $\bar{Q}s$ is average simulated value.

Percent bias (PBIAS) measures the average tendency of the simulated data to be larger or smaller than their observed data. A positive value PBIAS indicates model underestimation bias and negative value indicates model overestimation bias. The optimal value of PBIAS is 0.0, with low-magnitude values indicating accurate model simulation (Moriasi et al., 2007). PBIAS can be calculated as in equation 2.25:

$$PBIAS = 100\left(\frac{\sum_{i=1}^{n} Qo_i - \sum_{i=1}^{n} Qs_i}{\sum_{i=1}^{n} Qo_i}\right) \quad (3.25)$$

Where, Qo_i is observed value, $\overline{Q}o$ is average observed value, Qs_i is simulated value and $\overline{Q}s$ is average simulated value.

Table 3.5 General performance ratings for the recommended statistics

Performance Rate	R^2	NSE	PBIAS (%)
Very Good	0.70 -1.00	0.75 -1.00	PBIAS ≤ ±10
Good	0.60 - 0.70	0.65 - 0.75	±10 ≤ PBIAS≤ ±15
Satisfactory	0.50 - 0.60	0.50 - 0.65	±15 ≤ PBIAS≤ ±25
Unsatisfactory	< 0.50	< 0.5	PBIAS > ±25

3.8. Analysis of the Impact of Dynamic LULC Changes on Hydrological Responses

Modelling the hydrological responses to dynamic LULC changes in the big Akaki watershed is one of the most aims of this study. This study applied the SWAT hydrological model to assess the impact of static land use and dynamic land use data on hydrological responses of the big Akaki watershed. The two model setups used the same input data, same parameter but different land use data. The calibrated and validated SWAT model was used to assess and compare the impacts of static and dynamic LULC changes on hydrological responses based on 2000 LULC data for static model setup and 2000, 2010 and 2020 LULC data for dynamic setup. The two SWAT model setup simulations were carried out on monthly basis for a period of 2000-2018. The results from the dynamic model to the static baseline compared. The impact of dynamic LULC changes on hydrological responses such as surface runoff, evapotranspiration, water yield, lateral flow, groundwater flow, and sediment yield at basin and sub-basin scale was assessed.

3.9.Flow Chart for the Methodology

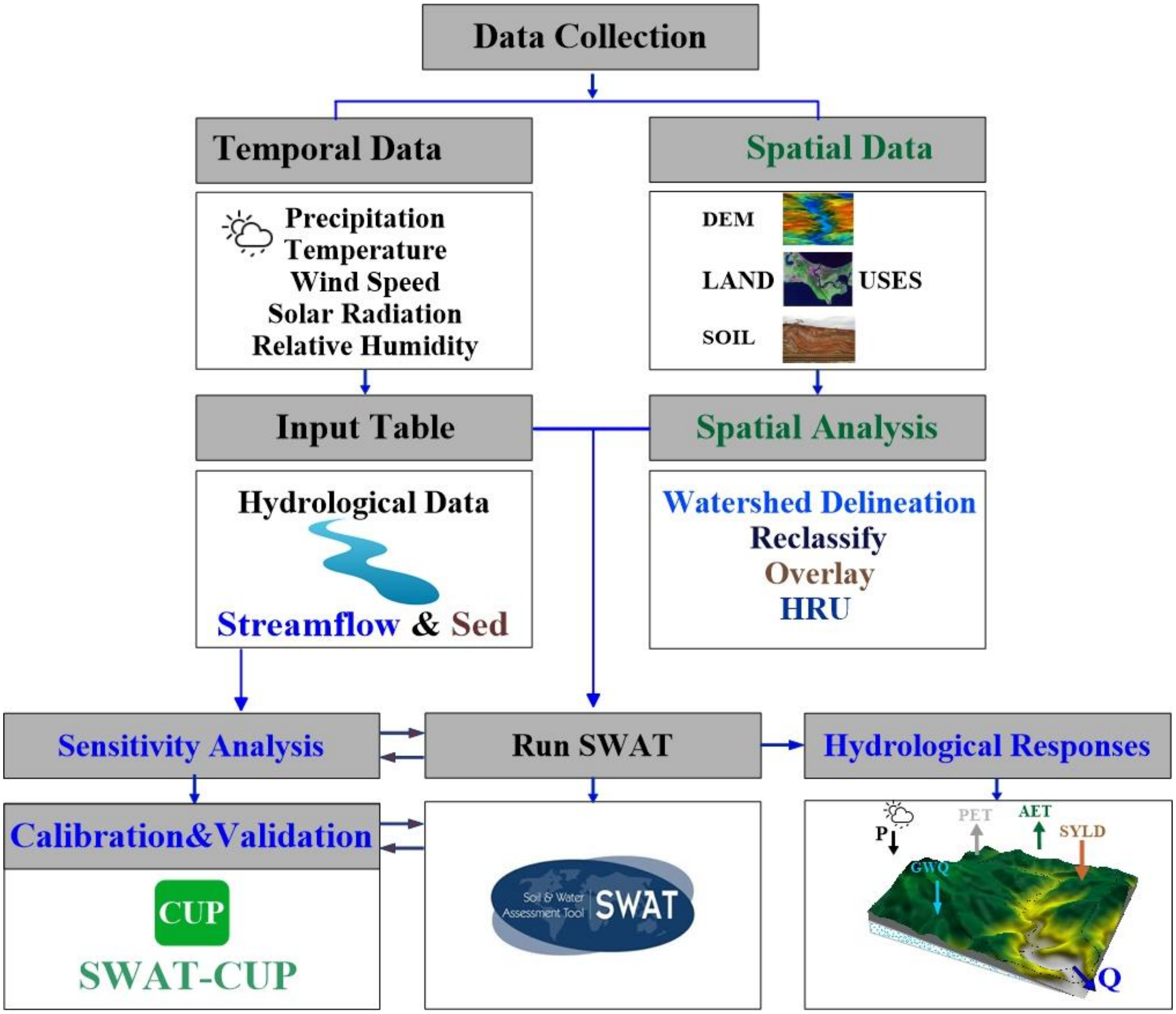

Figure 3. 1 Conceptual framework of the research methodology

4. RESULTS AND DISCUSSIONS

4.1. Land Use Land Cover Change

4.1.1. Land use land cover classification accuracy assessment

The maximum likelihood classification algorithm in the supervised classification method was used to categorize the Landsat images (Landsat 7 ETM+ and Landsat 8 OLI) for the land use period of 2000, 2010, and 2020, respectively into seven dominant LULC classes for the study period of 2000, 2010, and 2020 years in the big Akaki watershed. The error matrix accuracy assessment method was carried out to assess the agreement between labels assigned by the classifier (produced LULC map) and class allocations based on ground data (test data). Thus, the overall accuracy of the classified LULC map for 2000, 2010, and 2020 were 90.50%, 90.00%, and 89.10%, respectively. The kappa coefficient for the LULC maps of 2000, 2010, and 2020 were 0.83, 0.82, and 0.81, respectively. Since all kappa coefficient greater than 0.8, it presenting a very good agreement between classified map and ground truth data (Yang and Lo, 2002). Table 4.1 shows the user accuracy, producer accuracy, overall accuracy, and kappa coefficient for the 2020 LULC map. The accuracy assessments for the LULC map of 2000 and 2010 are illustrated in Appendix A.4.

Table 4.1 LULC classification accuracy assessment for 2020 LULC map

LULC Class	Agricultural	Built-up	Forest	Grassland	Shrubland	Waterbody	Bare land	Total	User accuracy (%)
Agricultural	**115**	**6**	4	8	0	0	1	134	85.82
Built-up	0	**28**	1	0	0	0	0	29	96.56
Forest	0	0	**17**	0	0	0	0	17	100
Grass land	0	1	0	**8**	0	0	0	9	88.89
Shrub land	0	0	0	0	**3**	0	0	3	100
Water body	0	0	0	0	0	**3**	0	3	100
Bare land	1	0	0	0	0	0	**5**	6	83.33
Total	116	35	22	16	3	3	6	201	
Producer accuracy (%)	99.14	80	77.27	50	100	100	83.33		
Overall accuracy	89.10%								
Kappa coefficient	0.81								

4.1.2. Land use land cover classification

The LULC classification was carried out using the maximum likelihood algorithm for 2000, 2010, and 2020 periods for this study. Seven major LULC classes were obtained and classified: agricultural, built-up, forest, grassland, shrubland, water body, and bare land. It can be observed that the agricultural land was the dominant LULC class for all land use periods (2000, 2010, and 2020) followed by built-up and forest land. The agricultural land was dominated in the eastern, southern, and central parts of the watershed whereas the western part of the watershed was mostly covered by built-up area. In the northern part especially in the Intoto Mountains, the forest land was the dominant LULC class. The grassland, shrubland, bare land and water body were other types of LULC classes that were distributed in different parts of the study area.

4.1.3. Land use land cover change detection

LULC change is the result of the long-time process of natural and anthropogenic activities. The LULC change showed a continuous expansion in the spatial extent of built-up area, shrubland and bare land whereas agricultural land and grassland showed a continuous decrement during the study period. The water body showed a slightly a decreasing trend while the forest land showed a slightly an increasing trend.

The LULC map of 2000 shows that the big Akaki watershed was dominated by agricultural land (78.46%), built-up (12.50%), and forest (4.68%) whereas grassland, water body, shrubland and bare land accounted for 3.48%, 0.65%, 0.02%, and 0.20%, respectively. In 2010 and 2020, the agricultural land was also the dominant land use class with area coverage of 78.11% and 75.81%, respectively. The built-up, forest land, grassland, shrubland, water body and bare land were covered 13.37%, 4.96%, 2.13%, 0.49%, 0.63% and 0.29% in 2010 and 15.97%, 4.96%, 2.05%, 0.49%, 0.46% and 0.26% in 2020, respectively. The temporal distribution of the LULC classes in 2000, 2010, and 2020 is indicated below in Table 4.2 and figure 4.2. Figure 4.1 illustrated also the spatial distribution of LULC class during 2000, 2010, and 2020 LULC periods respectively.

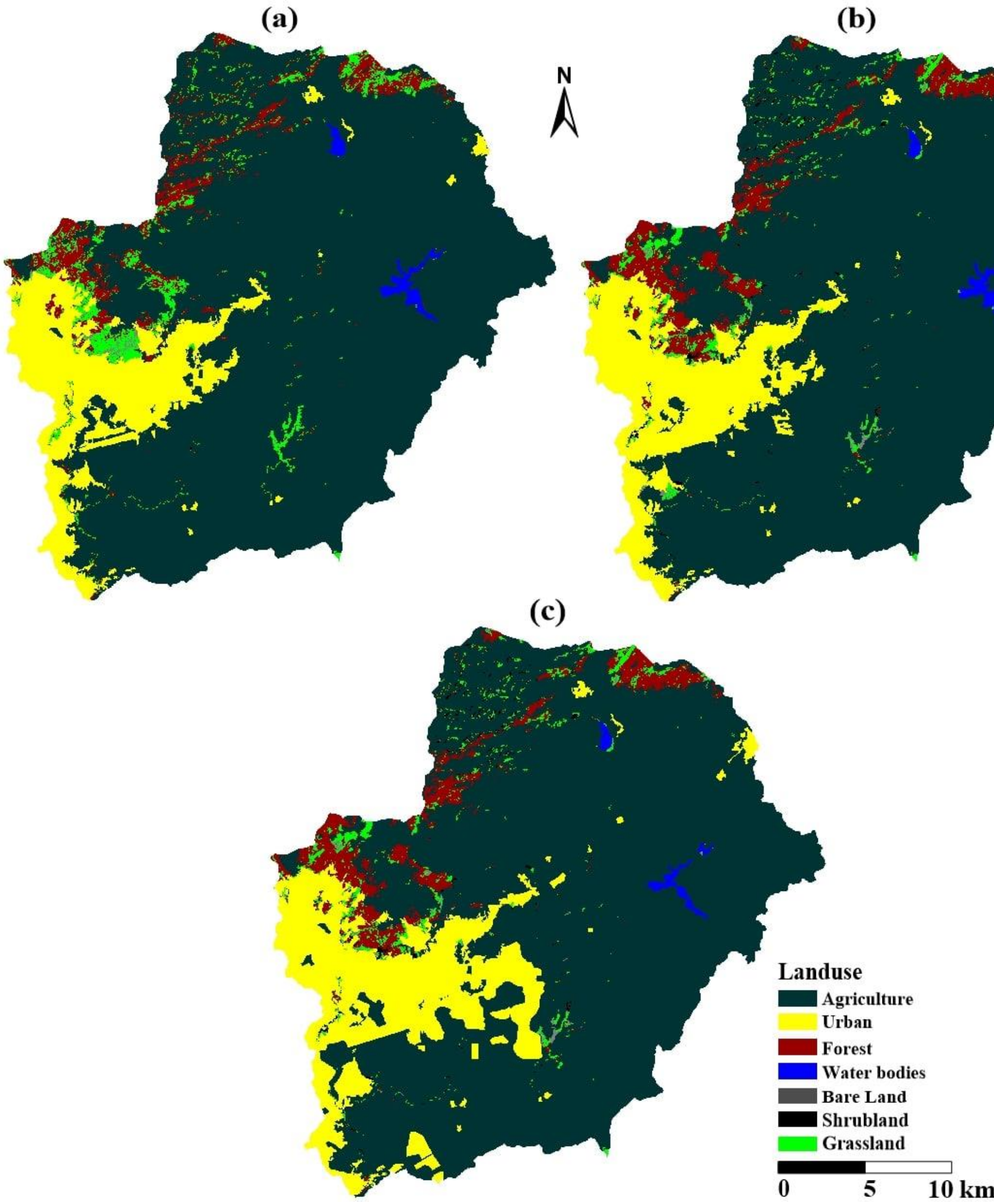

Figure 4. 1 LULC map for (a) 2000, (b) 2010, and (c) 2020 periods

The LULC data during the years 2000, 2010 and 2020, the dominant LULC changes were observed in agricultural land, built-up, grassland, and forest LULC classes as shown in Table 4.3. In the LULC change detection analysis for 10 years from 2000-2010, the area coverage of built-up, forest land, shrubland, and bare land increased by 7.23 Km^2 (0.78%), 2.34 Km^2 (0.28%), 3.96 Km^2 (0.49%) and 0.79 Km^2 (0.09%) with an annual increase rate of 0.72 km^2/yr, 0.23 Km^2/yr, 0.39 Km^2/yr and 0.08 Km^2/yr, respectively, whereas the areal coverage of agricultural land, grassland, and water body decreased by 2.91 Km^2 (0.35%), 11.29 Km^2 (1.35%)

and 0.12 Km^2 (0.02%) with an annual decrease rate of 0.29 Km^2/yr, 1.13 Km^2/yr and 0.012 Km^2/yr. Most of the agricultural land area was converted to built-up (78.10%), shrubland (7.91%), and forest land (5.39%) whereas grassland areas lost were changed to a forest (64.81 %), agricultural land (14.92%), shrubland (7.37%) and built-up (6.58 %).

Table 4.2 The temporal distribution of LULC classes in 2000, 2010 and 2020

LULC Class	2000 LULC		2010 LULC		2020 LULC	
	Area (Km^2)	Area (%)	Area (Km^2)	Area (%)	Area (Km^2)	Area (%)
Agricultural	653.70	78.46	650.79	78.11	631.61	75.81
Built-up	104.16	12.50	111.39	13.37	133.08	15.97
Forest	38.99	4.68	41.33	4.96	41.32	4.96
Grass land	29.02	3.48	17.73	2.13	17.09	2.05
Shrub land	0.19	0.02	4.15	0.49	4.06	0.49
Water body	5.39	0.65	5.27	0.63	3.83	0.46
Bare land	1.70	0.20	2.49	0.29	2.16	0.26
Total	833.15	100	833.15	100	833.15	100

During the years from 2010 to 2020, more changes in agricultural land, built-up and water bodies whereas fewer changes in forest land, shrubland, grassland, and bare land were observed when compared to the first decade (2000-2010). The built-up area was increased from 111.39 Km^2 in 2010 to 133.08 Km^2 in 2020 which indicated that the expansion of 21.69 Km^2 (2.60%) with the annual increasing rate of 2.17 Km^2/yr, While the agricultural land, grassland, water body, and bare land were decreased by 19.18 Km^2 (2.3%), 0.64 Km^2 (0.08), 1.44 Km^2 (0.17%) and 0.32 Km^2 (0.04 %) with an annual decreasing rate of 1.92 Km^2/yr, 0.06 Km^2/yr, 0.14 Km^2/yr and 0.032 Km^2/yr. In contrast to the first time frame (2000-2010), during the year from 2010 to 2020, the forest land and shrubland area remained constant. The rapid built-up expansion during the year 2020 was due to 92.71% of agricultural land and 27.32% of grassland lost to urban and infrastructure construction because of government settlement policy derived from growth and transformation plan launched in 2010 to meet the house demand of urban community. A detailed LULC change detection matrix for 2000-2020 has been presented in Table 4.4. The LULC change detection matrix for the remaining periods (2000-2010 and 2010-2020) has been illustrated in Appendix A.5.

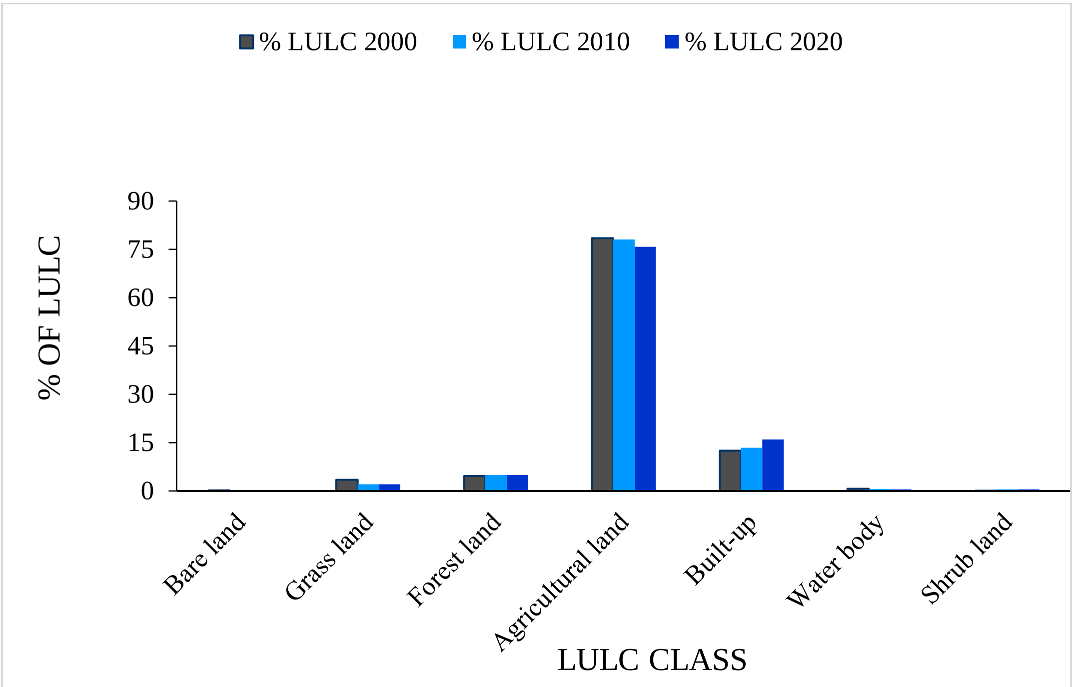

Figure 4. 2 Temporal patterns of LULC at big Akaki watershed

During the study period of 20 years (2000 to 2020), there was an increment in built-up, forest land, shrubland, and bare land areas, whereas the agricultural land, grassland, and water body were showed a decreasing trend. The built-up, forest land, shrubland and bare land were increased by 28.92 Km^2 (3.47%), 2.33 Km^2 (0.28%), 3.87 Km^2 (0.47%) and 0.46 Km^2 (0.06%) with the annual increasing rate of 1.45 Km^2/yr, 0.12 Km^2/yr, 0.19 Km^2/yr and 0.023 Km^2/yr, respectively. In contrast, the agricultural land, grassland, and water body showed a decreasing trend with the change of 22.09 Km^2 (2.65%), 11.93 Km^2 (1.43%), and 1.56 Km^2 (0.19%) with an annual decreasing rate of 1.10 Km^2/yr, 0.59 Km^2/yr and 0.09 Km^2/yr, respectively.

Table 4.3 LULC change detection during 2000-2010, 2010-2020 and 2000-2020

LULC Class	2000-2010 Change			2010-2020 Change			2000-2020 Change		
	Area (Km^2)	Area (%)	Rate (Km^2/yr)	Area (Km^2)	Area (%)	Rate (Km^2/yr)	Area (Km^2)	Area (%)	Rate (Km^2/yr)
Agricultural	-2.91	-0.35	-0.29	-19.18	-2.30	-1.92	-22.09	-2.65	-1.10
Built-up	+7.23	+0.87	+0.72	+21.69	+2.60	+2.17	+28.92	+3.47	+1.45
Forest	2.34	+0.28	+0.23	-0.01	0.00	-0.001	+2.33	+0.28	+0.12
Grassland	-11.29	-1.35	-1.13	-0.64	-0.08	-0.06	-11.93	-1.43	-0.59
Shrubland	+3.96	+0.48	+0.39	-0.09	-0.01	-0.01	+3.87	+0.47	+0.19
Water body	-0.12	-0.02	-0.012	-1.44	-0.17	-0.14	-1.56	-0.19	-0.08
Bare land	+0.78	+0.10	+0.08	-0.32	-0.04	-0.032	+0.46	+0.06	+0.023

The decline in agricultural land and grassland during the study period was due to the expansion of built-up areas in cities such as Addis Ababa because of economic growth, population growth, and migration from other parts of the country for job-seeking, construction of real statehouses, condominiums, industrial parks and other infrastructures at the expenses of agricultural land and grassland (Shawul et al., 2019; Worako, 2016). The increment of forest land from the period of 2000 to 2020 in the big Akaki watershed was due to the government's green legacy strategy to build a green economy and recover the degraded lands to achieve MDG and SDG goals. Research results from previous studies illustrate a similar conclusion. For instance, Shawul and Chakma (2019) reported that the expansion of built-up was observed in the upper Awash river basin at the expense of agricultural land and other natural vegetation due to population growth and socio-economic development in Addis Ababa and surrounding cities over the years of 1974 to 2014. Worako (2016) depicted that the built-up area was raised from 1985 to 2015 at the expense of agricultural land in Akaki watershed. The study reflects that coverage of forests also increased due to the green-based economic development slogan of the government and attention given to the rehabilitation of the degraded areas by government organizations, non-governmental organizations, and other stakeholders. Another study conducted in Addis Ababa and the surrounding Oromia special zone showed that the built-up area was growing from 1.5% in 1984 to 6.7% in 2015 at the expense of agricultural land and mixed woodland. They concluded that the built-up area was the most dynamic land cover type (Mohamed and Worku, 2019).

Table 4.4 LULC change detection matrix of 2000-2020

		2000						
		AL	BU	FL	GL	ShL	WB	BaL
2020	AL	616.26	5.66	4.26	3.22	0.04	1.54	0.04
	BU	34.03	96.49	0.75	1.38	0.03	0	0.09
	FL	1.04	0.62	26.57	12.44	0	0.01	0.57
	GL	0.87	0.87	4.84	9.06	0.04	0.16	0.68
	ShL	0.39	0.19	1.78	1.4	0.05	0.02	0.07
	WB	0.16	0	0	0.01	0	3.66	0
	BaL	0.11	0.06	0.55	1.12	0.01	0.04	0.17

Note: AL= Agricultural land, BU= Built-up, FL= Forest land, GL= Grassland, ShL= Shrubland, WB= Water body and BaL= Bare land

4.2. Streamflow Modelling

4.2.1. Streamflow sensitivity analysis

Sensitivity analysis is important for predicting streamflow sufficiently for a given watershed model (Kassa, 2009). It is a method of identifying the most important sensitive parameters for calibration, validation, and uncertainty analysis of SWAT model (Arnold et al., 2012; Gashaw et al., 2018; Moriasi et al., 2007).

The sensitivity of streamflow of big Akaki watershed was performed using monthly observed data recorded at Akaki gauge station. The global sensitivity analysis was performed using the Sequential Uncertainty Fitting-2 (SUFI-2) algorithm in SWAT Calibration and Uncertainty Program (SWAT- CUP). Accordingly, 16 parameters that have the potential to influence the big Akaki watershed were selected for sensitivity analysis for both static and dynamic model setup based on reviewing previous research works/literature done in different parts watershed and the manual incorporated in SWAT-CUP. The ranges of variation of these parameters are based on absolute SWAT values as indicated in Appendix A.6 is selected. In this analysis, after conducting a number of simulations, the SUFI-2 of SWAT-CUP ranked the most sensitive parameters in consecutive order based on their P-values and t-stat. The larger in absolute value, the value of t-stat, and the smaller the p-value was accepted as the more sensitive the parameter (Abbaspour et al., 2007). The most sensitive streamflow parameters were selected for calibration and validation processes as given below in Figure 4.3.

The result of the analysis as shown in Table 4.5 indicates that parameters namely: Curve number (CN2), Baseflow alpha factor (ALPHA_BF), Groundwater delay (GW_DELAY), Saturated soil conductivity (SOL_K), Soil evaporation compensation factor (ESCO.bsn), Groundwater recharge to deep aquifer (RCHRG_DP), Groundwater 'revap' coefficient (GW_REVAP), Hydraulic conductivity in main channel (CH_K2), Threshold depth of water in the shallow aquifer for 'revap' to occur (REVAPMN) and Available water capacity of the soil layer (SOL_AWC) are the most sensitive parameters for the big Akaki watershed.

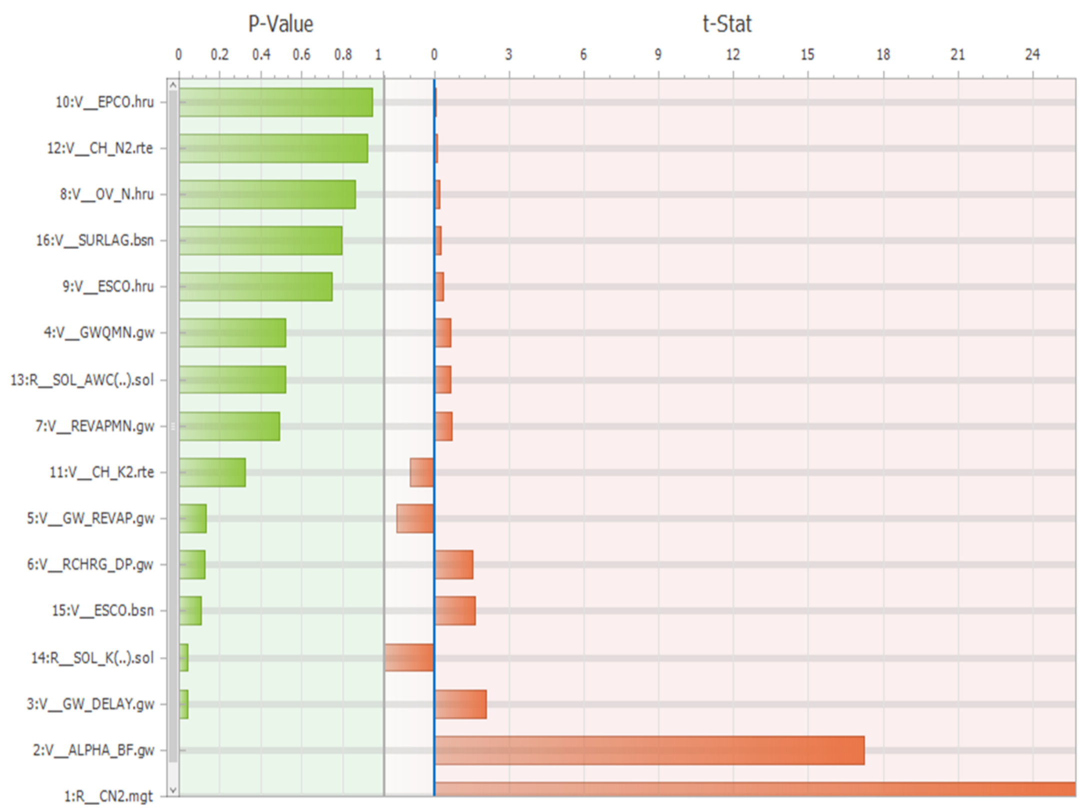

Figure 4. 3 Streamflow sensitive parameters

Surface runoff parameters such as CN_2.mgt, Sol_K.sol, CH_K_2.rte and Sol_AWC.sol were more effective parameters to change in streamflow. The base flow parameters such as ALPHA_BF.gw, GW_DELAY.gw, RCHRG_DP.gw, GW_REVAP.gw and REVAPMN.gw were more sensitive parameters for this study area.

Table 4.5 Streamflow parameter sensitivity rank

Parameter Name	Min value	Max value	Fitted value	t-value	p-value	Rank of sensitivity
CN_2	-0.25	0.25	0.22	25.73	0.00	1
ALPHA_BF	0	1	0.07	17.23	0.00	2
GW_DELAY	0	500	135.99	2.06	0.04	3
SOL_K	-0.25	0.25	0.23	-2.01	0.04	4
ESCO	0	1	0.58	1.61	0.11	5
RCHRG_DP	0	1	0.62	1.53	0.13	6
GW_REVAP	0.02	0.40	0.35	-1.52	0.13	7
CH_K_2	0.01	150	119.43	-0.99	0.32	8
REVAPMN	0	500	88.17	0.69	0.49	9
SOL_AWC	-0.25	0.25	0.18	0.64	0.52	10

4.2.2. Streamflow calibration and validation

The streamflow calibration was applied at Akaki gauge using SUFI-2 algorithm in SWAT-CUP. The first two years (2000-2001) of the simulation were used as a model warm-up to establish proper model initialization conditions and to stabilize the model. The model was calibrated for the period of 2002-2008. The model calibration was performed on monthly bases through the adjustment of sensitive parameters derived from sensitivity analysis. The performance of the model was tested at every stage of the model simulation iteration by changing the parameter value repeatedly within the allowable range until the simulated streamflow agreed with the measured streamflow. Subsequently, the simulated and measured streamflow was validated on the same time steps for the periods of 2009-2012 without further adjustment of calibrated flow parameters.

The SWAT model performance was evaluated by comparing the observed and simulated streamflow data series. The performance indicators such as coefficient of determination (R^2), Nash-Sutcliff efficiency (NSE), and Percent of bias (P_{Bias}) were used to evaluate the SWAT model performance. The performance efficiency values in both calibration and validation proved that SWAT-2012 estimated the streamflow satisfactorily for monthly streamflow time steps for this study. The value of R^2, NSE and P_{Bias} was 0.80, 0.73 and 21.40, respectively for calibration and 0.82, 0.61 and 37.70, respectively for validation for both static and dynamic model set up as indicated in Table 4.6.

Table 4.6 SWAT model performance for streamflow during the calibration and validation periods

Sn.	Performance index	Calibration (2002-2008)	Validation (2009-2012)
1	Coefficient of determination (R^2)	0.80	0.82
2	Nash-Sutcliff efficiency (NSE)	0.73	0.61
3	Percent of bias (P_{Bias})	21.40	37.70

According to performance rating criteria proposed by Moriasi et al. (2007) the values of R^2, NSE, and P_{Bias} for monthly streamflow simulation can be rated as satisfactory to very good for both the calibration and validation periods except for the P_{Bias} was unsatisfactory (37.70) during validation. The unsatisfactory result of P_{Bias} value during the validation period was due to the measured streamflow data quality problem. The positive value of P_{Bias} showed that the model underestimating the streamflow during both the calibration and validation.

The graphical analysis of measured and simulated data as illustrated in Figures 4.4 and 4.5 clearly presents the general trends in the data and differences between model simulations

(Shawul et al., 2019; Kassa, 2009). The simulated and measured streamflow hydrograph and scatter plot during calibration and validation are indicated in Figures 4.4 and 4.5, respectively.

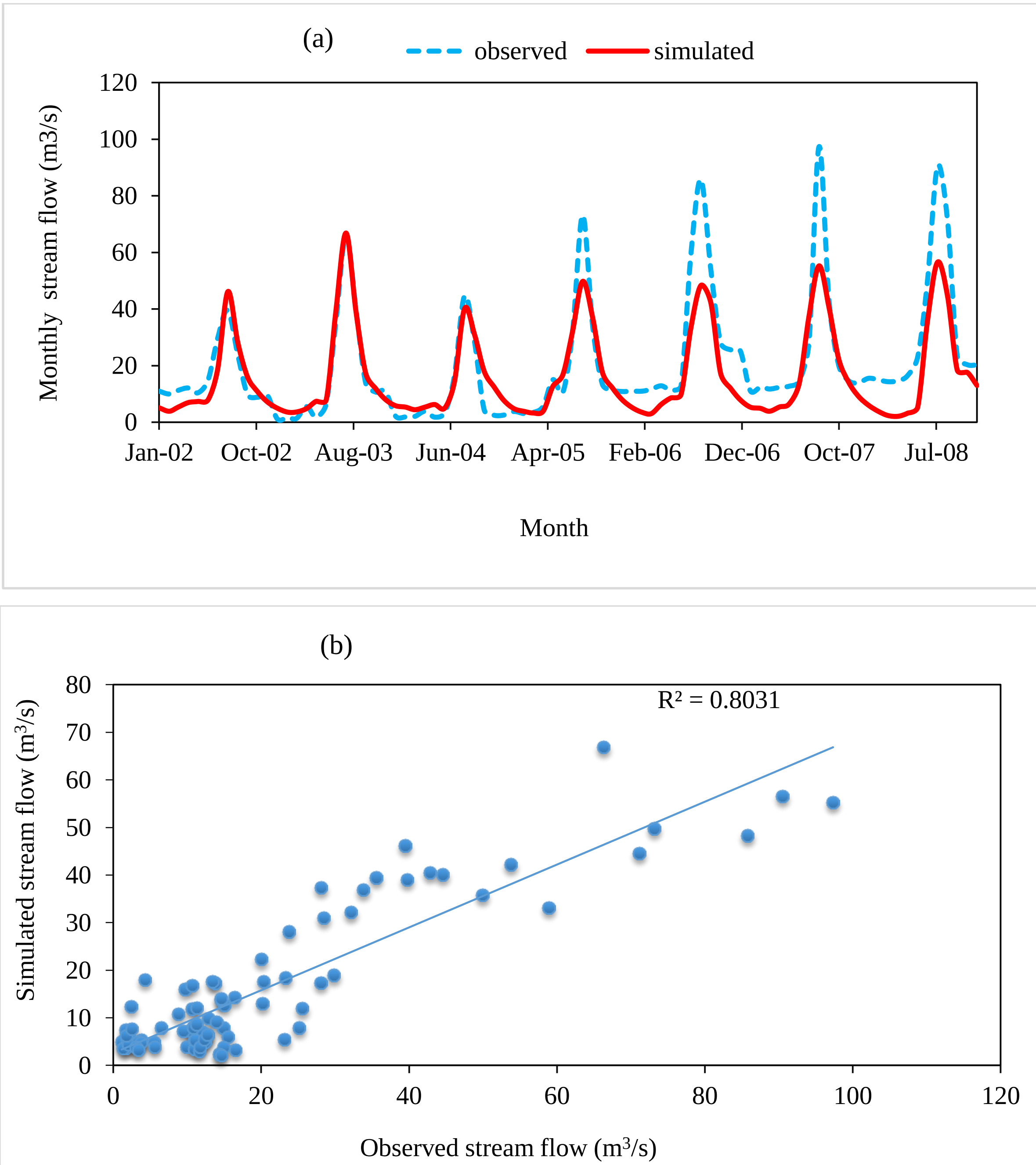

Figure 4. 4 Observed and simulated monthly streamflow hydrograph (a) and scatter plot (b) during calibration periods

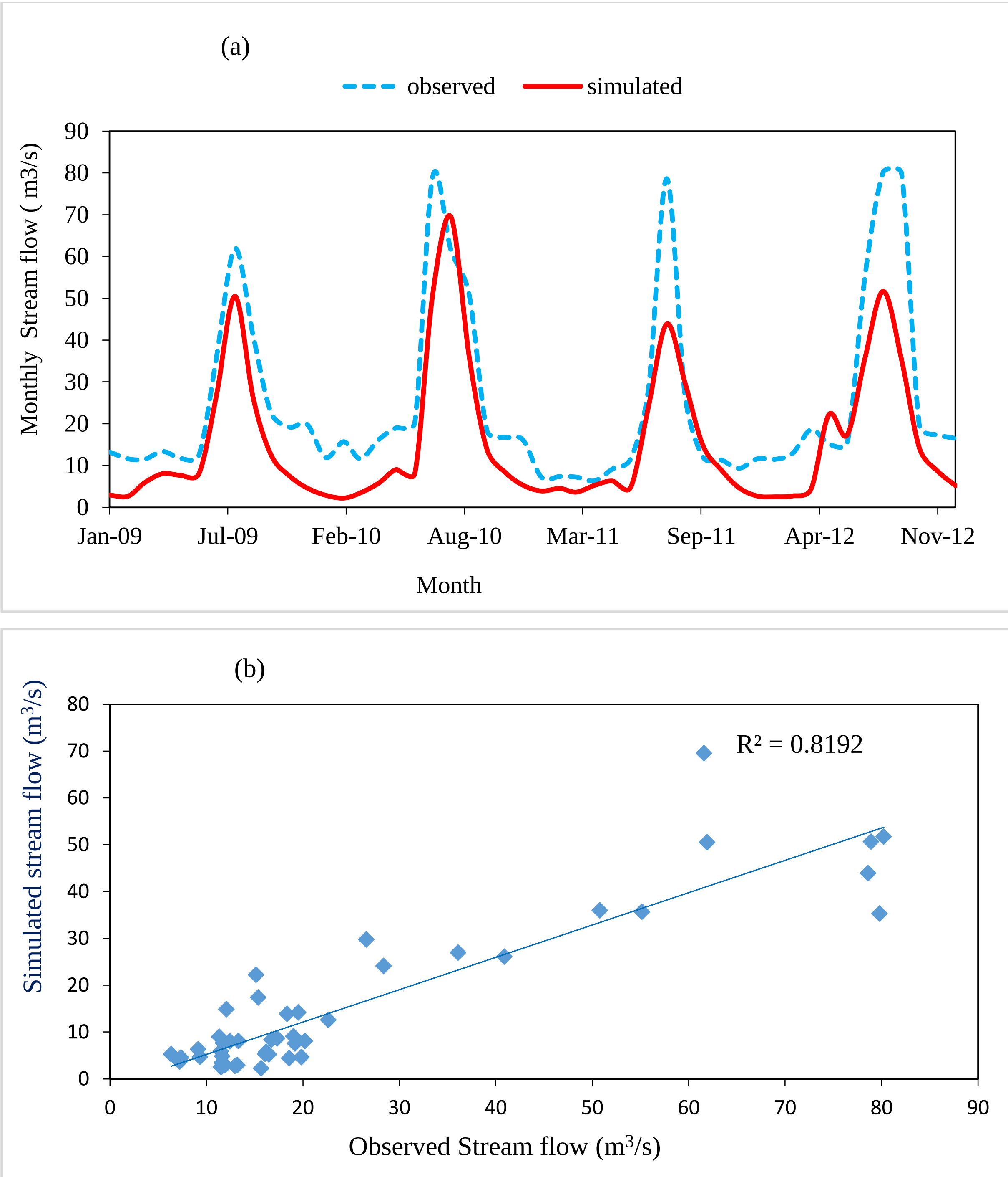

Figure 4. 5 Observed and simulated monthly streamflow hydrograph (a) and scatter plot (b) during validation periods

The model underestimates the flow during peak rainy season months and overestimates during dry months. This is may be due to the uneven representation of rainfall and other climate data inputs, uneven distribution of rain gauge stations in the catchment, the spatio-temporal variability of rainfall data and other instrumental errors and model limitations. These trends were also reported in other previous studies such as Shawul et al. (2019), Teklay et al. (2019), Zeberie (2019), and Aghsaei et al. (2020).

4.2.3. Streamflow uncertainty analysis

The goodness of fit and the degree to which the calibrated model accounts for the uncertainties was assessed by two measures (P-factor and R-factor) in the Sequential Uncertainty Fitting, version 2 (SUFI-2) programs in SWAT CUP (Abbaspour et al., 2004) for this study. P-factor refers to the degree to which all uncertainties are accounted for and which is the percentage of measured data bracketed by the 95% prediction uncertainty (95PPU) whereas R-factor is a measure of the quality of the calibration and indicates the thickness of the 95PPU and the average thickness of the 95PPU band divided by the standard deviation of the measured data (Abbaspour et al., 2007). The output of the uncertainty from the SUFI-2 uncertainty analysis technique of SWAT-CUP program is presented in Figure 4.6 and Figure 4.7 for calibration and validation, respectively. The uncertainty measure of SUFI-2 showed a P-factor of 0.75 and R-factor of 1.00 for calibration and a P-factor of 0.63 and R-factor of 0.98 for validation.

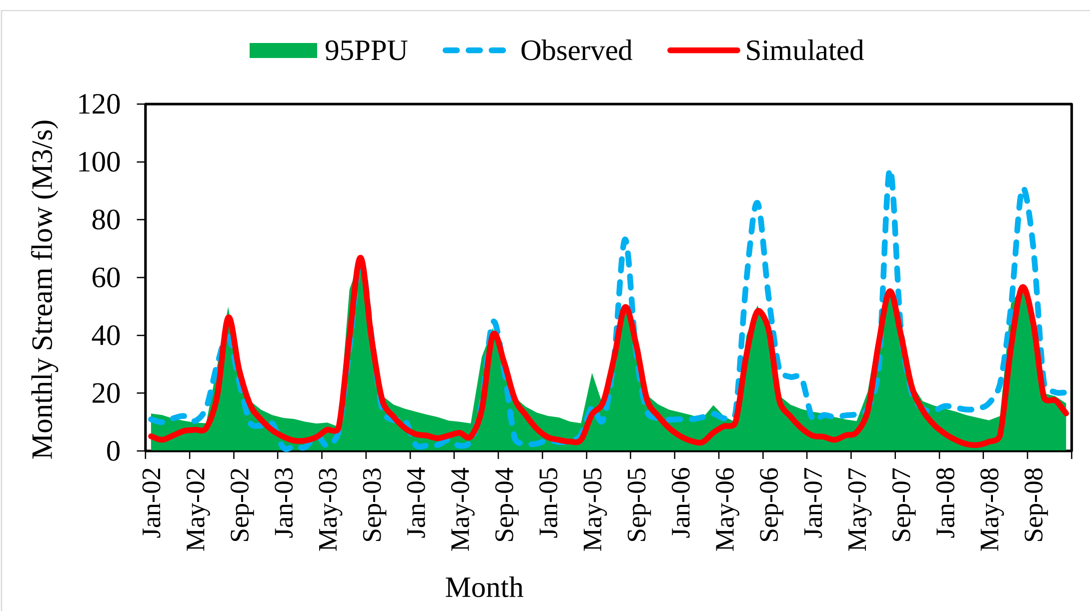

Figure 4. 6 Monthly streamflow calibration showing the 95PPU uncertainty intervals

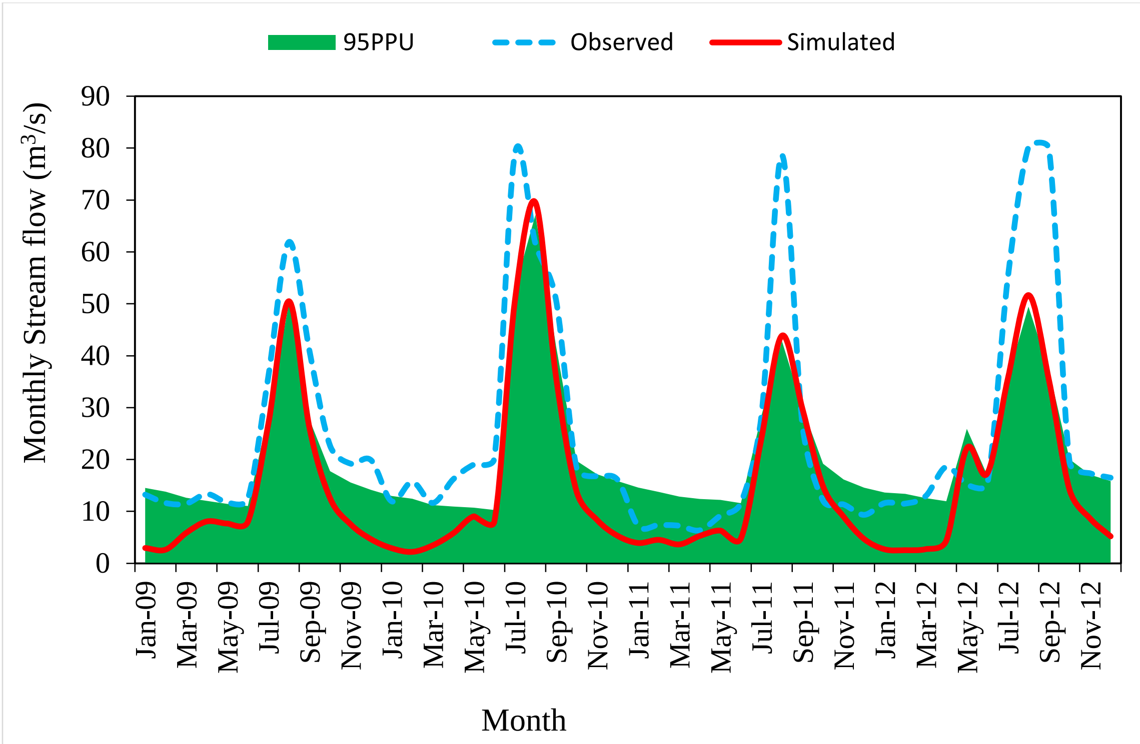

Figure 4. 7 Monthly streamflow validation showing the 95PPU uncertainty intervals

The P-factor and R-factor for both calibration and validation periods showed that the SWAT model was able to capture most of the uncertainties since the P-value is greater than 0.70 and R-factor is less than 1.50 as recommended by Abbaspour et al. (2015) for discharge data. The result obtained from uncertainty analysis in this study was in a similar trend to results reported in other previous studies: for instance, Kassa (2009) conducted research on the Hare watershed and obtained the P-factor of 0.65 and 0.62, and R-factor of 0.58 and 0.40, respectively for calibration and validation. Similarly, Abbaspour et al. (2015) applied a SWAT model in Europe to model hydrology and water quality at a continental scale and conducted that a large number of the outlets fall in desirable regions of P-factor and R-factor indices.

4.3. Sediment Yield Modeling

4.3.1. Sediment yield sensitivity analysis

The sensitivity of sediment yield of big Akaki watershed was performed using monthly observed data recorded at Akaki gauge station. The global sensitivity analysis was performed using Sequential Uncertainty Fitting-2 (SUFI-2) algorithm in SWAT Calibration and Uncertainty

Program (SWAT- CUP). Accordingly, 13 parameters that have the potential to influence the big Akaki watershed were selected for sensitivity analysis for both static and dynamic model setup based on reviewing the previous research works done in different parts watershed and the manual incorporated in SWAT-CUP. The ranges of variation of these parameters are based on absolute SWAT values as indicated in Appendix A.7. In this analysis, after conducting a number of simulations, the SUFI-2 of SWAT-CUP ranked the most sensitive parameters in consecutive order based on their P-values and t-stat. The most sensitive sediment yield parameters were selected for calibration and validation processes as given below in Figure 4.8.

The result of the analysis as shown in Table 4.7 indicates that parameters namely: Curve number (CN2), Sediment routing method (CH_EQN), Channel cover factor (CH_COV2), Biological mixing efficiency (BIOMIX), Channel erodibility factor (CH_ERODMO), USLE equation soil erodibility factor (USLE_K), Linear parameter for calculating the maximum amount of sediment that can be re-entrained during channel sediment routing (SPCON) and USLE equation support practice (USLE_P) are the most sensitive parameters for the big Akaki watershed which is in agreement with other previous studies such as Aghsaei et al. (2020); Molla et al. (2020) and, Biru and Kumar (2017).

Table 4.7 Sediment yield parameter sensitivity rank

Parameter Name	Min value	Max value	Fitted value	t-value	p-value	Rank of sensitivity
CN_2	-0.25	0.25	0.021	-13.15	0.00	1
CH_EQN	0	4	3.32	9.86	0.00	2
CH_COV2	0.001	1	0.97	1.99	0.05	3
BIOMIX	0	1	0.94	-1.59	0.11	4
CH_ERODMO	0	1	0.63	1.54	0.12	5
USLE_K	0	0.60	0.21	-0.87	0.38	6
SPCON	0.0001	0.01	0.002	-0.64	0.52	7
USLE_P	0	1	0.25	0.59	0.55	8

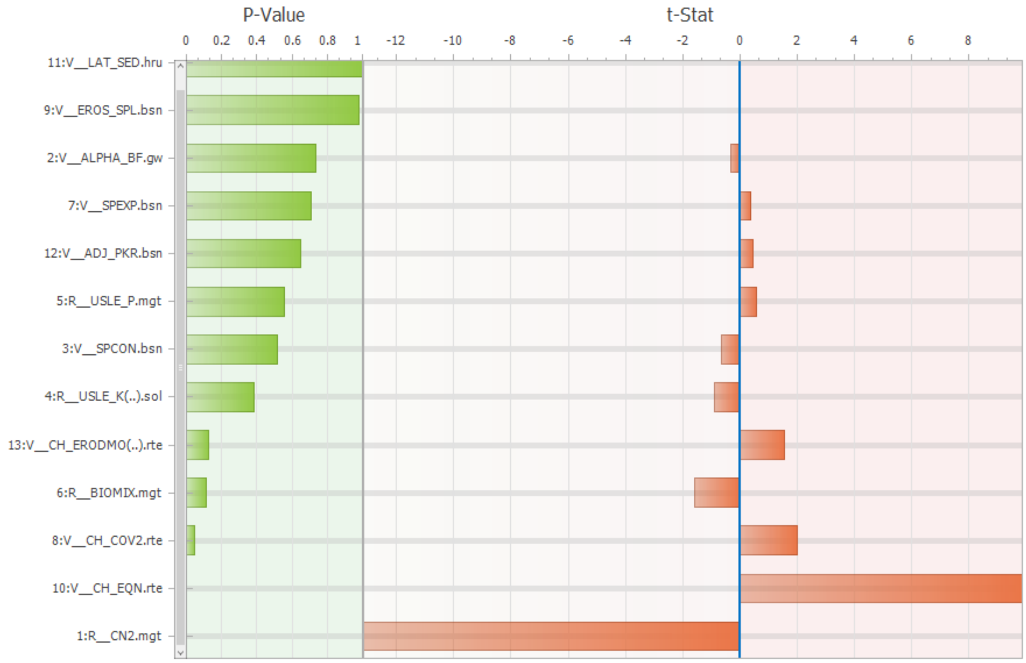

Figure 4. 8 Sediment yield sensitive parameters

Generally, from 13 parameters selected for sediment sensitive analysis, the parameter such as Sediment concentration in lateral flow and groundwater flow (LAT-SED), the splash erosion coefficient (EROS_SPL), Baseflow alpha factor (ALPHA_BF), Exponent parameter for calculating sediment re-entrained in channel sediment routing (SPEX) and Peak rate adjustment factor for sediment routing in the sub-basin (ADJ_PKR) were less sensitive to the study area.

4.3.2. Sediment yield calibration and validation

The sediment yield calibration was applied at Akaki gauge station using SUFI-2 algorithm in SWAT-CUP after streamflow calibration and validation was conducted. Like streamflow calibration and validation, the first two years (2000-2001) of the simulation were used as a model warm-up to establish proper model initialization conditions and to stabilize the model. The model was calibrated for the period of 2002-2008. The model calibration was performed on monthly bases through the adjustment of sensitive parameters derived from sensitivity analysis. The performance of the model was tested at every stage of the model simulation iteration by changing the parameter value repeatedly within the allowable range until the simulated sediment yield agreed with the measured sediment yield. Subsequently, the simulated and measured sediment yield was validated on the same time steps for the periods of 2009-2012 without further adjustment of calibrated sediment yield parameters.

The SWAT model performance was evaluated by comparing the observed and simulated sediment yield data series. The performance indicators such as coefficient of determination (R^2), Nash-Sutcliff efficiency (NSE) and Percent of bias (P_{Bias}) were used to evaluate the SWAT model performance. The performance efficiency values in both calibration and validation proved that SWAT-2012 estimated the sediment yield satisfactorily for monthly time steps for this study. The value of R^2, NSE and P_{Bias} was 0.84, 0.81 and 17.10, respectively for calibration and 0.68, 0.54 and 39.10, respectively for validation for both static and dynamic model set up as indicated in Table 4.8.

Table 4.8 SWAT model performance for sediment yield during the calibration and validation periods

Sn.	Performance index	Calibration (2002-2008)	Validation (2009-2012)
1	Coefficient of determination (R^2)	0.84	0.68
2	Nash-Sutcliff efficiency (NSE)	0.81	0.54
3	Percent of bias (P_{Bias})	17.10	39.10

According to performance rating criteria proposed by Moriasi et al. (2007) the values of R^2, NSE, and P_{Bias} for monthly sediment yield simulation can be rated as satisfactory to very good for both the calibration and validation periods. The graphical analysis of measured and simulated data as illustrated in Figures 4.9 and 4.10 clearly presents the general trends in the data and differences between model simulations. The simulated and measured sediment yield hydrograph and scatter plot during calibration and validation are indicated below in Figures 4.9 and 4.10, respectively.

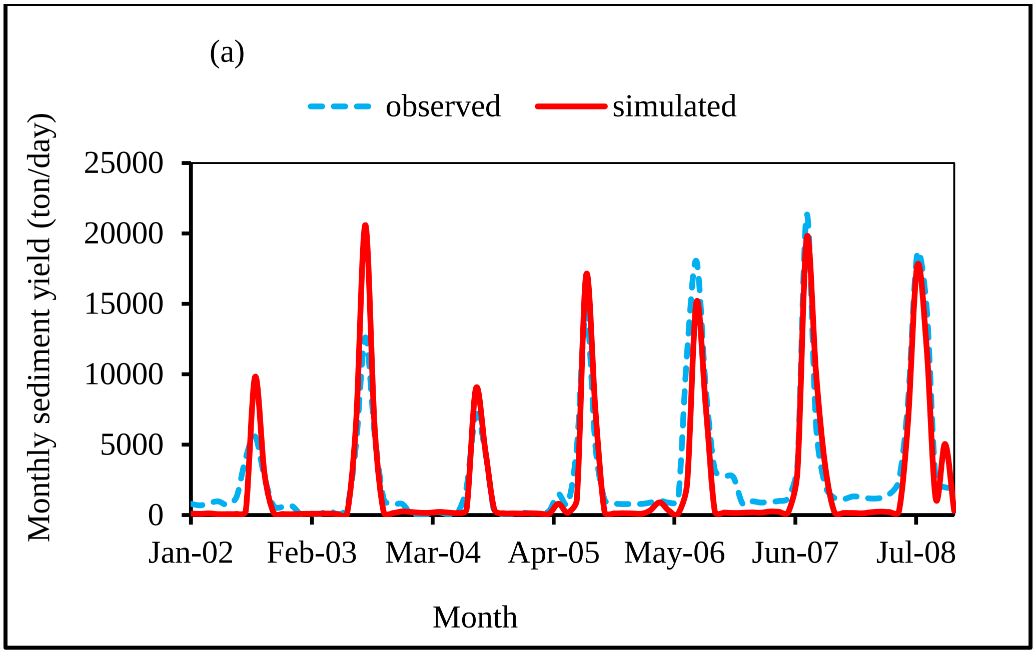

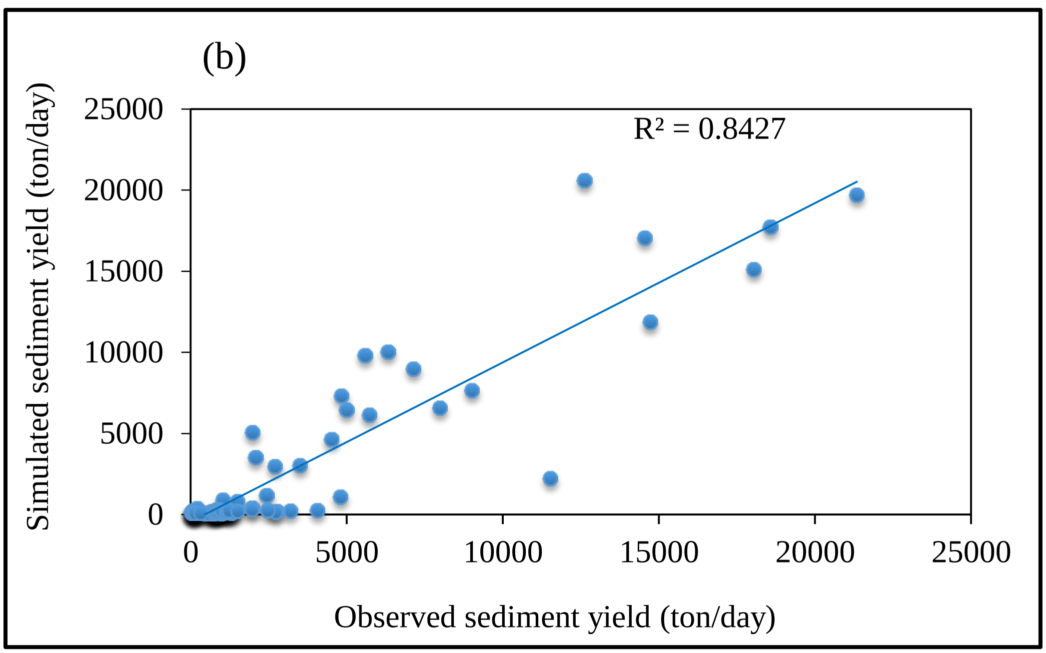

Figure 4. 9 Observed and simulated monthly sediment yield hydrograph (a) and scatter plot (b) during calibration periods

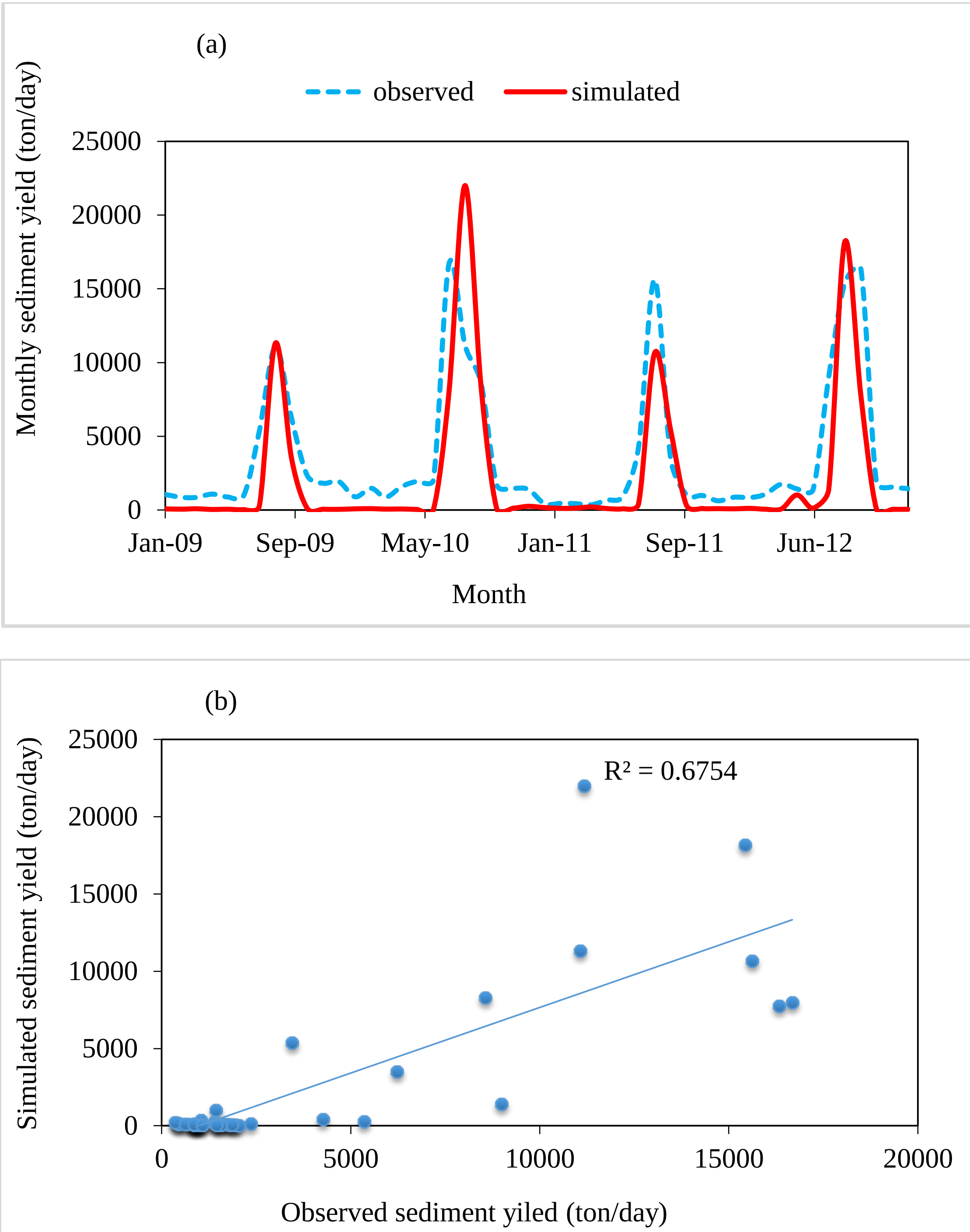

Figure 4. 10 Observed and simulated monthly sediment yield hydrograph (a) and scatter plot (b) during validation periods

The graphical inspection in Figure 4.9 and 4.10 shows that the model overestimated the sediment yield in most of the peak flow period (wet season) and underestimate during the low flow period (dry season).

4.3.3. Sediment yield uncertainty analysis

The goodness of fit and the degree to which the calibrated model accounts for the uncertainties was assessed by two measures (P-factor and R-factor) in the Sequential Uncertainty Fitting, version 2 (SUFI-2) in the SWAT CUP (Abbaspour et al., 2004) for this study. The output of the uncertainty from the SUFI-2 uncertainty analysis technique of SWAT-CUP program is presented in Figure 4.11 and Figure 4.12 for calibration and validation, respectively. The uncertainty measure of SUFI-2 showed a P-factor of 0.69 and R-factor of 3.89 for calibration and a P-factor of 0.60 and R-factor of 3.39 for validation.

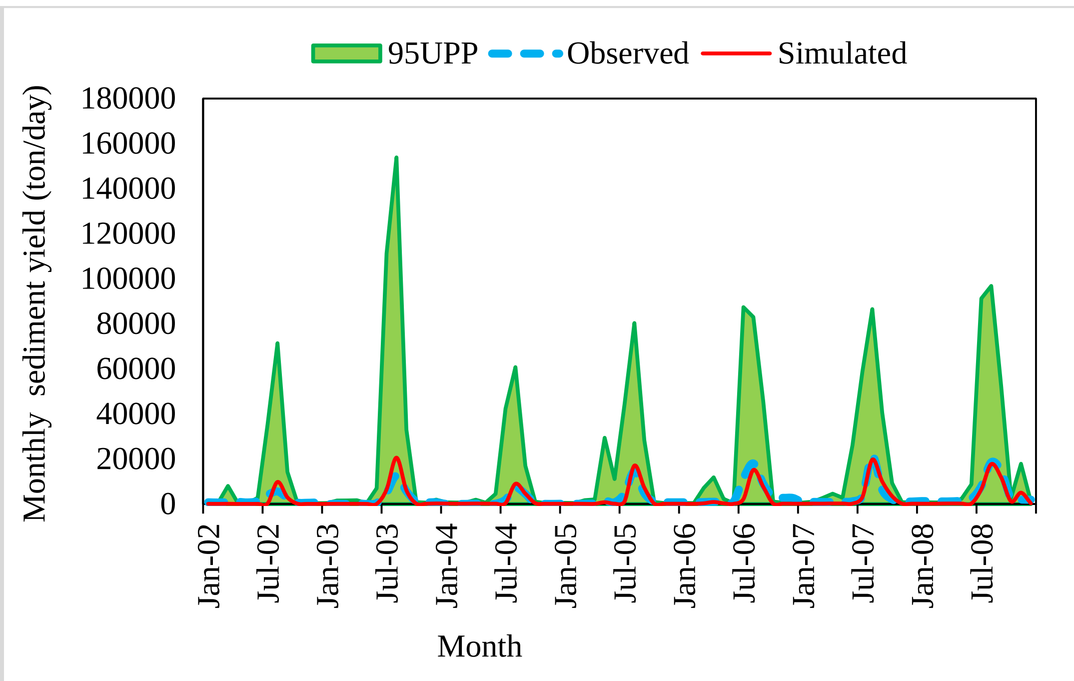

Figure 4. 11 Monthly sediment yield calibration showing the 95PPU uncertainty intervals

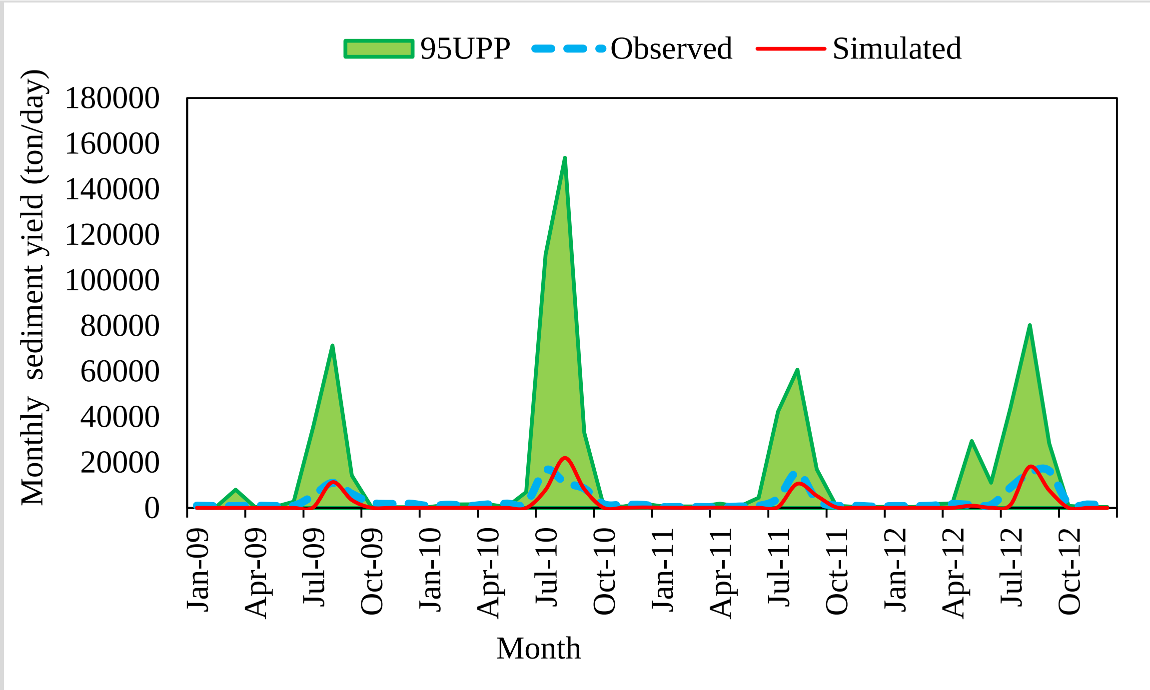

Figure 4. 12 Monthly sediment yield validation showing the 95PPU uncertainty intervals

The P-factor and R-factor for both calibration and validation periods showed that the SWAT model was able to capture most of the uncertainties since the P-value was 0.69 and R-factor was 3.89 for calibration and P-value was 0.60 and R-factor was 3.39 for validation. For sediment, a smaller P-factor and larger R-factor could be acceptable according to the SWAT-CUP user manual provided by Kerim C.Abbaspour. The result obtained from uncertainty analysis in this study was in a similar trend to the result reported by Abbaspour et al. (2015) applied a SWAT model in Europe to model hydrology and water quality at a continental scale and conducted that a large number of the outlets fall in desirable regions of P-factor and R-factor indices.

4.4. Assessment of Hydrological Response to Static and Dynamic LULC Change

The calibrated and validated results of a static model run and dynamic model run were used to analyze the spatio-temporal effects of dynamic LULC change on the hydrological response based on historical LULC of 2000, 2010 and 2020. The long-term hydrologic simulation from the year 2000 to 2018 was performed on a monthly time step to analyze the impact of dynamic LULC changes on water balance components and sediment yield at basin and sub-basin scales. The hydrological water balance components such as surface runoff (SurfQ), lateral flow (LatQ), groundwater flow (GWQ), groundwater recharge(GWR), actual evapotranspiration (ET), water yield (WYLD), and sediment yield (SYLD) were analyzed by comparing the model run with static LULC setup and model run with dynamic LULC setup at the basin, sub-basin level both spatially and temporarily.

4.4.1. Hydrological response at the basin level

The average annual water balance values at the basin level were simulated by static and dynamic LULC data. The impact of LULC on SurfQ, LatQ, GWQ, GWR, ET, WYLD, streamflow, and SYLD in the big Akaki watershed were analyzed. The hydrological response difference between the two applied model setups (Static and Dynamic) provided the isolated impact of the LULC change (Aghsaei et al., 2020; Teklay et al., 2019). The dynamic model setup (use of 2000, 2010 and 2020 LULC) yields slightly higher SurfQ, WYLD, SYLD, and streamflow and lower LatQ, GWQ, GWR and ET compared to the static model setup (only 2000 LULC). The expansion of built-up area at the expense of agricultural land and grassland increases SurfQ, streamflow, and WYLD and decreases the LatQ, GWQ, GWR and ET. The study conducted by Shawul et al. (2019) argued that the expansion of the urban area due to the expansion of Addis Ababa city at the expense of pasture and shrubland area experienced an increment in the SurfQ and a decrement of GWQ in the Akaki sub-basin.

The estimated annual SurfQ, WYLD and streamflow were increased by 2.51mm (1.10%), 0.67mm (0.20%) and 0.30m^3/s (0.34%), respectively whereas the LatQ, GWQ, GWR and ET were decreased by 1.18mm (11.10%), 0.63mm (0.70%), 0.56mm (0.42%) and 2.90mm (0.60%), respectively in the dynamic land use model compared to the static land use model as shown in Table 4.9. The relative expansion of built-up area by 27.76% and the reduction of agricultural land and grass land by 3.38% and 41.10%, respectively results in the increase of SurfQ, streamflow and WYLD and consequently decreases the LatQ, GWQ, GWR and ET. The improvement of the forest land and shrubland coverage from 4.68% and 0.02% in 2000 to 4.96% and 0.49% in 2020 respectively was observed due to government green legacy initiatives derived from MDG and SDG. However, these improvements result in an insignificant impact on the hydrological response at the basin level because of the contrasting impact of the expansion in built-up areas and reduction in agricultural and grassland which is in line with the findings reported by Shawul et al. (2019). Aragaw et al. (2021) reported that the basin average annual SurfQ showed an increasing pattern, from 151.40mm to 175.00mm, whereas the GWQ, LatQ, and GWR show a reduction from 89.00mm to 79.90mm, 69.20mm to 65.00mm and 287.90mm to 277.70mm, respectively during the study period of 1988 to 2018 due to contraction of evergreen forest and grassland and the expansion of cultivated land and urban area resulted in increases in impervious surface cover in Gidabo river basin. The research study conducted in Be river catchment in Vietnam depicted that SurfQ and soil water content increased by 18.40% and 12.80%, respectively, while GWQ, LatQ, and GWR decreased by 5.80%, 4.60%, and 4.00%, respectively due to agricultural land expansion and deforestation during 1978 to 2000 (Khoi and Suetsugi, 2014). Gyamfi et al. (2016) also discussed that urbanization was the strongest contributor to increases in SurfQ, and WYLD. Wagner et al. (2019) also discussed that the dynamic LULC change in Mula and Mutha rivers catchment resulted in an increase of WYLD and a decrease of ET when compared to a model run with a static LULC.

Table 4.9 Average annual water balance components and sediment yield of big Akaki watershed at basin level

Variable	Static LULC	Dynamic LULC
Surface runoff (mm)	232.48	234.99
Lateral flow (mm)	10.68	9.50
Groundwater flow (mm)	94.75	94.12
Groundwater recharge (mm)	132.82	132.26
Evapotranspiration (mm)	497.90	495.00
Total water yield (mm)	344.55	345.22
Stream flow (m^3/s)	87.10	87.40
Sediment yield (t/ha)	29.22	40.05

The average seasonal water balance variability due to static and dynamic LULC at the basin level was also evaluated during the wet season (June to September) and dry season (October to May). The estimated seasonal hydrological response to LULC changes as shown in Table 4.10, the hydrological response for wet seasons was more pronounced in the dynamic LULC scenario compared with the wet season hydrological responses in the static LULC scenario. The streamflow was increased by 0.31m^3/s (0.40%) during the wet season (June to September) due to the SurfQ increased by 3.32mm (1.73%) because of the rapid expansion of the built-up area in Addis Ababa and surrounding cities into the pre-urban agricultural lands. Thus, these LULC conversions accelerated the surface runoff by reducing the groundwater recharge and infiltration due to impervious surfaces. The WYLD was also increased by 0.56mm (0.23%), whereas LatQ, GWQ, GWR, and ET were decreased by 0.57mm (7.79%), 1.02mm (2.50%), 0.58mm (0.49%) and 0.76mm (0.29%), respectively in dynamic LULC model run compared with the model run with static LULC. Conversely, the streamflow was reduced by 0.19m^3/s (0.61%) during the dry season since the groundwater contribution (baseflow) reduced as a result of grassland and agricultural land reduction in most of the study area. Generally, the SurfQ, GWQ, GWR and ET were diminished by 0.81mm (2.00%), 0.09mm (0.20%), 0.04mm (0.28%) and 2.15mm (0.99%), respectively during dry season.

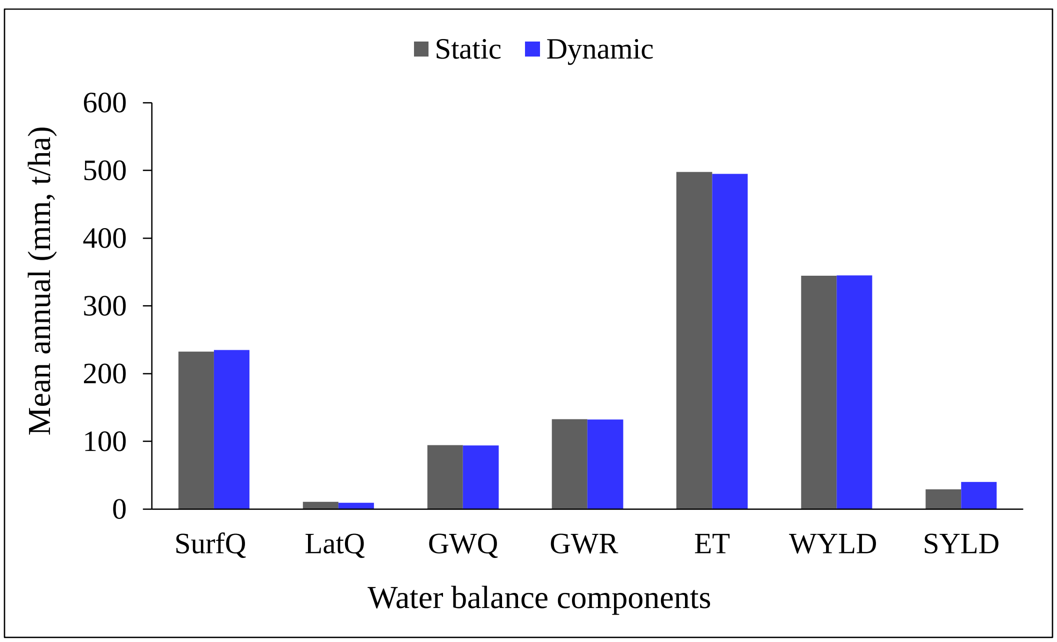

Figure 4. 13 Average annual water balance for static and dynamic LULC

The annual, wet, and dry sediment yield (SYLD) was increased by 10.83 t/ha, 8.61 t/ha, and 2.23 t/ha, respectively in the model run with dynamic LULC. The annual increment of SYLD by 10.83 t/ha (37.10%) is a result of the raise of SurfQ by 2.51mm since there is a direct relationship between surface runoff and sediment yield. The absolute reduction of agricultural land (by 2.65%) and grassland (by 1.43%) and the expansion of bare land (by 0.06%) result in the increment of SurfQ as well as SYLD.

Table 4.10 Average seasonal water balance components and sediment yield of big Akaki watershed at basin level

Variables	Wet Season		Dry Season	
	Static LULC	Dynamic LULC	Static LULC	Dynamic LULC
Surface runoff (mm)	192.00	195.32	40.44	39.63
Lateral flow (mm)	7.31	6.74	3.36	2.76
Groundwater flow (mm)	40.90	39.88	54.33	54.24
Groundwater recharge (mm)	118.80	118.05	14.33	14.29
Evapotranspiration (mm)	272.72	271.96	225.13	222.98
Total water yield (mm)	242.90	243.46	101.63	101.72
Stream flow (m^3/s)	76.00	76.31	30.95	30.76
Sediment yield (t/ha)	23.57	32.18	5.65	7.88

The finding of this study is consistent with other several studies. For instance, Gashaw et al. (2018) indicated that the increasing trend of annual and wet season streamflow and a decreasing trend of dry season streamflow due to the continuous increment of cultivated land and built-up area and extraction of vegetation covers in the Andassa watershed of the Blue Nile basin during 1985-2045 periods. They concluded that SurfQ and WYLD increased by 55.80mm and 23.70mm, respectively, whereas the GWQ and LatQ have decreased by 25.50mm and 5.50mm. A study in the Gummara watershed also depicted that the SurfQ and peak flow increased by 11.60mm and 2.40m^3/s, respectively due to the agricultural land expansion by 11.10% and forest land reduction by 2.30% between the 1985 and 2015 periods (Teklay et al., 2019). Similarly, the increasing trend of annual ET, WYLD, SYLD, and SurfQ and the decreasing trend in GWQ and LatQ was observed in the dynamic land use model (Aghsaei et al., 2020). They concluded that the dynamic land use implementation was more influential on monthly hydrological response than annual response. Wagner et al. (2019) in Mula and Mutha rivers catchment, India, reported an increase of WYLD and a decrease of ET for dynamic assessment with the linear land use change scenario where the urban area increased in most parts of the sub-basin.

4.4.2. Hydrological response at the sub-basin level

The dynamic LULC change effect on hydrological response was more pronounced at the sub-basin level than basin level (Aghsaei et al., 2019). Aragaw et al. (2021) also articulated that more significant changes of hydrological water balances were observed at the sub-basin level because of the uneven spatial distribution of LULC alterations.

The sub-basin level average water balance such as SurfQ, GWQ, ET, WYLD and SYLD were assessed by correlating their change in magnitude and direction with major LULC change at the sub-basin level between 2000 and 2020 LULC as illustrated in Figure 4.14. The sub-basins which experienced higher built-up expansion at the expense of agricultural land and grassland showed increments in the SurfQ, and WYLD and decrements in GWQ and ET. During the study period, the agricultural land use area decreased in sub-basins 1, 5, 8, 13, 15, 17, 18, 19, 21, 23, 25, 26, and 27 with a maximum decrement of 36.08% in sub-basin 15, while increased slightly in sub-basins 3, 4, 6, 7, 9, 10, 11, 12 and 20 with the maximum increment of 3.58% in sub-basin 4.

The built-up area increased in sub-basins 1, 5, 8, 13, 14, 15, 17, 18, 19, 21, 23, 25, 26 and 27 with the maximum expansion of 38.12% in sub-basin 15, while decreased in sub-basin 11 by 1.92%. The forest coverage was slightly increased in sub-basins 3, 6, 7, 14, 20, 23, 26, and 27, and decreased in sub-basins 1, 5, 11, 12, 13, 17 and 25 while no significant change in 2, 4, 8, 9, 10, 15, 16, 18, 19, 21, 22 and 24. The grassland area was decreased in all sub-basins except in sub-basin 25, with the maximum decrement of 6.61% in sub-basin 15. The expansion of built-up area at the expense of agricultural land and grassland in most of the sub-basins resulted higher SurfQ and WYLD in the dynamic model setup.

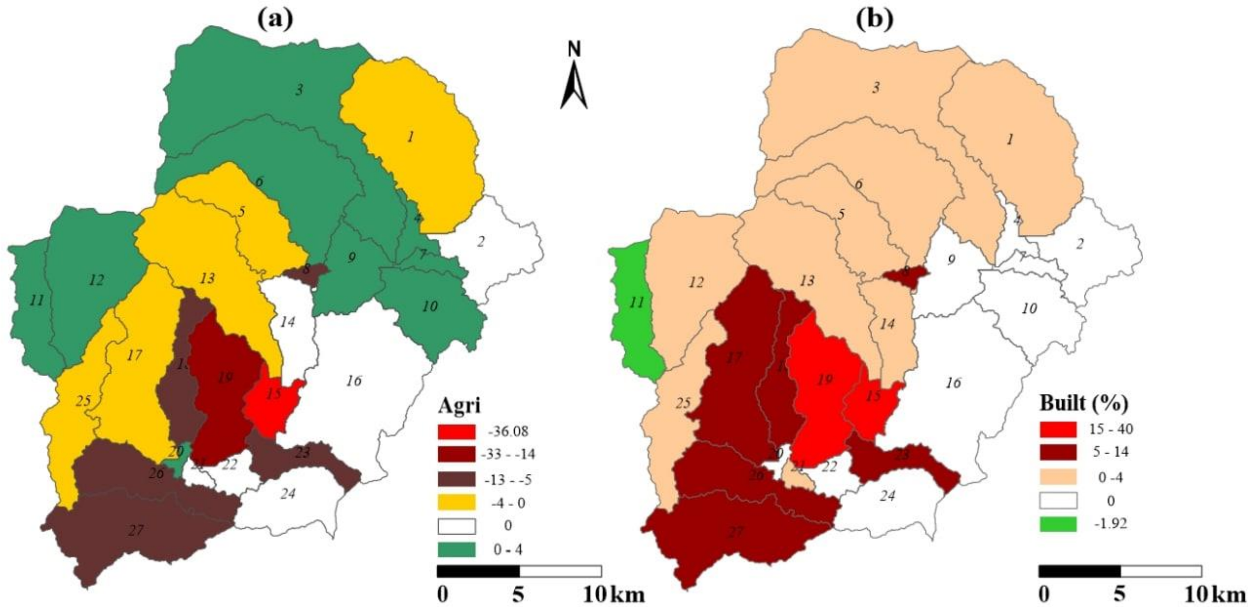

Figure 4. 14 Individual LULC change at sub-basin level of big Akaki watershed

The changes in long-term average annual SurfQ range from a decrease of 3.24mm in sub-basin 12 to an increase of 10.15mm in sub-basin 13 for a model run with dynamic LULC compared with the static one. The highest increment (10.15mm) of SurfQ in sub-basin 13 was due to the expansion of built-up by 1.44% and the decrement of agricultural land and grassland by 0.95% and 1.88%, respectively. The expansion of built-up by 38.12%, 32.71%, 13.84%, 7.12% and 7.05% in sub-basin 15, 19, 18, 26 and 23, respectively, increased the SurfQ by 0.96mm, 0.3mm, 0.91mm, 2.05mm and 3.25mm, respectively. The decrement of SurfQ in sub-basin 12 by 3.24mm was because of the expansion of forest land from 24.03% in 2000 to 28.04% in 2020 by 4.01%.

The average annual GWQ change was increased in sub-basin 13, 14, 15, and 21 while decreased in sub-basin 3, 5, 11, 17, and 25. Sub-basin 13 experienced the highest increment (6.12mm) GWQ change due to the increment of forest land from 4.63% to 5.46% and reduction of agricultural land from 87.23% to 86.28% between 2000 and 2020. While sub-basin 5 showed the highest decrement of GWQ by 2.58mm due to the expansion of the built-up area by 1.32%. The WYLD also shows an increment in sub-basin 5, 13, 14, 16, 20, 21, 23, 25, 26 and 27 with the maximum increment in sub-basin 13 by 8.78mm, whereas sub-basin 6, 11, 12, 17 and 19 showed a decrement with the highest decrement in sub-basin 11 by 1.29mm. This is in agreement with the increase of SurfQ and WYLD and decreases of GWQ due to expansion built-up and reduction of forest land reported in other research studies (Gashaw et al., 2018; Shawul et al., 2019; Teklay et al., 2019).

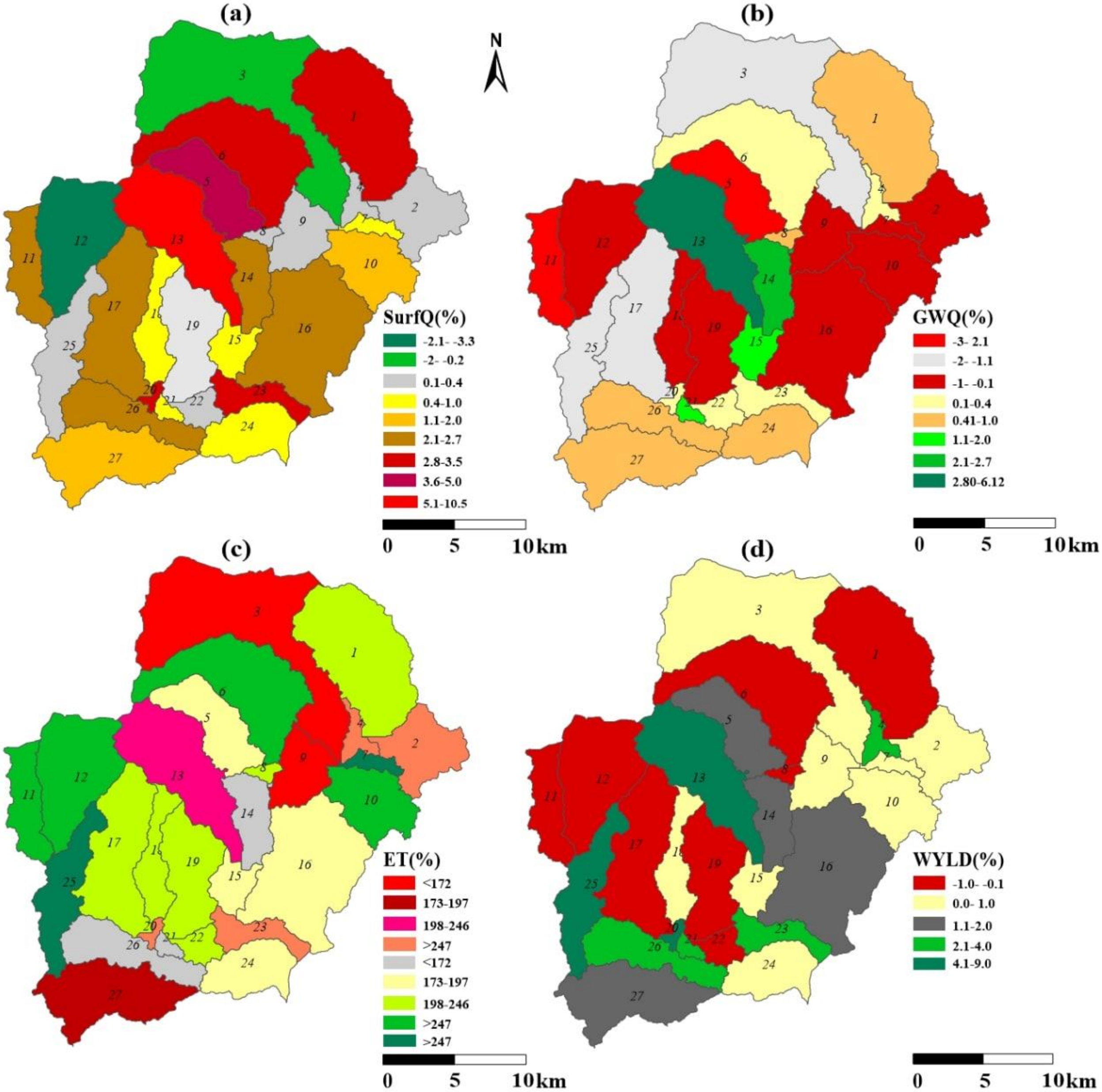

Figure 4. 15 Water balance components change at sub-basin level of big Akaki watershed

The change in average annual ET ranges from a decrease of 32.34mm in sub-basin 9 to an increase of 5.72mm in sub-basin 7 for the model run with dynamic LULC compared with the static one due to sub-basin 7 occupied by water bodies (lagedadi reservoir). The largest increment of ET also showed in sub-basin 7, 10, 11 and 25 by 5.72mm, 1.96mm, 2.07mm and

2.37mm, respectively, due to the increment of forest land. Whereas, sub-basin 2, 3, 4, 9, 13, 20, 21 and 27 showed the largest decrement in average annual ET by 2.3mm, 19.35mm, 4.83mm, 32.34mm, 9.34mm, 3.85mm, 2.01mm, 2.31mm and 12.94mm, respectively due to the expansion of built-up area and reduction of forest land during the study period between 2000 and 2020.

The impact of dynamic LULC change on average annual SYLD at the sub-basin level ranges from a decrease of 4.74t/ha in sub-basin 6 to an increase of 0.78t/ha in sub-basin 3. This finding is in agreement with other studies' reports. For instance, Shawul et al. (2019) revealed that the sub-basin level impact of LULC changes were more pronounced than at the basin level on hydrological response. They concluded that the expansion of built-up and agricultural land resulted in relatively higher SurfQ and lower GWQ and ET. Berihun et al. (2019) also reported that the conversion of natural vegetation covers such as grassland, bushland, and forest land to cultivated land contributed to the decrease in mean annual ET in contrasting agro-ecological environments of the upper Blue Nile basin during the study period of 1982 to 2016/17.

4.4.3. Spatial distribution of surface runoff and sediment yield for dynamic LULC

For the SWAT model simulated with a dynamic LULC model setup, the annual water balance values of the big Akaki watershed indicated high spatial variation due to TJETBT1ET3T-8(a)4(ti)-e6(l)-11(

SYLD (sub-basin 11, 25, and 27) were dominated by built-up LULC types and flat slope (0-10% slope class). The built-up area generated the least SYLD because the surface covered by impervious structures such as buildings, asphalt, and concrete materials prohibited the rainfall and surface runoff from eroding the topsoil which causes sediment yield. Identifying the critical sediment-prone sub-basins is very useful to control soil erosion and implement proper watershed management and planning (Serur and Adi, 2022; Tesema and Leta, 2020).

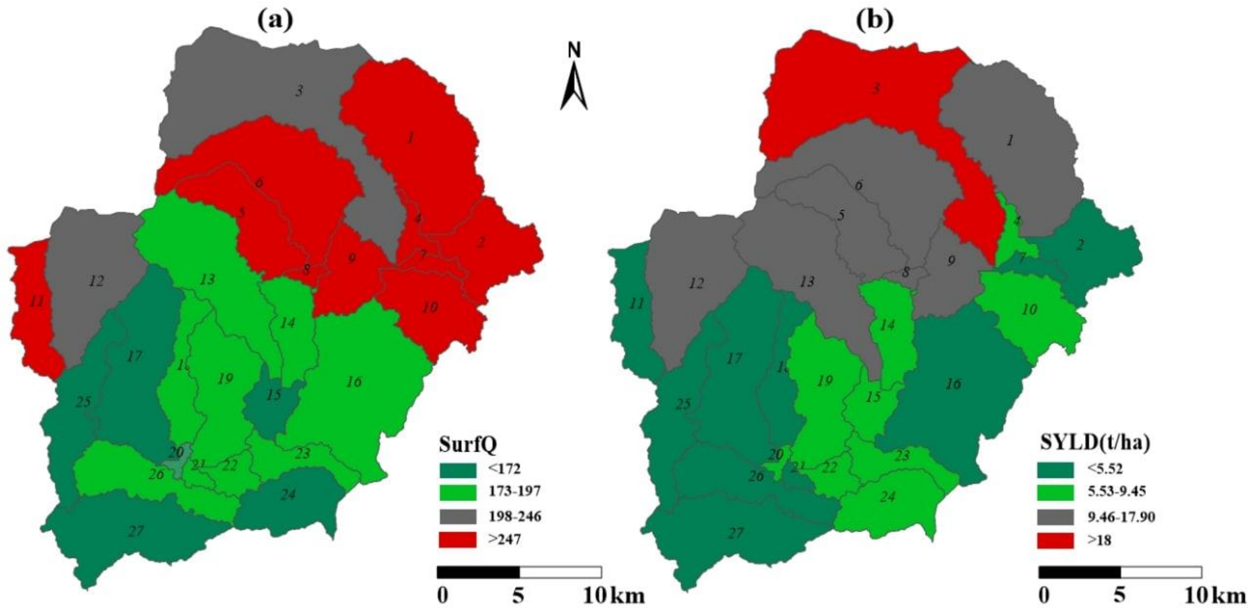

Figure 4. 16 SurfQ (a) and SYLD (b) generated at each sub-basin for dynamic LULC of big Akaki watershed

According to Hurni (1985), for different agro-ecological zones of Ethiopia, the tolerable soil loss rate ranges 2 t/ha/yr to 18 t/ha/yr. Accordingly, the finding in this study (big Akaki watershed) depicted that the simulated SYLD in sub-basin 3 (21.24 t/ha/yr) exceeded the maximum tolerable soil loss rate (18 t/ha/yr). According to Hurni (1985) document on soil loss rate, most of the big Akaki watershed was within a tolerable range.

SurfQ and SYLD had a direct relationship since the SurfQ facilitates the SYLD process by eroding the top soil particle and transporting it to the downstream parts. The sub-basins that generate a high amount of SurfQ also generate a high amount of SYLD and vice versa. But this relationship of SurfQ and SYLD is indirectly related in some sub-basins. For instance, sub-basin 2, 7, and 11 generated a high amount of SurfQ but generated a relatively small amount of SYLD.

Sub-basin 11 generates a high amount of SurfQ with an average annual value of 257.23mm but generates a small amount of SYLD with an average annual value of 3.22 t/ha because the sub-basin was covered with a built-up area, 82.32% ET1189 with 49.47% of 0-10 and 36.17% of 10-20 slope classes. This indicated that SurfQ is not the only factor in SYLD generation, but also other factors such as LULC, topography, slope, soil characteristics, and agricultural practices are affected the SYLD generation significantly.

This finding is in agreement with other studies' reports. For instance, Zeberie (2019) discussed that the Akaki watershed experienced the SYLD from a very high sediment prone area (21.75 t/ha) to a low sediment potential source area (< 3 t/ha). They finalized that the SYLD-prone sub-basins were dominantly covered with intensively cultivated land, grassland, and bare soil with a very steep slope. Tesema and Leta (2020) also identified the two sub-basin in the Kesem dam watershed that generated the highest SYLD with annual average values of 24 to 29 t/ha/yr which are dominantly covered with shrubland and steep slope topographic characteristics. Similarly, Liu et al. (2015) reported that high soil erosion occurs in crop areas with a relatively steep slope, while low erosion occurs in flat areas with near-zero slopes.

5. CONCLUSIONS AND RECOMMENDATIONS

5.1. Conclusions

Quantification of the hydrological responses and sediment yields to the land use and land cover (LULC) change at spatial and temporal scales is very important for water resources planning, development, and management. This study assesses the impact of dynamic LULC changes on hydrological responses using the SWAT hydrological models in the big Akaki watershed. The remote sensing satellite image data of 2000, 2010, and 2020 were classified with the help of ERDAS Imagine 2015 and Arc-GIS 10.4 to assess the spatio-temporal change in LULC in the study area.

The major LULC classes were agricultural land, built-up area, forest land, grassland, shrubland, water body, and bare land. The analysis of the three LULC periods showed that the big Akaki watershed experienced a significant change in LULC during the study period of two decades. The major LULC changes were from agricultural land and grassland to the built-up area. The built-up area, forest land, shrubland and bare land were increased by 6.96%, 5.98%, 2350.00%, and 45.00%, whereas the agricultural land, grassland and water body were diminished by 0.45%, 38.79% and 3.08%, respectively for the period of 2000-2010. During the period of 2010-2020, the built-up area was increased by 19.45%, whereas agricultural land, grassland, water body, and bare land were decreased by 2.90%, 3.76%, 26.98% and 10.34%, respectively. The forest land and shrubland were remain constant during this period interval. The rapid expansion of built-up at the expense of agricultural and grassland was due to population growth and socio-economic development in the study area. The expansion of construction works, industrial and infrastructures into pre-urban areas was a reason for dynamic change in LULC. However, the forest land showed a slightly increasing trend because of the government soil and water conservation and afforestation policy that was implemented following the Ethiopian millennium with the motto of “green legacy”.

The impact of the dynamic LULC changes on hydrological responses was evaluated using the SWAT hydrological model by comparing the model run with static LULC (only use of 2000 LULC) and the model run with dynamic LULC (use of 2000, 2010, and 2020 LULC). The SWAT-LUT software was used to incorporate the dynamic LULC into the SWAT land use update module. The SWAT model was calibrated for the period of 2002-2008 and validated for the period of 2009-2012 for streamflow and sediment yield at the big Akaki gauge station using SWAT-CUP. The SWAT model evaluation showed that for both model setups (static and dynamic), the coefficient of determination (R^2), Nash Sutcliffe efficiency (NSE) percent of bias (P_{Bias}) as well as the uncertainty analysis indices: P-factor and R-factor for both calibration and validation were found in the acceptable range.

The dynamic LULC changes have a major impact on hydrological responses and sediment yield of the study watershed. The average annual basin value of SurfQ, WYLD, streamflow and SYLD were increased by 2.51mm (1.10%), 0.67mm (0.20%), 0.30m^3/s (0.34%) and 10.83t/ha (37.10%), respectively whereas, the LatQ, GWQ, GWR and ET were reduced by 1.18mm (11.10%), 0.63mm (0.70%), 0.56mm (0.42%) and 2.9mm (0.60%), respectively in dynamic model setup compared to the static model setup. The average seasonal basin level water balance was also evaluated in wet and dry seasons. The streamflow and SYLD increased from 76.00m^3/s and 23.57t/ha to 76.31m^3/s and 32.18 t/ha, respectively due to the SurfQ increased from 192.00mm to 195.32mm. The other water components showed a decreasing trend when implementing the dynamic LULC model setup in wet season. During the dry season, the streamflow was decreased by 0.19m^3/s due to the contribution of base flow were decreased.

The effect of LULC change is more pronounced at the sub-basin level than at a basin level. The average annual SurfQ, WYLD and SYLD were increased by 10.15mm, 7.78mm and 0.78t/ha in sub-basin 13, 13 and 3, respectively. Whereas GWQ and ET were reduced by 2.58mm and 32.34mm in sub-basin 5 and 9, respectively. The expansion of built-up area and bare land at the expense of agricultural land and other natural vegetation, generally increased the wet season flow, SurfQ, WYLD and SYLD, and decreased the dry season flow, LatQ, GWQ, GWR and ET.

The model run with a dynamic LULC setup indicated that higher spatial variation of annual water balance values. The spatial variations LULC, topography, soil properties, and rainfall characteristics in the watershed may cause these spatial variations of SurfQ and SYLD. The sub-basins situated in the upstream part of the study watershed generated higher SurfQ and SYLD.

Generally, the outcomes from this study has shown that the SWAT model simulation with dynamic land use maps improved the hydrological response estimations than the static one in the big Akaki watershed. Since the dynamic model setup estimates accurately the spatio-temporal hydrological responses by solving the stationarity problem. It helps to assess the impacts of LULC change, climate change and land management practices on a watershed. Therefore, this study gives important information on watershed responses to LULC and ways of sustainable watershed planning and management for policymakers, decision-makers, water science specialists, and other stakeholders.

5.2. Recommendations

From the research result, the following core recommendations are drawn:

- The dynamic LULC simulation approach employed in this research thesis can serve as a turning point for research studies in other river basins. All most all LULC impact assessments on water resource components solely depend on the static LULC approach in Ethiopia. However, to account the spatio-temporal variability of the watershed accurately, the dynamic LULC approach model simulation is more preferable.
- The input data availability and quality are one of the paramount criteria for distributed physical hydrological modelling. The weather data, streamflow and sediment yield data that were used for this study have data missing and quality problems. Since the SWAT hydrological model requires intensive input data, the concerned body should work jointly in an integrated way to improve the required data quality.
- The study did not consider the reservoir and other water storage due to the unavailability of regulated flow data. Thus, better to incorporate (add) the reservoir in SWAT model simulation.
- The study illustrated that there are sub-basin with a generation of higher sediment yield. Therefore appropriate water and land management options are necessary to reduce the sediment yield. The author recommends to apply the best management practice to maintain and conserve the watershed sustainably.
- The author of this research thesis believes that this study has put the foundation for the future detailed dynamic LULC changes impact assessment on hydrological responses in different river watersheds of Ethiopia.

REFERENCES

AAWSA, BCEOM, SEURECA and Tropics. 2000. Addis Ababa water supply project Stage-IIIA Groundwater-Phase II, modeling of Akaki well field, V1, main report, Addis Ababa Water and Sewerage Authority, Addis Ababa, Ethiopia.

Abbaspour, K. C., Rouholahnejad, E., Vaghefi, S., Srinivasan, R., Yang, H., & Kløve, B. (2015). A continental-scale hydrology and water quality model for Europe: Calibration and uncertainty of a high-resolution large-scale SWAT model. Journal of Hydrology, 524, 733–752. https://doi.org/10.1016/j.jhydrol.2015.03.027

Abbaspour, K., Vejdani, M., & Haghighat, S. (2007). SWAT-CUP calibration and uncertainty programs for SWAT. Proc.Intl. Congress on Modelling and Simulation (MODSIM'07).

Abbaspour, K.C., Johnson, C.A., van Genuchten, M.T., 2004. Estimating uncertain flow and transport parameters using a sequential uncertainty fitting procedure. Vadose Zone Journal 3 (4), 1340–1352.

Abbott, M. B., Bathurst, J. C., Cunge, J. A., O'Connell, P. E., & Rasmussen, J. (1986). An introduction to the European Hydrological System — Systeme Hydrologique Europeen, "SHE", 1: History and philosophy of a physically-based, distributed modelling system. Journal of Hydrology, 87(1–2), 45–59. https://doi.org/10.1016/0022-1694(86)90114-9

Abdulkareem, J. H., Sulaiman, W. N. A., Pradhan, B., & Jamil, N. R. (2018). Long-Term Hydrologic Impact Assessment of Non-point Source Pollution Measured Through Land Use/Land Cover (LULC) Changes in a Tropical Complex Catchment. Earth Systems and Environment, 2(1), 67–84. https://doi.org/10.1007/s41748-018-0042-1

Abraham, T., & Nadew, B. (2018). Impact of Land Use Land Cover Dynamics on Water Balance, Lake Ziway Watershed, Ethiopia. 9(4), 15.

Aghsaei, H., Mobarghaee Dinan, N., Moridi, A., Asadolahi, Z., Delavar, M., Fohrer, N., & Wagner, P. D. (2020). Effects of dynamic land use/land cover change on water resources and sediment yield in the Anzali wetland catchment, Gilan, Iran. Science of The Total Environment, 712, 136449. https://doi.org/10.1016/j.scitotenv.2019.136449

Alam, K., Qureshi, S., & Blaschke, T. (2011). Monitoring spatio-temporal aerosol patterns over Pakistan based on MODIS, TOMS and MISR satellite data and a HYSPLIT model. Atmospheric Environment, 45(27), 4641–4651. https://doi.org/10.1016/j.atmosenv.2011.05.055

Alemu, Z.A., Dioha, M.O. Climate change and trend analysis of temperature: the case of Addis Ababa, Ethiopia. Environ Syst Res **9,** 27 (2020). https://doi.org/10.1186/s40068-020-00190-5.

Al-Fares, W. (2013). Historical Land Use/Land Cover Classification Using Remote Sensing. Springer International Publishing. https://doi.org/10.1007/978-3-319-00624-6

Aliye, M. A., Aga, A. O., Tadesse, T., & Yohannes, P. (2020). Evaluating the Performance of HEC-HMS and SWAT Hydrological Models in Simulating the Rainfall-Runoff Process for Data Scarce Region of Ethiopian Rift Valley Lake Basin. Open Journal of Modern Hydrology, 10(04), 105–122. https://doi.org/10.4236/ojmh.2020.104007

Amin, A., & Nuru, N. (2020). Evaluation of the Performance of SWAT Model to Simulate Stream Flow of Mojo River Watershed: In the Upper Awash River Basin, in Ethiopia. Hydrology, 8(1), 7. https://doi.org/10.11648/j.hyd.20200801.12

Andualem, T. G., & Gebremariam, B. (2015). Impact Of Land Use Land Cover Change On Stream Flow And Sediment Yield: A Case Study Of Gilgel Abay Watershed, Lake Tana Sub-Basin, Ethiopia. 3(11), 15.

Aragaw, H. M., Goel, M. K., & Mishra, S. K. (2021). Hydrological responses to human-induced land use/land cover changes in the Gidabo River basin, Ethiopia. Hydrological Sciences Journal, 66(4), 640–655. https://doi.org/10.1080/02626667.2021.1890328

Aredo, M. R., Hatiye, S. D., & Pingale, S. M. (2021). Impact of land use/land cover change on stream flow in the Shaya catchment of Ethiopia using the MIKE SHE model. Arabian Journal of Geosciences, 14(2), 114. https://doi.org/10.1007/s12517-021-06447-2

Arnold, J. G., Moriasi, D. N., Gassman, P. W., Abbaspour, K. C., White, M. J., Srinivasan, R., Santhi, C., Harmel, R. D., Van Griensven, A., Van Liew, M. W., Kannan, N., & Jha, M. K. (2012). SWAT: Model use, calibration, and validation. Transactions of the ASABE, 55(4), 1491–1508.

Asnake Molla, Brook Abate, Yohannes Behonegne. Assessment of Sediment Inflow in Dire Dam Reservoir Using SWAT Model, Dire Catchment, Ethiopia. Control Science and Engineering. Vol. 4, No. 2, 2020, pp. 16-31. doi: 10.11648/j.cse.20200402.11

Assfaw, A. T. (2020). Modeling Impact of Land Use Dynamics on Hydrology and Sedimentation of Megech Dam Watershed, Ethiopia. The Scientific World Journal, 2020, 1–20. https://doi.org/10.1155/2020/6530278

Azorin-Molina, C., Guijarro, J. A., McVicar, T. R., Trewin, B. C., Frost, A. J., & Chen, D. (2019). An approach to homogenize daily peak wind gusts: An application to the Australian series. International Journal of Climatology, 39(4), 2260–2277. https://doi.org/10.1002/joc.5949

Balascio, C. C., D. J. Palmeri, and H. Gao. 1998. Use of a genetic algorithm and multi-objective programming for calibration of a hydrologic model.Trans. ASAE 41(3): 615-619.

Barakat, A., Ouargaf, Z., Khellouk, R., El Jazouli, A., & Touhami, F. (2019). Land Use/Land Cover Change and Environmental Impact Assessment in Béni-Mellal District (Morocco)

Using Remote Sensing and GIS. Earth Systems and Environment, 3(1), 113–125. https://doi.org/10.1007/s41748-019-00088-y

Beaty, P. A Brief History of ERDAS IMAGINE. Available online: http://field guide.blogspot.com/2009/04/brief-history-of-erdas-imagine.html (accessed on 19 May 2021).

Bekele, D., Alamirew, T., Kebede, A., Zeleke, G., & Melesse, A. M. (2019). Land use and land cover dynamics in the Keleta watershed, Awash River basin, Ethiopia. Environmental Hazards, 18(3), 246–265. https://doi.org/10.1080/17477891.2018.1561407

Ben Khélifa, W., & Mosbahi, M. (2021). Modeling of rainfall-runoff process using HEC-HMS model for an urban ungauged watershed in Tunisia. Modeling Earth Systems and Environment. https://doi.org/10.1007/s40808-021-01177-6

Beven, K., Binley, A., 1992. The future of distributed models – model calibration and uncertainty prediction. Hydrological processes 6(3), 279-298

Birhanu, A., Masih, I., van der Zaag, P., Nyssen, J., & Cai, X. (2019). Impacts of land use and land cover changes on hydrology of the Gumara catchment, Ethiopia. Physics and Chemistry of the Earth, Parts A/B/C, 112, 165–174. https://doi.org/10.1016/j.pce.2019.01.006

Biru, Z., & Kumar, D. (2018). Calibration and validation of SWAT model using stream flow and sediment load for Mojo watershed, Ethiopia. Sustainable Water Resources Management, 4(4), 937–949. https://doi.org/10.1007/s40899-017-0189-1

Bosch, J. M., & Hewlett, J. D. (1982). A review of catchment experiments to determine the effect of vegetation changes on water yield and evapotranspiration. Journal of Hydrology, 55(1–4), 3–23. https://doi.org/10.1016/0022-1694(82)90117-2

Cheng, S. (2011). The best relationship between lumped hydrograph parameters and urbanized factors. Natural Hazards, 56(3), 853–867. https://doi.org/10.1007/s11069-010-9596-4

Chipman, Jonathan W._ Kiefer, Ralph W._ Lillesand, Thomas M et al. - Remote sensing and image interpretation-John Wiley & Sons (2015).pdf. (n.d.-a).

Chowdhury, M., Hasan, M. E., & Abdullah-Al-Mamun, M. M. (2020). Land use/land cover change assessment of Halda watershed using remote sensing and GIS. The Egyptian Journal of Remote Sensing and Space Science, 23(1), 63–75. https://doi.org/10.1016/j.ejrs.2018.11.003

Congalton, R. G., 1981, The Use of Discrete Multivariate Analysis for the Assessment of Landsat Classification Accuracy, Blacksburg: Virginia Polytechnic Institute and State University, Master’s thesis.

Congalton, R. G., and R. A. Mead, 1983, “A Quantitative Method to Test for Consistency and

Correctness in Photointerpretation," Photogrammetric Engineering & Remote Sensing, 49(1):69–74.

Congalton, R. G., and K. Green, 2009, Assessing the Accuracy of Remotely Sensed Data: Principles and Practices, 2nd Ed., Boca Raton: CRC Press, 183 p.

CSA. (2021). Population Size of Towns by Sex, Region, Zone and Weredas.

Cuomo, A., & Guida, D. (2021). Hydro-Geomorphologic-Based Water Budget at Event Time-Scale in A Mediterranean Headwater Catchment (Southern Italy). Hydrology, 8(1), 20. https://doi.org/10.3390/hydrology8010020

Czernecki, B., Głogowski, A., & Nowosad, J. (2020). Climate: An R Package to Access Free In-Situ Meteorological and Hydrological Datasets For Environmental Assessment. Sustainability, 12(1), 394. https://doi.org/10.3390/su12010394

Daba, M. H. (2018). Sensitivity of SWAT Simulated Runoff to Temperature and Rainfall in the Upper Awash Sab-Basin, Ethiopia. Hydrology: Current Research, 09(01). https://doi.org/10.4172/2157-7587.1000293

Dahmen, E. R., & Hall, M. J. (1990). Screening of hydrological data: Tests for stationarity and relative consistency. ILRI.

Daofeng, L., Ying, T., Changming, L., & Fanghua, H. (2004). Impact of land-cover and climate changes on runoff of the source regions of the Yellow River. Journal of Geographical Sciences, 14(3), 330–338. https://doi.org/10.1007/BF02837414

Demlie, M., Wohnlich, S., Gizaw, B., & Stichler, W. (2007). Groundwater recharge in the Akaki catchment, central Ethiopia: Evidence from environmental isotopes (δ18O, δ2H and3H) and chloride mass balance. Hydrological Processes, 21(6), 807–818. https://doi.org/10.1002/hyp.6273

Deribew, K. T., & Dalacho, D. W. (2019). Land use and forest cover dynamics in the North-eastern Addis Ababa, central highlands of Ethiopia. Environmental Systems Research, 8(1), 8. https://doi.org/10.1186/s40068-019-0137-1

Desta, H., & Lemma, B. (2017). SWAT based hydrological assessment and characterization of Lake Ziway sub-watersheds, Ethiopia. Journal of Hydrology: Regional Studies, 13, 122–137. https://doi.org/10.1016/j.ejrh.2017.08.002

Devia, G. K., Ganasri, B. P., & Dwarakish, G. S. (2015). A Review on Hydrological Models. Aquatic Procedia, 4, 1001–1007. https://doi.org/10.1016/j.aqpro.2015.02.126

Dwarakish, G. S., & Ganasri, B. P. (2015). Impact of land use change on hydrological systems: A review of current modeling approaches. Cogent Geoscience, 1(1), 1115691. https://doi.org/10.1080/23312041.2015.1115691

Fan, M., & Shibata, H. (2015). Simulation of watershed hydrology and stream water quality under land use and climate change scenarios in Teshio River watershed, northern Japan. Ecological Indicators, 50, 79–89. https://doi.org/10.1016/j.ecolind.2014.11.003

FAO (2002). Land-Water Linkages in Rural Watersheds Case Study Series. Food and Agriculture Organization of the United Nations, Rome, Italy

Gashaw, T., Tulu, T., Argaw, M., & Worqlul, A. W. (2018). Modeling the hydrological impacts of land use/land cover changes in the Andassa watershed, Blue Nile Basin, Ethiopia. Science of The Total Environment, 619–620, 1394–1408. https://doi.org/10.1016/j.scitotenv.2017.11.191

Gebresamuel, G., Singh, B. R., & Dick, Ø. (2010). Land-use changes and their impacts on soil degradation and surface runoff of two catchments of Northern Ethiopia. Acta Agriculturae Scandinavica, Section B - Plant Soil Science, 60(3), 211–226. https://doi.org/10.1080/09064710902821741

Getachew, B., Manjunatha, B. R., & Bhat, H. G. (2021). Modeling projected impacts of climate and land use/land cover changes on hydrological responses in the Lake Tana Basin, upper Blue Nile River Basin, Ethiopia. Journal of Hydrology, 595, 125974. https://doi.org/10.1016/j.jhydrol.2021.125974

Girmay H, Assefa G (1979) The Addis Ababa-Nazreth volcanics: A miocene-pleistocene volcanic succession in the Ethiopian Rift. SINET: Ethiopia J Sci 12(1): 1-24

Guijarro, J. A. (2018). Homogenization of climatic series with Climatol. https://doi.org/10.13140/RG.2.2.27020.41604

Guzha, A. C., Rufino, M. C., Okoth, S., Jacobs, S., & Nóbrega, R. L. B. (2018). Impacts of land use and land cover change on surface runoff, discharge and low flows: Evidence from East Africa. Journal of Hydrology: Regional Studies, 15, 49–67. https://doi.org/10.1016/j.ejrh.2017.11.005

Guzman, C. D., Tilahun, S. A., Zegeye, A. D., & Steenhuis, T. S. (2013). Suspended sediment concentration–discharge relationships in the (sub-) humid Ethiopian highlands. Hydrology and Earth System Sciences, 17(3), 1067-1077.

Gyamfi, C., Ndambuki, J.M., and Salim, R.W., 2016. Hydrological responses to land use/cover changes in the Olifants basin, South Africa. Water, 8 (12), 588.

Halefom, A., Teshome, A., Sisay, E., & Ahmad, I. (2018). Dynamics of Land Use and Land Cover Change Using Remote Sensing and GIS: A Case Study of Debre Tabor Town, South Gondar, Ethiopia. Journal of Geographic Information System, 10(02), 165–174. https://doi.org/10.4236/jgis.2018.102008

Heber Green, W., & Ampt, G. A. (1911). Studies on Soil Phyics. The Journal of Agricultural Science, 4(1), 1–24. https://doi.org/DOI: 10.1017/S0021859600001441

Higgins, A., Restrepo, J. C., Ortiz, J. C., Pierini, J., & Otero, L. (2016). Suspended sediment transport in the Magdalena River (Colombia, South America): Hydrologic regime, rating parameters and effective discharge variability. International Journal of Sediment Research, 31(1), 25-35.

Hu, S., & Shrestha, P. (2020). Examine the impact of land use and land cover changes on peak discharges of a watershed in the midwestern United States using the HEC-HMS model. Papers in Applied Geography, 6(2), 101–118. https://doi.org/10.1080/23754931.2020.1732447

J. G. Arnold, D. N. Moriasi, P. W. Gassman, K. C. Abbaspour, M. J. White, R. Srinivasan, C. Santhi, R. D. Harmel, A. van Griensven, M. W. Van Liew, N. Kannan, & M. K. Jha. (2012). SWAT: Model Use, Calibration, and Validation. Transactions of the ASABE, 55(4), 1491–1508. https://doi.org/10.13031/2013.42256

Jansson, M. B. (1996). Estimating a sediment rating curve of the Reventazon river at Palomo using logged mean loads within discharge classes. Journal of Hydrology, 183(3-4), 227-241.

Jensen, J. R. (n.d.). Introductory Digital Image Processing: A Remote Sensing Perspective. 659.

Kasa, L., Zeleke, G., Alemu, D., Hagos, F., & Heinimann, A. (2010). IMPACT OF URBANIZATION OF ADDIS ABEBA CITY ON PERI-URBAN ENVIRONMENT AND LIVELIHOODS. 30.

Kassa, T., & Forech, G. (2009). Watershed Hydrological Responses to Changes in Land Use and Land Cover, and Management Practices at Hare Watershed , Ethiopia. Ph.D Thesis, University of Siegen, Germany, 229.

Kennedy, J., & Eberhart, R. (1995, November). Particle swarm optimization. In Proceedings of ICNN'95-international conference on neural networks (Vol.4,pp. 1942-1948). IEEE

Khalil, A. (2021). Inhomogeneity detection in the rainfall series for the Mae Klong River Basin, Thailand. Applied Water Science, 11(9), 147. https://doi.org/10.1007/s13201-021-01474-6

Khan, K. N. (2002). A Geographic Information System Based Spatially Distributed Rainfall-Runoff Model (Doctoral dissertation, University of Pittsburgh).

Khoi, Dao Nguyen. 2016. " Comparison of the HEC-HMS and SWAT Hydrological Models in Simulating the Stream Flow." Journal of Science and Technology 53(5A): 189-95

Kibria, K., Ahiablame, L., Hay, C., & Djira, G. (2016). Streamflow Trends and Responses to Climate Variability and Land Cover Change in South Dakota. Hydrology, 3(1), 2. https://doi.org/10.3390/hydrology3010002

Koneti, S., Sunkara, S., & Roy, P. (2018). Hydrological Modeling with Respect to Impact of Land-Use and Land-Cover Change on the Runoff Dynamics in Godavari River Basin Using the HEC-HMS Model. ISPRS International Journal of Geo-Information, 7(6), 206. https://doi.org/10.3390/ijgi7060206

Krause, P., Boyle, D. P., & Bäse, F. (2005). Comparison of different efficiency criteria for hydrological model assessment. Advances in Geosciences, 5, 89–97. https://doi.org/10.5194/adgeo-5-89-2005

Kuczera, G., Parent, E., 1998. Monte Carlo assessment of parameter uncertainty in conceptual catchment models: the Metropolis algorithm. Journal of Hydrology 211 (1-4), 69-85.

Kumar, N., Tischbein, B., Kusche, J., Beg, M. K., & Bogardi, J. J. (2017). Impact of land-use change on the water resources of the Upper Kharun Catchment, Chhattisgarh, India. Regional Environmental Change, 17(8), 2373–2385. https://doi.org/10.1007/s10113-017-1165-x

Kusimi, J. M. (2008). Assessing land use and land cover change in the Wassa West District of Ghana using remote sensing. GeoJournal, 71(4), 249–259. https://doi.org/10.1007/s10708-008-9172-6

Lambin, E. F., Geist, H. J., and Lepers, E. (2003). Dynamics of Land Use Land Cover. https://doi.org/10.1146/annurev.energy.28.050302.105459

Lemma, H., Frankl, A., Dessie, M., Poesen, J., Adgo, E., & Nyssen, J. (2020). Consolidated sediment budget of Lake Tana, Ethiopia (2012–2016). Geomorphology, 371, 107434.

Li, Z., & Fox, J. M. (2012). Mapping rubber tree growth in mainland Southeast Asia using time-series MODIS 250 m NDVI and statistical data. Applied Geography, 32(2), 420–432. https://doi.org/10.1016/j.apgeog.2011.06.018

Liu, J. G., & Mason, P. J. (2009). Essential Image Processing and GIS for Remote Sensing: Liu/Essential Image Processing and GIS for Remote Sensing. John Wiley & Sons, Inc. https://doi.org/10.1002/9781118687963

Liu, Y., Yang, W., Yu, Z. et al. Estimating Sediment Yield from Upland and Channel Erosion at A Watershed Scale Using SWAT. Water Resour Manage **29,** 1399–1412 (2015). https://doi.org/10.1007/s11269-014-0729-5

Magar, R. B., & Jothiprakash, V. (2011). Intermittent reservoir daily-inflow prediction using lumped and distributed data multi-linear regression models. Journal of Earth System Science, 120(6), 1067–1084. https://doi.org/10.1007/s12040-011-0127-9

Marshall, L., Nott, D., & Sharma, A. (2005). Hydrological model selection: A Bayesian alternative: HYDROLOGICAL MODEL SELECTION. Water Resources Research, 41(10). https://doi.org/10.1029/2004WR003719

Merritt, W. S., Letcher, R. A., & Jakeman, A. J. (2003). A review of erosion and sediment transport models. Environmental Modelling & Software, 18(8–9), 761–799. https://doi.org/10.1016/S1364-8152(03)00078-1

Mohamed, A., & Worku, H. (2019). Quantification of the land use/land cover dynamics and the degree of urban growth goodness for sustainable urban land use planning in Addis Ababa and the surrounding Oromia special zone. Journal of Urban Management, 8(1), 145–158. https://doi.org/10.1016/j.jum.2018.11.002

Moriasi, D. N., Arnold, J. G., Van Liew, M. W., Bingner, R. L., Harmel, R. D., & Veith, T. L. (2007). Model evaluation guidelines for systematic quantification of accuracy in watershed simulations. Transactions of the ASABE, 50(3), 885–900.

Munoth, P., & Goyal, R. (2020). Impacts of land use land cover change on runoff and sediment yield of Upper Tapi River Sub-Basin, India. International Journal of River Basin Management, 18(2), 177–189. https://doi.org/10.1080/15715124.2019.1613413

Musie, M., Sen, S., & Chaubey, I. (2020). Hydrologic Responses to Climate Variability and Human Activities in Lake Ziway Basin, Ethiopia. Water, 12(1), 164. https://doi.org/10.3390/w12010164

Nash, J. E., & Sutcliffe, J. V. (1970). River flow forecasting through conceptual models part I — A discussion of principles. Journal of Hydrology, 10(3), 282–290. https://doi.org/10.1016/0022-1694(70)90255-6

Neitsch, S. L., Arnold, J. G., Kiniry, J. R., & Williams, J. R. (2011). Soil & Water Assessment Tool Theoretical Documentation Version 2009. Texas Water Resources Institute, 1–647. https://doi.org/10.1016/j.scitotenv.2015.11.063

Neitsch SL, J.G. Arnold, J.R. Kiniry, R. Srinivasan, and J.R. Williams, 2005, Soil and Water Assessment Tool, Theoretical Documentation: Version 2005. USDA Agricultural Research Service and Texas A&M Blackland Research Center: Temple.

Nelson, S. A., & Khorram, S. (2018). Image Processing and Data Analysis with ERDAS IMAGINE®. CRC Press.

Nimac, I., & Perčec Tadić, M. (2017). Complete and homogeneous monthly air temperature series for the construction of 1982-2010 climatological normals in Croatia. Geofizika, 34(2), 225–249. https://doi.org/10.15233/gfz.2017.34.13

P. W. Gassman, M. R. Reyes, C. H. Green, & J. G. Arnold. (2007). The Soil and Water Assessment Tool: Historical Development, Applications, and Future Research Directions. Transactions of the ASABE, 50(4), 1211–1250. https://doi.org/10.13031/2013.23637

Pal, N., Pal, S., & IntelligenceUnit, M. (1993). A REVIEW ON IMAGE SEGMENTATION TECHNIQUES. 18.

Paul, P. K., Zhang, Y., Ma, N., Mishra, A., Panigrahy, N., & Singh, R. (2021). Selecting hydrological models for developing countries: Perspective of global, continental, and country scale models over catchment scale models. Journal of Hydrology, 600, 126561. https://doi.org/10.1016/j.jhydrol.2021.126561

Raes, D., Willems, P., & Gbaguidi, F. (2006). RAINBOW - a software package for hydrometeorological frequency analysis and testing the homogeneity of historical data sets. 15.

Rahman, A., Kumar, S., Fazal, S., & Siddiqui, M. A. (2012). Assessment of Land use/land cover Change in the North-West District of Delhi Using Remote Sensing and GIS Techniques. Journal of the Indian Society of Remote Sensing, 40(4), 689–697. https://doi.org/10.1007/s12524-011-0165-4

Rawat, J. S., & Kumar, M. (2015). Monitoring land use/cover change using remote sensing and GIS techniques: A case study of Hawalbagh block, district Almora, Uttarakhand, India. The Egyptian Journal of Remote Sensing and Space Science, 18(1), 77–84. https://doi.org/10.1016/j.ejrs.2015.02.002

Razad, A. Z. A., Samsudin, S. H., Abbas, N. A., Setu, A., Mohd Sidek, L., Jung, K., & Sharip, Z. (2019, November). Sediment yield modeling as sediment management strategies towards sustainability of hydropower reservoirs in Malaysia. In International Conference on Dam Safety Management and Engineering (pp. 26-37). Springer, Singapore.

Setegn, S.G., Srinivasan, R., Melesse, A.M. and Dargahi, B. (2010), SWAT model application and prediction uncertainty analysis in the Lake Tana Basin, Ethiopia. Hydrol. Process., 24: 357- 367. https://doi.org/10.1002/hyp.7457

Serur, A. B., & Adi, K. A. (2022). Multi-site calibration of hydrological model and the response of water balance components to land use land cover change in a rift valley Lake Basin in Ethiopia. Scientific African, 15, e01093.

Serur, A. B., & Sarma, A. K. (2016). Evaluation of the ArcSWAT Model in Simulating Catchment Hydrology: In Weyib River Basin, Bale Mountainous Area of Southeastern Ethiopia. International Journal of Innovative and Emerging Research in Engineering, 3(2), 9.

Shawul, A. A., & Chakma, S. (2019). Spatiotemporal detection of land use/land cover change in the large basin using integrated approaches of remote sensing and GIS in the Upper Awash basin, Ethiopia. Environmental Earth Sciences, 78(5), 141. https://doi.org/10.1007/s12665-019-8154-y

Shawul, A. A., Chakma, S., & Melesse, A. M. (2019). The response of water balance components to land cover change based on hydrologic modeling and partial least squares regression (PLSR) analysis in the Upper Awash Basin. Journal of Hydrology: Regional Studies, 26, 100640. https://doi.org/10.1016/j.ejrh.2019.100640

Sime, C.H., Demissie, T.A. & Tufa, F.G. Surface runoff modeling in Ketar watershed, Ethiopia. J. Sediment. Environ. **5,** 151–162 (2020). https://doi.org/10.1007/s43217-020-00009-4

Singh, V. P., & Woolhiser, D. A. (2002). Mathematical Modeling of Watershed Hydrology. Journal of Hydrologic Engineering, 7(4), 270–292. https://doi.org/10.1061/(ASCE)1084-0699(2002)7:4(270)

Tadele, K., & Förch, G. (2007). Impact of Land Use / Cover Change on Streamflow: The Case of Hare River Watershed, Ethiopia. 7.

Tadese, M., Kumar, L., Koech, R., & Kogo, B. K. (2020). Mapping of land-use/land-cover changes and its dynamics in Awash River Basin using remote sensing and GIS. Remote Sensing Applications: Society and Environment, 19, 100352. https://doi.org/10.1016/j.rsase.2020.100352

Tesema, T. A., & Leta, O. T. (2020). Sediment Yield Estimation and Effect of Management Options on Sediment Yield of Kesem Dam Watershed, Awash Basin, Ethiopia. Scientific African, 9, e00425. https://doi.org/10.1016/j.sciaf.2020.e00425

Tewabe, D., & Fentahun, T. (2020). Assessing land use and land cover change detection using remote sensing in the Lake Tana Basin, Northwest Ethiopia. Cogent Environmental Science, 6(1), 1778998. https://doi.org/10.1080/23311843.2020.1778998

The Guardian, 2007, Global food crisis looms as climate change and population growth strip fertile land. The Guardian, August 30

Tolera, M. B., & Chung, I.-M. (2021). Integrated Hydrological Analysis of Little Akaki Watershed Using SWAT-MODFLOW, Ethiopia. Applied Sciences, 11(13), 6011. https://doi.org/10.3390/app11136011

Tolera, M., Chung, I.-M., & Chang, S. (2018). Evaluation of the Climate Forecast System Reanalysis Weather Data for Watershed Modeling in Upper Awash Basin, Ethiopia. Water, 10(6), 725. https://doi.org/10.3390/w10060725

Tsehayu K, Hailemariam T (1990) Engineering geological map of Addis Ababa. Ethiopian Institute of Geological Surveys, Addis Ababa

Tso, B., & Mather, P. M. (2009). Classification methods for remotely sensed data (2nd ed). CRC Press.

USGS. (2016). Landsat-Earth Observation Satellites [Fact Sheet].

Van Griensven, A., Meixner, T., 2006. Methods to quantify and identify the sources of uncertainty for river basin water quality models. Water Science and Technology 53 (1), 51–59.

Welde, K., & Gebremariam, B. (2017). Effect of land use land cover dynamics on hydrological response of watershed: Case study of Tekeze Dam watershed, northern Ethiopia. International Soil and Water Conservation Research, 5(1), 1–16. https://doi.org/10.1016/j.iswcr.2017.03.002

Weng, Q. (2010). Remote sensing and GIS integration: Theory, methods, and applications. McGraw-Hill Professional ; McGraw-Hill [distributor. http://www.dawsonera.com/abstract/9780071606547

Williams, J.R., 1975, Sediment-yield predictions with universal equation using runoff energy factor. In Present and Prospective Technology for Predicting Sediment Yield and Sources. U.S. Dept. Agr., ARS-S-40. Washington, D.C. p. 244-252.

Woldesenbet, T. A., Elagib, N. A., Ribbe, L., & Heinrich, J. (2017). Hydrological responses to land use/cover changes in the source region of the Upper Blue Nile Basin, Ethiopia. Science of The Total Environment, 575, 724–741. https://doi.org/10.1016/j.scitotenv.2016.09.124

Worako, A. W. (2016). Land Use Land Cover Change Detection by Using Remote Sensing Data in Akaki River Basin. International Journal of Environment, 1(1), 10.

Yadeta, D., Kebede, A., & Tessema, N. (2020). Potential evapotranspiration models evaluation, modelling, and projection under climate scenarios, Kesem sub-basin, Awash River basin, Ethiopia. Modeling Earth Systems and Environment, 6(4), 2165-2176.

Yang, X., & Lo, C. P. (2002). Using a time series of satellite imagery to detect land use and land cover changes in the Atlanta, Georgia metropolitan area. International Journal of Remote Sensing, 23(9), 1775-1798.

Zhang, H., Wang, B., Liu, D. L., Zhang, M., Leslie, L. M., & Yu, Q. (2020). Using an improved SWAT model to simulate hydrological responses to land use change: A case study of a catchment in tropical Australia. Journal of Hydrology, 585, 124822. https://doi.org/10.1016/j.jhydrol.2020.124822

Zhu, C., & Li, Y. (2014). Long-Term Hydrological Impacts of Land Use/Land Cover Change From 1984 to 2010 in the Little River Watershed, Tennessee. International Soil and Water Conservation Research, 2(2), 11–21. https://doi.org/10.1016/S2095-6339(15)30002-2

APPENDICES

Appendix A

Appendix A .1 Soil parameters of the study area

SNAM	NLAYERS	HYDGRP	SOL_ZMX	SOL_CRK	TEXTURE	SOL-Z	SOL_BD	SOL_K	SOL_CBN	CLAY	SILT	SAND	ROCK	SOL_ALB	USLE_K
ET1137	2	D	1000	0.5	SCL	300	1.57	6.22	0.63	27	22	51	1	0.39	0.15
ET1154	2	C	1000	0.5	SCL	300	1.57	6.22	0.63	27	22	51	1	0.39	0.15
ET1189	2	D	1000	0.5	C	300	1.33	1.35	2.45	49	27	24	1	0.11	0.11
ET1266	2	D	1000	0.5	C	300	1.31	0.73	1.07	54	25	21	1	0.29	0.13
ET957	2	D	1000	0.5	C	300	1.43	1.33	0.78	42	28	30	1	0.35	0.15

Appendix A .2 Algorithm for filling missing rainfall data

```
library(climatol)
#daily PCP
daily2climatol('PCP stations.txt',c(1,3,2,4,0,0),2:5,'PCP',sep=',',na.strings='NA')
homogen('PCP', 2000, 2018, expl=TRUE)
homogen('PCP', 2000, 2018, std=2)
dahstat('PCP', 2000, 2018, stat='series')

#daily TMAX
daily2climatol('Tmax stations.txt',c(1,3,2,4,0,0),2:5,'Tmax',sep=',',na.strings='NA'
homogen('Tmax', 2000, 2018, expl=TRUE)
dd2m('Tmax', 2000, 2018)
homogen('Tmax-m', 2000, 2018)
homogen('Tmax', 2000, 2018, dz.max=7, metad=TRUE)
dahstat('Tmax', 2000, 2018, stat='series')

#daily TMIN
daily2climatol('Tmin stations.txt',c(1,3,2,4,0,0),2:5,'Tmin',sep=',',na.strings='NA'
homogen('Tmin', 2000, 2018, expl=TRUE)
dd2m('Tmin', 2000, 2018)
homogen('Tmin-m', 2000, 2018)
homogen('Tmin', 2000, 2018, dz.max=7, metad=TRUE)
dahstat('Tmin', 2000, 2018, stat='series')
```

Appendix A .3 Average annual rainfall of stations in the study area

Year	AAObse	AA Bole	Akaki	Intoto	Dire Gidib
2000	1032.2	781.9	763.8	1412	911.5
2001	1136	1051.4	731.1	1473.4	1088.5
2002	977.3	826.7	663.2	1459.8	847.3
2003	1010.5	858.9	781.7	1673.4	1276.2
2004	1047.7	855.7	616.8	1558.4	640.4
2005	1111.2	944.5	948.7	1610.2	1089.1
2006	1064.3	926.2	814.9	1580.3	938.5
2007	1204.5	943	850.6	1580.9	1135
2008	1002.6	923	836.6	1749.2	1108
2009	957.7	812.5	870	1472.9	929.7
2010	1181.4	886.7	866.9	1675	1224.4
2011	969.4	791.5	658.7	1356.4	941.4
2012	926.7	757.1	751.5	1674.6	880.2
2013	1054	899.1	689.3	1999.7	1108.4
2014	974.1	747.2	736	1366.2	869.2
2015	937.7	696.8	675.5	1472.7	766.2
2016	1080.2	849.9	809.6	1575.4	1025.2
2017	913.3	827	674.3	1771.5	1009.2
2018	1083.7	886.2	786.3	1744.6	1141.9

Appendix A .4 LULC classification accuracy assessment

i. 2000 LULC map

LULC Class	Agricultural	Built-up	Forest	Grass land	Shrub land	Water body	Bare land	Total	User accuracy (%)
Agricultural	120	0	1	7	0	0	6	134	89.6
Built-up	1	23	2	0	0	0	0	26	88.5
Forest	0	0	14	0	0	0	0	14	100
Grass land	2	0	0	12	0	0	0	14	85.7
Shrub land	0	0	0	0	3	0	0	3	100
Water body	0	0	0	0	0	4	0	4	100
Bare land	0	0	0	0	0	0	6	6	100
Total	123	23	17	19	3	4	12	201	
Producer accuracy (%)	97.6	100	82.4	63.2	100	100	50		
Overall accuracy	90.5%								
Kappa	0.83								

coefficient

ii. 2010 LULC map

LULC Class	Agricultural	Built-up	Forest	Grass land	Shrub land	Water body	Bare land	Total	User accuracy (%)
Agricultural	122	0	5	9	0	0	2	138	88.5
Built-up	2	24	1	0	0	0	0	27	88.9
Forest	0	0	15	0	0	0	0	15	100
Grass land	0	0	0	10	0	0	0	10	100
Shrub land	0	0	0	0	3	0	0	3	100
Water body	0	0	0	0	0	3	0	3	100
Bare land	1	0	0	0	0	0	4	5	80
Total	125	24	21	19	3	3	6	201	
Producer accuracy (%)	97.6	100	71.4	52.6	100	100	66.7		
Overall accuracy	90.0%								
Kappa coefficient	0.82								

Appendix A .5 LULC change detection matrix

i. For 2000-2010

		2000						
		AL	BU	FL	GL	ShL	WB	BaL
2010	AL	641.28	2.62	3.38	2.85	0.04	0.31	0.04
	BU	9.49	99.67	0.78	1.25	0.03	0	0.04
	FL	0.66	0.56	27.14	12.37	0	0.01	0.54
	GL	0.96	0.87	4.92	9.56	0.04	0.19	0.75
	ShL	0.32	0.19	1.95	1.41	0.05	0.02	0.08
	WB	0.44	0	0.02	0.01	0	4.84	0
	BaL	0.28	0.07	0.62	1.19	0.01	0.05	0.18

ii. For 2010-2020

		2010						
		AL	BU	FL	GL	ShL	WB	BaL
	AL	621.68	5.5	0.89	0.78	0.36	1.61	0.23
	BU	26.21	105.21	0.12	0.83	0.15	0	0.24
	FL	0.83	0.17	39.12	1.01	0.11	0	0.01
2020	GL	0.75	0.19	0.98	14.23	0.18	0	0.17
	ShL	0.28	0.04	0.12	0.23	3.22	0	0
	WB	0.09	0	0	0.03	0	3.67	0.01
	BaL	0.1	0.03	0.01	0.17	0	0	1.75

Appendix A .6 Streamflow parameters and parameter ranges used for a sensitivity analysis

Name	Min	Max	Description	Process
CN2.mgt	35	98	SCS runoff CN for moisture condition II	Runoff
ALPHA_BF.gw	0	1	Baseflow alpha factor (days)	Groundwater
GW_DELAY.gw	0	500	Groundwater delay (days)	Groundwater
GWQMN.gw	0	5000	Threshold depth of water in the shallow aquifer required for return flow to occur (mm)	Groundwater
GW_REVAP.gw	0.02	0.2	Groundwater 'revap' coefficient	Groundwater
RCHRG_DP.gw	0	1	Groundwater recharge to deep aquifer (fraction)	Groundwater
REVAPMN.gw	0	500	Threshold depth of water in the shallow aquifer for 'revap' to occur (mm)	Groundwater
OV_N.hru	0.01	30	Manning's "n" value for overland flow	Evaporation
ESCO.hru	0	1	Soil evaporation compensation factor	Evaporation
EPCO.hru	0	1	Plant evaporation compensation factor	Evaporation
CH_K2.rte	-0.01	500	Hydraulic conductivity in main channel (mm/hrs)	Channel
CH_N2.rte	-0.01	0.3	Manning coefficient for main channel	Channel
SOL_AWC.sol	0	1	Available water capacity of the soil layer (mm/mm soil)	Soil
SOL_K.sol	0	2000	Saturated soil conductivity (mm/hrs)	Soil
ESCO.bsn	0	1	Soil evaporation compensation factor	Evaporation
SURLAG.bsn	0.05	24	Surface runoff lag coefficient	Runoff

Appendix A .7 Sediment yield parameters and parameter ranges used for a sensitivity analysis

Name	Min	Max	Description
CN2.mgt	35	98	SCS runoff CN for moisture condition II
ALPHA_BF.gw	0	1	Baseflow alpha factor (days)
SPCON.bsn	0.0001	0.01	Linear parameter for calculating the maximum amount of sediment that can be reentrained during channel sediment routing
USLE_K.sol	0	0.6	USLE equation soil erodibility (K) factor
USLE_P.mgt	0	1	USLE equation support practice
BIOMIX.mgt	0	1	Biological mixing efficiency
SPEX.bsn	1	1.5	Exponent parameter for calculating sediment reentrained in channel sediment routing
CH_COV_2.rte	-0.001	1	Channel cover factor
EROS_SPL.bsn	0.9	3.1	The splash erosion coefficient
CH_EQN.rte	0	4	Sediment routing method
LAT_SED.hru	0	5000	Sediment concentration in lateral flow and groundwater flow
ADJ_PKR.bsn	0.5	1	Peak rate adjustment factor for sediment routing in the sub-basin
CH_ERODMO.rte	0	1	Channel erodibility factor

Appendix B

Appendix B. 1 Homogeneity test plot for rainfall station

i. AA Bole

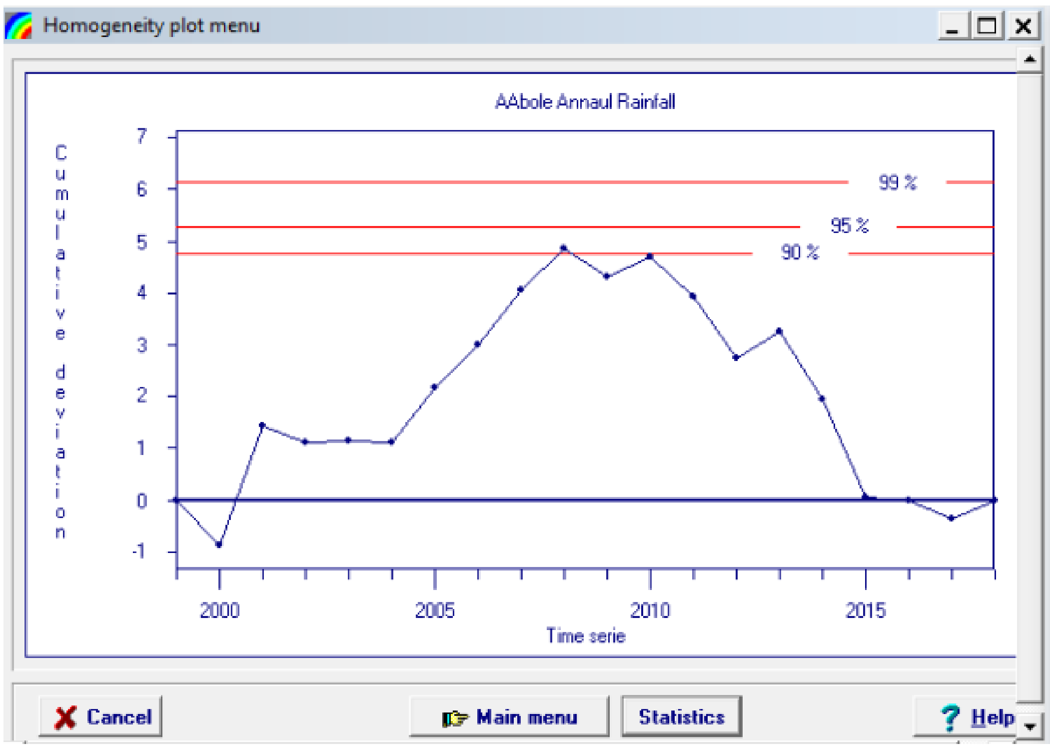

ii. Akaki

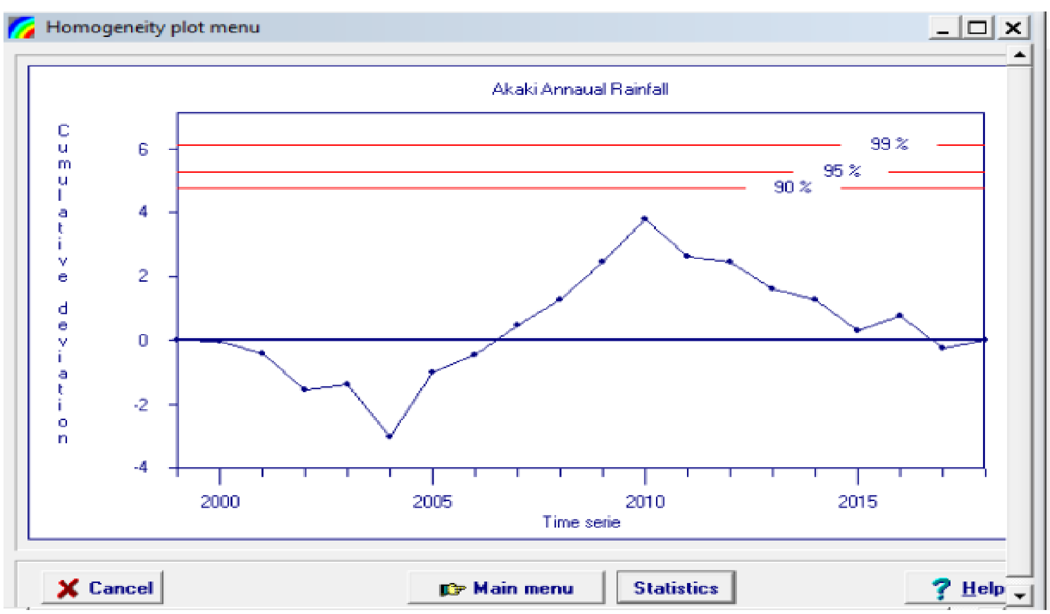

iii. Dire Gidib

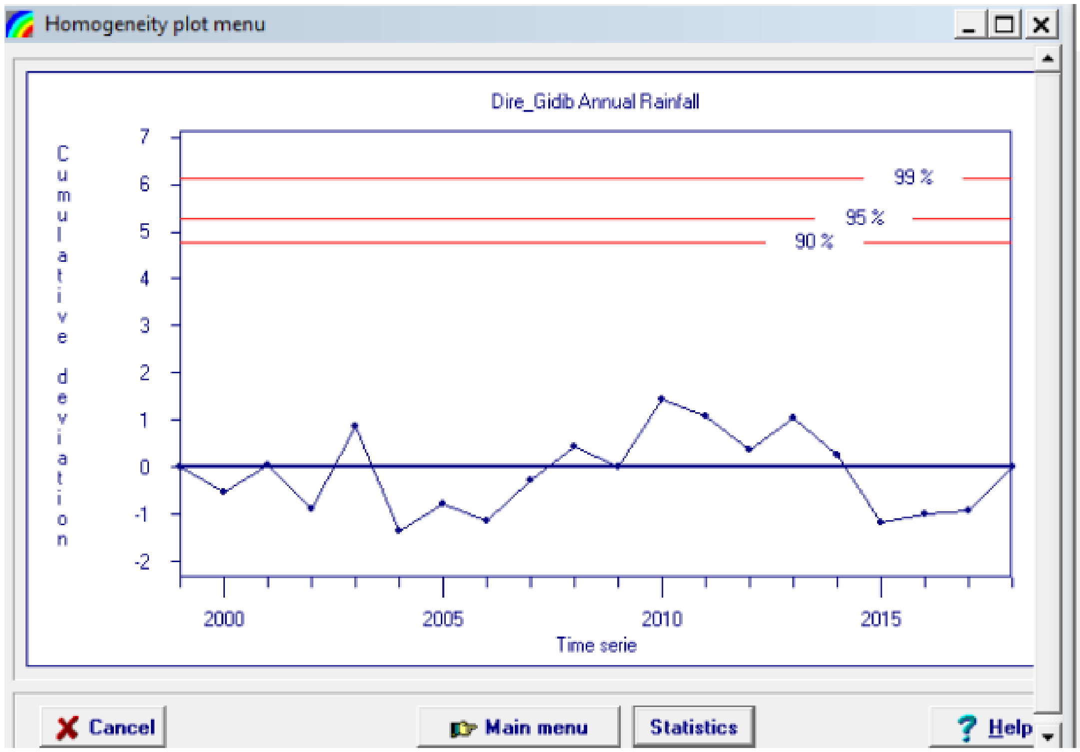

iv. Intoto

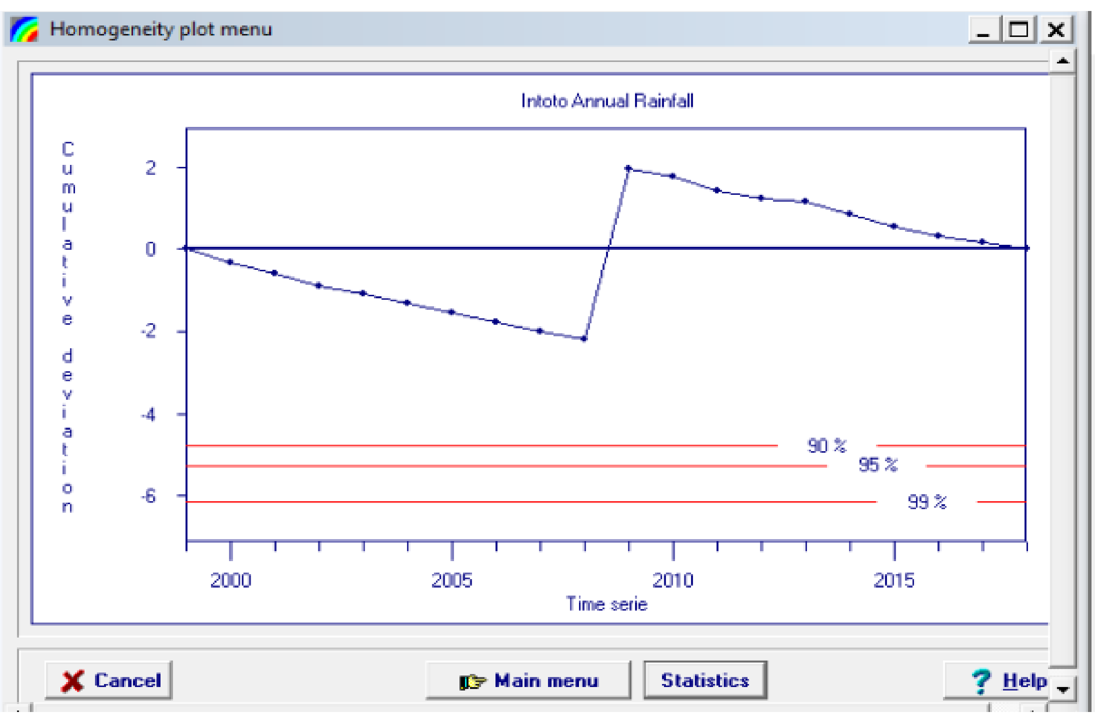

Appendix B. 2 Average seasonal water balance for a model run with static and dynamic LULC

i. Wet Season

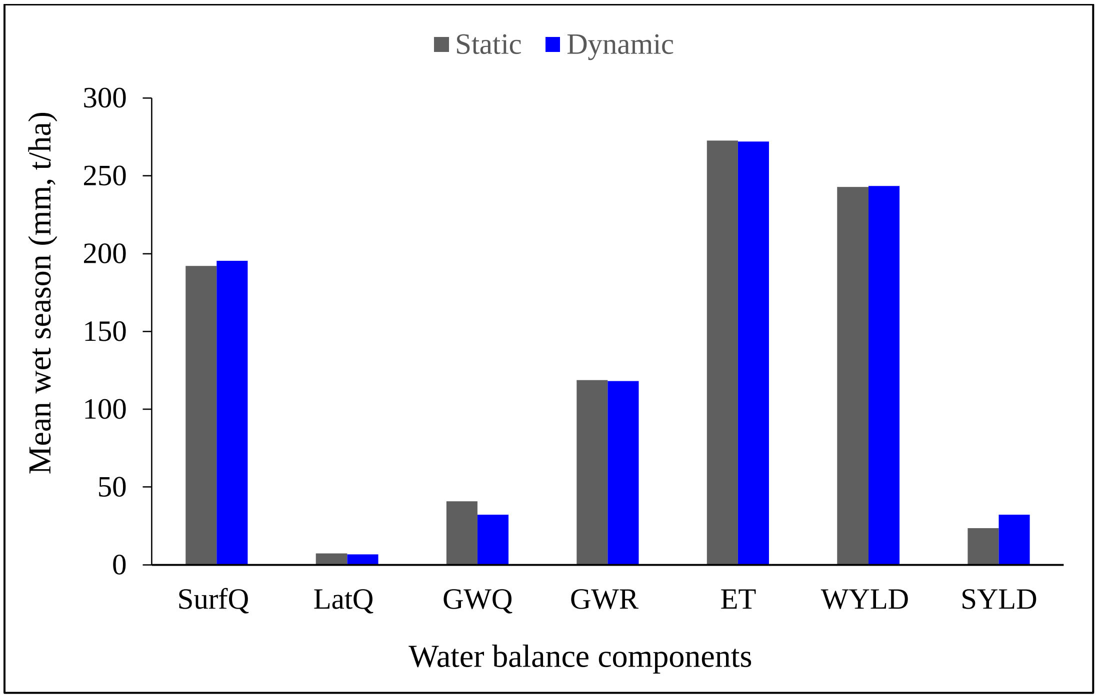

ii. Dry Season